

Aus dem Institut für Klinische Neuroimmunologie
der Ludwig-Maximilians-Universität München
Direktor: Prof. Dr. Kerschensteiner



Understanding the role of epithelial MyD88 signals in the early development of Experimental Autoimmune Encephalomyelitis (EAE)

Dissertation
zum Erwerb des Doktorgrades der Naturwissenschaften
an der Medizinischen Fakultät
der Ludwig-Maximilians-Universität München

vorgelegt von
Verónica E. Solís González.

aus
David, Panama

2022

Mit Genehmigung der Medizinischen Fakultät
der Universität München

Betreuer(in): Priv. Doz. Dr. Naoto Kawakami

Zweitgutachter(in): Prof. Dr. Elfriede Nößner

Dekan: Prof. Dr. med. Thomas Gudermann

Tag der mündlichen Prüfung: 17. Oktober 2022

A mi hermano, cuya reciente y temprana partida se talló profundamente en mi alma.

Para ti, este fruto de esfuerzo de muchos años.

Table of Contents

Zusammenfassung	1
Summary	3
List of Figures	5
List of Tables	7
List of Abbreviations	8
Introduction	12
1.1 Multiple Sclerosis	12
1.1.1 Pathogenesis	13
1.1.2 Etiology.....	14
1.2 Experimental Autoimmune Encephalomyelitis.....	15
1.2.1 Induced EAE Murine Models.....	15
1.2.2 Spontaneous EAE Murine Models.....	15
1.3 Innate Triggers of the Nervous System Autoimmunity.....	17
1.3.1 The host-microbial crosstalk	17
1.3.2 MyD88: a modulator in the host-microbial control	18
1.3.3 MyD88, the microbiota and gut immune compartment in CNS autoimmunity	21
1.4 Activation of T lymphocytes.....	23
1.4.1 Calcium influx as an early marker for T lymphocyte activation	23
1.4.2 NFAT translocation as a visual marker of T cell activation	25
Objectives	27
2. Materials and Methods.....	29
2.1 Materials.....	29
2.1.1 Mice.....	29
2.1.2 Cell Lines.....	31
2.1.3 Buffers and Solutions	31
2.1.4 Antibodies	34
2.1.5 Primers	36
2.1.6 Plasmids.....	37
2.1.7 Kits.....	37

2.2 Methods.....	38
2.2.1 Mouse Routine.....	38
2.2.1.1 Tail Genomic DNA Isolation and PCR Genotyping.....	38
2.2.1.2 Leukocyte Isolation from Peripheral Blood.....	38
2.2.1.3 Isolation of serum from total blood.....	38
2.2.1.4 Mononuclear Leukocyte Isolation from Organs.....	39
2.2.1.5 Generation of bone marrow derived dendritic cells (BMDCs).....	40
2.2.1.6 Adoptive cell transfer.....	40
2.2.1.7 FITC-Dextran gavage.....	40
2.2.1.8 Ovalbumin gavage.....	41
2.2.1.9 Active induction of Experimental Autoimmune Encephalomyelitis (EAE).....	41
2.2.2 Flow Cytometry.....	41
2.2.3 Enzyme-linked Immunosorbent Assay (ELISA).....	43
2.2.4 Fecal DNA extraction and 16S rRNA qPCR.....	44
2.2.5 16S ribosomal RNA (rRNA) gene sequence analysis.....	44
2.2.6 Cloning and Sequencing.....	45
2.2.7 Tissue histology and immunofluorescence microscopy.....	46
2.2.8 Cell Culture.....	46
3. Results.....	52
3.1 The Interplay between the Gut Microbiota and MyD88-dependent Pathways in the Development of EAE.....	52
3.1.1. Deletion of MyD88 in intestinal epithelial cells (IECs) leads to severe EAE.....	52
3.1.2 The effect of IECs MyD88-dependent pathways in epithelial barrier function.....	54
3.1.3. The effect of intestinal MyD88-dependent pathways in adaptive immune responses.....	57
3.1.4. The Effect of epithelial-specific MyD88 signaling in the composition of the gut microbiota.....	63
3.2 Establishing Tools to Identify Molecular Mimicry Events in Gut Tissues as a Trigger Mechanism for EAE.....	66
3.2.1 Generation a MOG-specific T cell Hybridoma as an antigen-screening In-Vitro Tool.....	66
3.2.2 Establishing an in-vivo system for assessing T cell activation events in the gut.....	74
4. Discussion.....	79
4.1 Understanding the role of epithelial MyD88 signals in the pathogenesis and course of spontaneous EAE.....	79

4.1.1. Influence of intrinsic MyD88 signals in IECs in the integrity of the gut epithelial cell wall and commensal gut bacterial translocation 81

4.1.2. Effect of intestinal epithelial MyD88 signals' in cells from the innate and adaptive immune system 85

4.1.5 Composition of the local gut microbiota in steady-state MyD88^{ΔIEC} mice 87

4.2 The challenges of establishing in-vivo and in-vitro experiments to assess T cell activation in the gut 90

4.2.1. Designing an T-cell hybridoma as in-vitro tool for antigen screening 91

4.2.2. Establishing an in-vivo approach for the study of early T cell activation events in EAE 92

References 95

Resources & Contributions 104

Acknowledgements..... 105

Affidavit 106

Confirmation of congruency 107

Zusammenfassung

Die Wechselwirkung zwischen symbiotischen Darmbakterien und dem Immunsystem beeinflusst nicht nur das Gleichgewicht des Immunsystems, sondern ist auch ein wichtiger Faktor bei der Entstehung bestimmter Krankheiten. Dieses Zusammenspiel wird als *host-microbe crosstalk* bezeichnet und beschreibt mehrere Signalketten, welche zu einer gesunden Darmflora beitragen. Eine Störung des Gleichgewichts zwischen Darmbakterien, Enterozyten und Zellen des lokalen Immunsystems kann zu einer Überstimulation des Immunsystems führen und verschiedene Autoimmunerkrankungen auslösen. Aktuelle Studien zeigen einen direkten Einfluss von Darmbakterien auf das darmassoziierte lymphatische Gewebe (GALT) des Immunsystems, allerdings ist der zugrunde liegende Mechanismus größtenteils unbekannt.

In dieser Arbeit wurde die Bedeutung von MyD88 Signalen innerhalb des Epithels auf den *host-microbe crosstalk* untersucht, sowie deren Einfluss auf die Entstehung von *Experimental Autoimmune Encephalomyelitis* (EAE). Mäuse mit MyD88-Knockout in Darmschleimhauts-zellen (MyD88^{ΔIEC} Mäuse) wurden auf Veränderungen ihres Darmfloragleichgewichts, ihrer Zytokinproduktion und der Zusammensetzung ihres Darmmikrobioms untersucht. Berichten zufolge spielen MyD88 Signale innerhalb des Epithels eine entscheidende Rolle bei der Entstehung von EAE, da bei Knockout Mäusen ein stärkerer Verlauf als bei Kontrollgruppen beobachtet wurde. Ebenso war die Inzidenz an spontan auftretendem EAE bei Kreuzung der MyD88^{ΔIEC} Mäuse mit Opticospinal EAE (OSE) Mäusen erhöht. Der beobachtete Phenotyp dieser Mäuse könnte auf eine geschwächte lokale Th2 Antwort zurückgeführt werden, gemeinsam mit einer leichten Reduktion von IL-4 und IL-10 Zytokine und begleitet von einer deutlichen Verringerung an *Small intestine lamina propria* (SiLPL) FoxP3⁺ Treg Zellen. Allerdings wurden keine Veränderung der lokalen Th1/Th17 Antwort in den untersuchten MyD88^{ΔIEC} *steady-state* Mäusen beobachtet.

Wir können eine Translokation von Darmbakterien in das Darmgewebe von MyD88^{ΔIEC} Mäusen ausschließen, da in angrenzenden Organen keine 16S rRNA gefunden wurde. Ebenso ergab eine Sequenzierung der V3/V4 Regionen der 16S rRNA keine Anzeichen auf eine signifikante Änderung der Darmflorakomposition, welche auf eine Dysbiose der MyD88^{ΔIEC} Mäusen hätte hinweisen können. Der Anteil an IgA im Stuhl der MyD88^{ΔIEC} Mäuse unterschied sich ebenfalls nicht von dem der Kontrollmäuse. Damit kann die Möglichkeit einer durch IgA behinderten Immunantwort ausgeschlossen werden.

Nachdem wir mehrere potentielle Mechanismen für den schwereren Krankheitsverlauf sowie die erhöhte Inzidenz von EAE in MyD88^{ΔIEC} Mäusen ausschließen können, stellen wir eine alternative Theorie vor. Wir vermuten, dass die erhöhte Darmwandpermeabilität bei MyD88^{ΔIEC} Mäusen es den lokalen dendritischen Zellen (DCs) erlaubt eine erhöhte Menge an Abfallprodukten von Fremdbakterien zu detektieren. Diese DCs könnten dann B- und T-Zellen innerhalb der Peyer-Platten aktivieren. Dadurch würde eine Entzündung ausgelöst welche wegen der reduzierten Menge an FoxP3⁺ Tregs Zellen innerhalb des SiLPL der MyD88^{ΔIEC} Mäuse außer Kontrolle gerät. In Kombination mit weiteren Störungen des Darmgleichgewichts (z.B. AMP Produktion, Tight-Junction Proteinexpressionsmuster, Probleme der Schleimhaut in Dünn- oder Dickdarm), würde dies die Beobachtungen während der Entwicklung von EAE in MyD88^{ΔIEC} Mäusen erklären.

Zusammenfassend kann man sagen, dass die fehlenden IEC-MyD88 abhängigen Signalkaskaden eine signifikante Verringerung der lokalen FoxP3⁺ Treg Zellkonzentration in der *intestinal lamina propria* in MyD88^{ΔIEC} Mäusen zur Folge haben, welche zur Schwere der EAE in diesen Mäusen beitragen könnte. Allerdings finden wir keinen Einfluss dieser Signalkaskaden auf die Konzentration von ausgeschiedenem IgA, die Zusammensetzung des Darmmikrobioms sowie die lokale Th1/Th17 Immunantwort im Darm von MyD88^{ΔIEC} *steady-state* Mäusen.

Summary

The interaction between the commensal microbiota and the immune system do not only influences functions that affect immune system homeostasis but also play a role in the development of disease. This interaction is widely known as the microbe-host crosstalk and it involves the interaction of several pathways that contribute to a healthy gut microenvironment. An imbalance in intestinal bacteria, enterocytes and cells from the local immune system is known to lead to overstimulation of the immune system, thereby contributing to the development of several autoimmune diseases. In the case of Multiple Sclerosis (MS), recent studies have shown that the microbiota plays an active role in influencing the local immune system of the gut-associated lymphoid tissue (GALT) but the exact mechanism behind this interaction remains largely unknown.

In this study, we explore the effect that epithelial MyD88 signals have in the microbial-host crosstalk and its possible influence in Experimental Autoimmune Encephalomyelitis (EAE) development. Intestinal epithelial cells (IECs) specific MyD88 knock-out mice (MyD88^{ΔIEC} mice) were assessed for changes in their intestinal homeostasis as well as profiled for their cytokine production and microbiota composition. Epithelial MyD88 signals have been observed to play an important role in the development of EAE as a more severe course of the disease was observed in these mice when compared to control littermates. Likewise, a higher incidence in the development of spontaneous EAE was observed when crossing MyD88^{ΔIEC} mice with Opticospinal EAE (OSE) mice. The phenotype observed in these mice could be attributed to a dampened Th2 local response, featuring a slight reduction in IL-4 and IL-10 cytokines that is accompanied with a significant reduction in small intestine lamina propria (SiLPL) FoxP3⁺ Treg cells. On the other hand, alterations in the local Th1/Th17 response were not observed in MyD88^{ΔIEC} steady-state mice.

In this work, we could exclude a potential translocation of gut bacteria into the gut tissues of MyD88^{ΔIEC} as we failed to detect the presence of 16S rRNA in peripheral organs. In addition, no significant changes in the overall microbiota composition that could hint to a dysbiosis in MyD88^{ΔIEC} mice were observed when sequencing the V3/V4 regions of 16S RNA genes. Furthermore, frequencies of fecal IgA in MyD88^{ΔIEC} mice did not differ from those of control mice, discarding the possibility of an impaired IgA-mediated immune response in gut tissues.

Having explored different mechanisms to explain the exacerbated course and increased incidence of EAE in MyD88^{ΔIEC} mice, we propose an alternative theory. We theorize that the slight increase in the gut

permeability observed in MyD88^{ΔIEC} mice in this work could allow local dendritic cells (DCs) to sample a higher number of commensal bacterial products from the luminal bacteria. Local DCs could in turn activate B and T cells within the Peyer's Patches; therefore, unleashing a pro-inflammatory response that cannot be controlled by local FoxP3⁺ Treg cells as MyD88^{ΔIEC} mice were found to have a significant decrease in FoxP3⁺ Tregs cells within the SiLPL. This, combined with other possible potential alterations in the gut homeostasis (such as AMP production, tight-junction expression profile and defects in the mucus layer of small intestine and colon) could offer an explanation to the phenotype observed when studying EAE development in MyD88^{ΔIEC} mice.

In summary, the lack IEC-MyD88 dependent signals are shown to significantly reduce the frequencies of local FoxP3⁺ Tregs in the intestinal lamina propria of the small intestine of MyD88^{ΔIEC} mice, a finding that might contribute to the increased EAE severity observed in these mice. However, these signals appear not to influence fecal IgA frequencies, overall microbiota composition and local gut Th1/Th17 immune response in MyD88^{ΔIEC} steady-state mice.

List of Figures

Figure 1.3.2.1	The role of the Toll-like receptor pathway in the Intestinal homeostasis	20
Figure 1.4.1.1	Scheme of the calcium-signaling cascade upon T cell activation	24
Figure 2.2.9.1	Schematic workflow of PEG-mediated T cell-hybridoma generation	48
Figure 3.1.1.1	Deletion of MyD88 in Intestinal Epithelial Cells (IECs) exacerbates the severity of active EAE	52
Figure 3.1.1.2	Lack of MyD88-dependent pathways in IECs play increases the incidence of spontaneous EAE	53
Figure 3.1.2.1	Epithelia cell wall and intestinal tissues remain intact regardless of MyD88 deficiency in IECs	54
Figure 3.1.2.2	MyD88 deficiency in IEC does not promote bacteria colonization of peripheral or gut-derived organs	55
Figure 3.1.2.3	Effect of epithelial MyD88-dependent signaling in the intestinal permeability of MyD88 ^{ΔIEC} mice	56
Figure 3.1.3.1	Effect of epithelial MyD88 on Th1/Th17 cells in lymphoid organs and GALT	57
Figure 3.1.3.2	Effect of epithelial MyD88 on Th2 cytokines of lymphoid organs and GALT	58
Figure 3.1.3.3	Effect of epithelial MyD88 on FoxP3 ⁺ regulatory T cells of lymphoid organs and GALT	59
Figure 3.1.3.4	Effect of epithelial MyD88 on the generation and recruitment of myeloid cells in spleen and GALT	60
Figure 3.1.3.5	The abundance of fecal IgA does not depend on gut epithelial MyD88 signaling.	61
Figure 3.1.3.6	Effect of epithelial MyD88 on the abundance of serum immunoglobulins IgA, IgM and IgG	61
Figure 3.1.4.1	Effect of epithelial MyD88 on segmented filamentous bacteria (SFB) abundance in fecal pellets	63
Figure 3.1.4.2	Effect of epithelial MyD88 signaling on caecal luminal microbiota	64

List of Figures

Figure 3.1.4.3	Effect of epithelial MyD88 signaling on taxonomical order of caecal luminal microbiota	65
Figure 3.2.1.1	pQC-NFAT-TRE-sGFP retroviral construct diagram.	66
Figure 3.2.1.2	Screening of MOG-specific T cell hybridoma positive clones by FACS Staining	67
Figure 3.2.1.3	Antigen-specific IL-2 production of reactive MOG-specific T cell hybridoma clones.	68
Figure 3.2.1.4	Screening of MOG-specific T cell hybridomas expressing NFAT-TRE-sGFP plasmid by FACS after being pre-treated with an ecotropic receptor booster treatment and stimulation with PMA/ionomycin	69
Figure 3.2.1.5	TCH-2D2-B9 T cell hybridoma cells don't incorporate pcDNA6-NFAT-TRE-sGFP plasmid efficiently	71
Figure 3.2.1.6	TCH-2D2-B9 T cell hybridoma appears to be resistant to transfection with different reagents	72
Figure 3.2.1.7	BW5147 lymphoma cells efficiently incorporate NFAT-TRE-sGFP via retroviral transduction	72
Figure 3.2.1.8	GFP expression by BW5147 lymphoma cells confirms stably expression of NFAT-TRE-sGFP	73
Figure 3.2.2.1	Schematic workflow of adoptive transfer of cells into mouse recipient	74
Figure 3.2.2.2	Frequencies of transferred B-cell depleted actin-GFP splenocytes recovered after 1-, 3-, 5-, and 7-days post-transfer from different organs from C57BL/6 mice	75
Figure 3.2.2.3	Frequencies of $V\alpha 2^+\beta 6^+$ cells recovered 24 hours after oral gavage with ovalbumin at 3 days post-transfer from different organs from recipient C57BL/6 mice	76
Figure 3.2.2.4	Retroviral transfection of B-cell depleted C57BL/6 splenocytes with NFAT-TRE-sGFP retroviral supernatant.	78
Figure 4.1	Proposed mechanism for a local gut inflammatory event that could lead to severe EAE in MyD88 ^{ΔIEC} mice.	89

List of Tables

Table 2.1.2	Cell Lines	31
Table 2.1.4.1	Flow Cytometry Antibodies	34
Table 2.1.4.2	Purified Antibodies and Avidin	35
Table 2.1.4.3	Antibodies for Enzyme-linked Immunosorbent Assay (ELISA)	35
Table 2.1.5.1	Primers for Genotyping	36
Table 2.1.5.2	Primers for Real-Time quantitative PCR	36
Table 2.1.5.3	Primers for Molecular Cloning	37
Table 2.1.6	Plasmids	37
Table 2.1.7	Kits	37

List of Abbreviations

2D2	MOG ₃₅₋₅₅ specific TCR transgenic
ABTS	2,2'-azino-bis(3-ethylbenzothiazoline-6-sulfonic acid
ACK	ACK Ammonium-Chloride-Potassium
aEAE	Actively-induced EAE – aEAE
Ag	Antigen
AMP	Antimicrobial peptide
APC	Antigen presenting cell
BBB	Blood–brain barrier
BCA	Bicinchoninic acid assay
BCR	B cell receptor
BES	N,N-bis[2-hydroxyethyl]-2-aminoethanesulfonic acid
BMDCs	Bone marrow derived dendritic cells
CFA	Complete Freund's adjuvant
CIS	Clinically isolated syndrome
cLPL	Colonic lamina propria
CNS	Central nervous system
CO ₂	Carbon dioxide
CRAC	Ca ²⁺ channels
CSF	Cerebral spinal fluid
DMEM	Dulbecco's Modified Eagle Medium
DNA	Deoxyribonucleic acid
EAE	Experimental autoimmune encephalomyelitis
EBV	Epstein–Barr virus
ELISA	Enzyme-linked immunosorbent assay
ER	Endoplasmic reticulum
EUB	Eubacterial
FACS	Fluorescence-activated cell sorting
FBS	Fetal bovine serum
FITC	Fluorescein isothiocyanate

List of Abbreviations

GALT	Gut-associated lymphoid tissues
GF	Germ-free
GFP	Green fluorescent protein
GM-CSF	Granulocyte-macrophage colony-stimulating factor
HAT	Hypoxanthine-aminopterin-thymidine medium
HBSS	Hank's Balanced Salt Solution
HEK	Human embryonic kidney
HEPES	4-(2-hydroxyethyl)-1-piperazineethanesulfonic acid
HRP	Horseradish peroxidase
IBD	Inflammatory bowel disease
IECs	Intestinal epithelial cells
IFN	Interferon
Ig	Immunoglobulin
IL	Interleukin
IS	Immunological synapse
LB	Luria Bertani
LPL	Lamina propria lymphocytes
MBP	Myelin basic protein
MEM	Minimum Essential Medium
MHC	Major histocompatibility complex
MLN	Mesenteric lymph nodes
MOG	Myelin oligodendrocyte glycoprotein
MS	Multiple Sclerosis
NFAT	Nuclear factor of activated T-cells
OSE	Opticospinal EAE
OT	Ovalbumin-specific TCR transgenic
OTU	Operational taxonomic units
PBS	Phosphate-buffered saline
PCR	Polymerase chain reaction

List of Abbreviations

PE	Phycoerythrin
PEG	Polyethylene glycol
PLP	Proteolipid protein
PP	Peyer's patches
PPMS	Primary progressive multiple sclerosis
PRR	pattern recognition receptors
PTX	Pertussis toxin
PURO	Puromycin
qPCR	Quantitative PCR
RA	Rheumatoid arthritis
rDNA	Ribosomal DNA
RBC	Red blood cell
rMOG	Recombinant MOG
RNA	RNA Ribonucleic acid
RPMI	Roswell Park Memorial Institute
RR	Relapsing remitting
RRMS	Relapsing remitting multiple sclerosis
sEAE	Spontaneous EAE
SFB	Segmented filamentous bacteria
slgA	Secretory IgA
SiLP	Small intestinal lamina propria
SLE	Systemic Lupus Erythematosus
SPF	Specific pathogen-free
SOCE	store-operated Ca ²⁺ entry
SPL	Spleen
SPMS	Secondary progressive multiple sclerosis
TAE	Tris-acetate
TCR	Specific T-cell receptor
TH	IgH MOG

List of Abbreviations

TLR	Toll-like receptors
TMB	3,3',5,5'-tetramethylbenzidine substrate
TNF	Tumor necrosis factor
TRE	Transcriptional response elements
Treg	Regulatory T cell
Tris	Tris(hydroxymethyl)aminomethane

Introduction

1.1 Multiple Sclerosis

Multiple sclerosis (MS) is a chronic autoimmune, inflammatory, demyelinating, and neurodegenerative disease of the central nervous system (CNS) that has a prevalence of around 2.3 million people worldwide with the highest prevalence observed in North America and Europe (Atlas of MS, 2013). MS patients are typically young adults exhibiting an onset between the ages of 20 and 40 years (Ransohoff et al. 2015). This disease has been reported to have a higher prevalence in women (Greer and McCombe 2011; Harbo et al. 2013). However, there have also been reports of patients experiencing their initial demyelinating event during childhood or adolescence (Yeshokumar et al. 2017).

Within MS, four clinical courses have been extensively described by the National Multiple Sclerosis Society Advisory Committee on Clinical Trials (Lublin and Reingold 1996): relapsing remitting MS (RRMS), secondary progressive MS (SPMS), primary progressive MS (PPMS) and progressive relapsing MS (PRMS). However, in 2012, due to the increased knowledge base of MS pathology, the Committee revised this classification and added the clinically isolated syndrome (CIS) course, which is defined as the first episode of inflammatory demyelination observed in the CNS that could progress into MS (Lublin et al. 2014). These patterns of disease evolution are known to share a common pathophysiology but each of them differs in symptom severity, expanded disability status scale (EDSS) score and CNS lesion morphology based on their clinical assessment. Initial phases of the disease are characterized by the presence of reversible episodes of neurological deficits (known as relapses). These relapses usually last days or weeks and are observed often in CIS and RRMS. (Brownlee et al. 2017; McDonald 2000). Over time, the reversible episodes develop a more permanent nature and the progression of the clinical disability become apparent, leading to SPMS (Lublin and Reingold 1996). On the other hand, only a minority of patients develops a progressive disease course from onset and these patients are classified as PPMS. PRMS is rare form of MS that is characterized by being progressive from the onset of the disease. PRMS exhibit acute relapses that can either fully regress or not, with periods of continuing progression between relapses.

The clinical manifestations of MS are heterogeneous and correlate to the location of active lesions within the nervous system. These lesions, or focal plaques, are characterized by areas of focal demyelination and are typically present along the CNS, including the brain, optic nerve, and spinal cord.

These lesions constitute the pathological hallmark of all MS phenotypes and typically found around post-capillary venules.

1.1.1 Pathogenesis

Although the pathogenic mechanisms behind MS development are still largely unknown, experimental, and clinical studies identify the immune system as the main protagonist behind the MS onset. It has been reported that both T cell and B cell-dependent mechanisms are involved.

A role for B cells in the development of MS relapses has been confirmed based on results stemming from selective B cell-targeting therapies, such as anti- CD20 antibodies (Hauser et al. 2017). On the other hand, based on both human and animal studies, it has been proposed that relapses are mainly mediated by abnormally activated (known as autoreactive) and/or inadequately regulated pro-inflammatory CNS-specific effector T cells, which include CD4⁺ T cells and CD8⁺ T cells. These cells are reported to traffic from the periphery into the CNS parenchyma where they cause local perivascular demyelination, glial cell activation and neuroaxonal injury (Baecher-Allan et al. 2018; Dendrou et al. 2015).

When investigating the pathogenesis of MS, the most commonly pro-inflammatory effector cells implicated are CD4⁺ T cells that express IL-17 (known as T helper 17 cells, or Th17 cells) and CD8⁺ T cells. These cells are observed to increase in number in the periphery and in the CNS of patients with MS. Furthermore, these cells are thought to contribute to direct injury of oligodendrocytes and neurons. However, the mechanisms used by these cells to cause direct injury to CNS-derived tissues are yet to be defined. In addition, Th17 CD4⁺ cells and CD8⁺ T cells are proposed to cause tissue injury indirectly through the activation of other cells, such as macrophages (Huber et al. 2013; Kebir et al. 2009; Kebir et al. 2007; van Langelaar et al. 2018).

It has been theorized that autoreactive T cells are capable of gaining access to their target organ and initiate a stream of pro-inflammatory events that lead to the recruitment of other relevant immune cell types, such as monocytes and B cells, only after a specific triggering event has occurred in peripheral organs. Additionally, leukocyte infiltration has been reported in both the grey and white matter in chronic and pre-symptomatic MS lesions (Ciccarelli et al. 2014).

1.1.2 Etiology

Although the etiology of MS is not clear, this disease is considered to be the result of a complex interplay of various risk factors that include genetic, environmental, viral infections through molecular mimicry (Haahr et al. 2004; Serafini et al. 2007) and most recently, the involvement of the gut microflora (Berer and Krishnamoorthy 2014; Berer et al. 2011; Burgueño and Abreu 2020; Kamada et al. 2013; Karmarkar and Rock 2013; Lee et al. 2011). Despite the fact that MS is not regarded as a hereditary disease, it has been observed that the prevalence of familial MS is roughly 13% for all MS phenotypes (Harirchian et al. 2018). The risk of MS development in age-adjusted monozygotic twins is 35%, as compared with 6% in dizygotic twins and 3% in siblings (Compston and Coles 2002). The main genetic risk factor known to-date is the major histocompatibility complex class II (MHC Class II), as there is a solid and constant association between MS and HLA DRB1*1501, DQA1*0102, and DQB1*0602 extended haplotype (Dyment et al. 2004).

The effect of environmental factors in MS development has been predominantly observed when analyzing the worldwide global distribution of the disease. In agreement with several reports, an increased risk of developing MS in countries located in higher geographic latitude have led to the conclusion that there is an existing correlation between MS and low sunlight exposure, as well as vitamin D deficiency (Handel et al. 2010; Marrie 2004).

In addition, due to the immune-mediated pathogenesis of MS, previous infectious diseases have been suggested as possible triggers that could contribute to the onset of MS. Of the various pathogens investigated, the Epstein–Barr virus (EBV) is the most consistently and robustly associated with this disease (Endriz et al. 2017; Olsson et al. 2017). The reason for this is that up to 100% of patients with MS are seropositive for EBV. Although, the process by which EBV infection increases the risk of MS is not clear, a molecular mimicry mechanism leading to the generation of cross-reactive T cells and antibodies has been proposed (Endriz et al. 2017; Olsson et al. 2017).

Finally, the intestinal microbiota has recently emerged as an additional potential triggering factor for MS (Berer and Krishnamoorthy 2014; Wekerle et al. 2013). In a recent revolutionary study, the transplant of fecal samples from selected twin pairs discordant for MS into a transgenic mouse model for spontaneous MS voided of its own microflora (germ-free mice) reported a significantly higher incidence of autoimmunity in mice that received MS twin-derived microbiota compared to mice that received the healthy twin-derived microbiota (Berer et al. 2017).

1.2 Experimental Autoimmune Encephalomyelitis

1.2.1 Induced EAE Murine Models

A multifaceted interplay between different immune cell types that lead to demyelination and remyelination in the CNS during the course of MS has been unraveled using animal models. These animal models do not only aid scientists in understanding the elusive pathology of the MS onset but also help in identifying new therapeutic approaches for MS treatment.

To date, experimental autoimmune encephalomyelitis (EAE), originally designated experimental allergic encephalitis, is a widely-accepted, standardized model for demyelinating diseases such as MS (Handel et al. 2011). In this model, the most usual way to induce EAE is through active immunization (known as actively-induced EAE or aEAE) with myelin proteins or peptides that are emulsified with an equal volume of complete Freund's adjuvant (CFA) containing *Mycobacterium tuberculosis* to create an antigen depot. Boosts with pertussis toxin are subsequently administered intraperitoneally on day 0 and day 2-post immunization in order to help in opening the blood–brain barrier (BBB), an event that allows immune cell infiltration into the CNS (Stromnes and Goverman 2006). Upon immunization, animals are controlled daily for weight and clinical signs of EAE, which are usually graded on a scale of 0 to 5, being score 0 normal and score 5 moribund.

In this model, the type of the disease course and pathology that results from the active induction are dependent on the mouse strain and the antigen used for immunization. For instance, aEAE of C57BL/6 mice with MOG₃₅₋₅₅ in CFA can induce a monophasic form of EAE (Lassmann 2007); whereas active immunization of SJL/J mice with PLP₁₃₉₋₁₅₁ leads to a relapsing-remitting disease that features epitope spreading (Vanderlugt et al. 2000). Myelin basic protein (MBP), myelin oligodendrocyte glycoprotein (MOG) and proteolipid protein (PLP) are the most frequently used antigens.

1.2.2 Spontaneous EAE Murine Models

aEAE is a method that has been proven extremely helpful when assessing immune cell infiltration and demyelination events after active immunization with CNS tissue or myelin peptides emulsified in CFA. As described above, this method is also a very versatile tool that allows the study of different EAE courses that result from the combination of mice strain and myelin antigens used for immunization.

However, the method has several limitations and is often not enough to investigate the highly dynamic nature of pathogenic immune cells across the different stages of activation, trafficking, recruitment, and infiltration of the CNS during the course of EAE. For instance, the CFA inoculation together myelin peptides in aEAE creates an exceedingly artificial environment for activation of autoreactive T cells that is not appropriate for investigating very early activation events that contribute to the natural development of disease. In addition, most mouse strains, including the C57BL/6 mice, develop a monophasic disease course that shows no relapses. Therefore, translating observations of aEAE studies into the human disease is very challenging as aEAE poorly reflects the disease course observed in the human disease.

The need for a tool that allows the study of EAE in a more natural way led to the development of the spontaneous models. One of these spontaneous models of EAE (sEAE) is the “opticospinal EAE” (OSE) mouse. This double-transgenic mouse was generated by crossing the 2D2 mice (Bettelli et al. 2003), with the Th (IgH^{MOG}) mice (Litzenburger et al. 1998). The resulting mouse line is characterized by having T cells that carry TCR specific for MOG₃₅₋₅₅ and B cells with a BCR that carries a rearranged heavy chain of a MOG-specific antibody. In this mice model, MOG-specific T cells and B cells simultaneously cooperate to develop spontaneous a chronic opticospinal EAE at around four to eight weeks of age, and shows a disease incidence of 60% (Krishnamoorthy et al. 2006). Another spontaneous model often used for the study of EAE is the “relapsing remitting” (RR) mouse. In this model, the mice are single transgenic in SJL background, and their T cells carry a TCR that recognizes MOG₉₂₋₁₀₆ peptide. What makes this model special is that transgenic T cells are reported to recruit MOG-specific B cells from the endogenous repertoire in order for EAE to develop. This combination of events leads to mice to develop a relapsing-remitting EAE at around two months of age, and show a disease incidence of 80% (Pollinger et al. 2009).

The abovementioned spontaneous EAE models feature a cooperation between T and B cells that play an important role in the onset of the disease without external manipulation. Both spontaneous models provide scientists with a powerful tool to help elucidating the triggering factors that determine the outbreak and course of human MS.

1.3 Innate Triggers of the Nervous System Autoimmunity

1.3.1 The host-microbial crosstalk

The human body, primarily the skin and mucosal surfaces, is populated by a wide range of microbial species (known as microbiota or microflora) (Peterson et al. 2009; Scher and Abramson 2011). From all other parts of the body, the oral-intestinal track has the maximum diversity and density of microbiota in the human body (Rodriguez et al. 2015; Scher and Abramson 2011). Most of these microorganisms are found in the distal intestine. It is now widely recognized that there is a bidirectional communication between the local gut microbiota and the host immune system. It is known that the intestinal microbiota plays an important role in influencing the development of host immunity and, in turn, the immune system also regulates the local gut microbiota through intestinal barrier maintenance and immune exclusion (Kamada et al. 2013). These interactions, often referred as host-microbial crosstalk, are homeostatic, tightly controlled, organized by both innate and adaptive immune responses and essential for triggering tolerant responses from the host required to produce healthy immune responses (Round et al. 2010).

Several studies performed in germ-free (GF) mice have led to the discovery of the important role that the gut microbiota plays in shaping the gut-associated lymphoid tissues (GALT). For instance, GF mice have been reported to have a significant reduction in the number and size of Peyer's patches (PPs) and mesenteric lymph nodes (MLNs) when compared to mice with normal commensal microbiota or to recolonized mice with conventional flora (Falk et al. 1998; Pollard and Sharon 1970). Furthermore, the gut microbiota has been reported to provide necessary polarizing signals to maintain a steady Th17 CD4⁺ T cells and regulatory T (Tregs) cell population, as it has been observed that GF mice have low numbers of Th17 CD4⁺ T cells when compared to control mice (Atarashi et al. 2008; Lochner et al. 2011). In addition, some specific commensal bacteria, such as *Bacteroides fragilis* and some strains of *Clostridia*, have been identified as key players in the differentiation of certain Tregs subsets (Atarashi et al. 2011; Mazmanian et al. 2008). Likewise, the presence of Th17 cells in gut tissues has been confirmed to promote the activation of intestinal epithelial defense mechanisms (Liang et al. 2006), suggesting a crucial role for these cells in maintaining the local mucosal homeostasis.

When the symbiotic relationship between the host and microbiota is disturbed, the gut microbiota can consequently contribute to disease development (Honda and Littman 2012; Littman and Pamer 2011). For instance, changes in the gut microbiota and its subsequent effect in the local immune system have been linked to extra-intestinal diseases such as type 1 diabetes, rheumatoid arthritis (RA), allergic airway

inflammation and MS (Berer et al. 2011; Hill et al. 2012; Mazmanian et al. 2008; Wen et al. 2008; Wu et al. 2010).

1.3.2 MyD88: a modulator in the host-microbial control

The gut immunological homeostasis is maintained by the interaction between the gut microbiota and the host immunity. The gut homeostasis is greatly dependent on the healthy state of the intestinal epithelium, as this layer of cells acts as the primary physical barrier between the vast enteric microbial community and internal host tissues. The interplay between the microflora and the intestinal epithelial cells (IECs) is greatly influenced by the events following the recognition of microbial products. Microbial products, widely termed pathogen-associated molecular patterns (PAMPs), are recognized by the host through the pattern recognition receptors (PRRs). PRRs are group of germ line-encoded receptors that are highly conserved throughout several species that include the Toll-like receptors (TLRs). Each TLR recognizes a different PAMP and all identified TLRs utilize the MyD88-dependent signaling pathway, except for TLR3, which uses the MyD88-independent TRIF pathway. This makes MyD88 a critical adaptor protein in innate immunity signal transduction that is common for all TLRs except for TLR3. Intrinsic MyD88-dependent signals in cells from innate immune cells, such as DCs, are thought to be pivotal for the induction of appropriate immune responses. Upon PAMP recognition, DCs go through a process of maturation in which the expression of MHC Class II and co-stimulatory molecules such as CD40 and B7 is upregulated. Such changes in the expression of these surface molecules and the release of pro-inflammatory cytokines not only regulate the activation of other innate cells but also has an important effect in the resulting adaptive immune response by determining T-cell polarization as well as humoral immunity via integration of activating signals (Akira and Takeda 2004; Merad et al. 2013).

In the gut, PRR activity leads to the expression of gene products that enhance the epithelial barrier function and promote innate immunity. Among these PRRs, the TLR family has been identified as major players in the development of several autoimmune diseases, such as Inflammatory Bowel Disease (IBD) (Morgan et al. 2014; Depaolo et al. 2008), SLE (Komatsuda et al. 2008; Pan et al. 2010), RA (Sorensen et al. 2008; Iwahashi et al. 2004) and ultimately MS (Derkow et al. 2013; Zekki et al. 2002). TLR signaling in gut tissues requires to be tightly regulated; as physiological TLR signaling favors intestinal homeostasis activities in healthy individuals but, excessive TLR signaling in response to invasive microbes rather aggravate local intestinal inflammation (Cario 2010).

MyD88-mediated signaling in IECs has been proven to be crucial for the maintenance of gut homeostasis as targeted deletion of MyD88 in IEC leads to a decreased production of Muc-2, antimicrobial peptides (AMP) RegIII γ , Defa-rs1, secretory IgA (sIgA), and decreases the activation of genes that codify tight junction proteins (Frantz et al. 2012; Guo et al. 2015). Additionally, it has been reported that deletion of MyD88 in IECs did not only reduce the expression of the RegIII γ in the small intestine at the terminal ileum but this reduction of RegIII γ promoted the bacteria colonization of small intestinal surfaces (Vaishnava et al. 2008). In addition, translocation of the gut-resident opportunistic pathogen *K. pneumoniae* and the commensal bacteria *E. coli* to mesenteric lymph nodes (MLN) in MyD88-deficient mice remarks an important role of MyD88 in keeping the integrity and permeability of the intestinal wall (Frantz et al. 2012; Fukata et al. 2005; Nighot et al. 2017).

Altogether, stimulation of the TLR on intestinal epithelial cells through PAMPs initiate a cascade of downstream events that orchestrate a coordinated response to limit bacterial invasion of the underlying tissue. These events include the induction of class-switch recombination of local IgM and IgA1 in order to generate and secrete IgA2 into the intestinal lumen; promote epithelial cell movement in order to favor epithelial cell-wall damage repair; and the release of antimicrobial peptides into the intestinal lumen to aid in the segregation of the microbiota from host tissues (Figure 1.3.2.1).

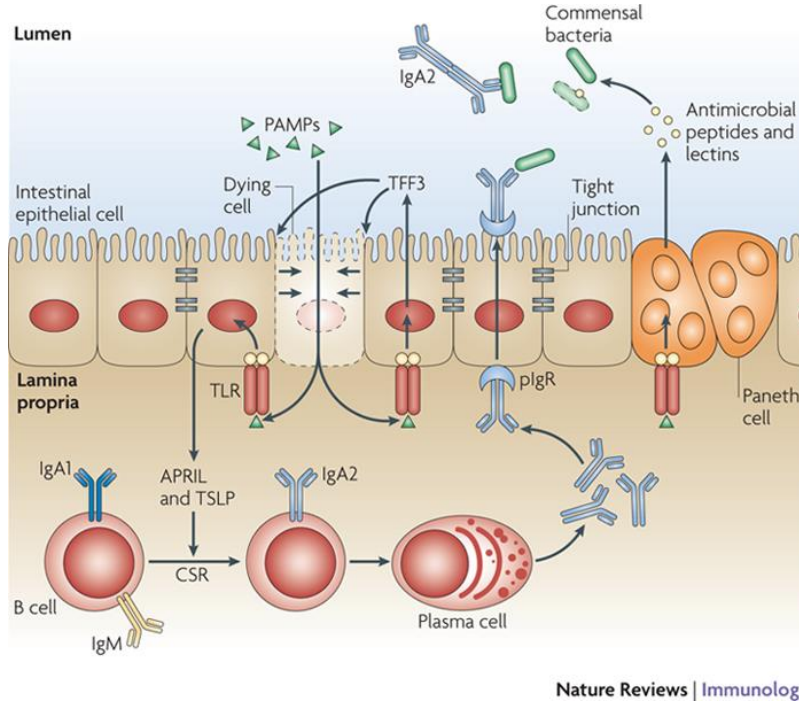


Figure 1.3.2.1. The role of the Toll-like receptor pathway in the Intestinal homeostasis.

Upon stimulation of Toll-like receptors on enterocytes, the expression of a proliferation-inducing ligand (APRIL) and thymic stromal lymphopoietin (TSLP) is induced. Both molecules are known to contribute to class switch recombination (CSR) of IgM antibodies and the conversion of IgA1 into protease-resistant IgA2. In gut tissues, IgA2 antibody is known to bind bacteria at the apical surface of intestinal epithelial cells in order to prevent bacterial invasion into the lamina propria. In addition, activation of TLR-2 in these tissues stimulates the production of trefoil factor 3 (TFF3). This event promotes the movement of cells from the epithelial monolayer of the intestine to repair gaps caused through invading bacteria. Paneth cells also respond to TLR stimulation by inducing the production of antimicrobial peptides (AMP) and lectins, for instance α -defensins and REG3 γ . (License number: 5112910140973. Adapted from (Abreu 2010b).

1.3.3 MyD88, the microbiota and gut immune compartment in CNS autoimmunity

A connection between the commensal gut microbiota and CNS autoimmunity became clear upon findings from Berer et al., that show that germ-free RR mice remain protected from EAE development throughout their lives until they are recolonized with conventional flora from SPF mice (Berer et al. 2011). Upon re-colonization, previously healthy GF RR mice promptly developed EAE, indicating that the gut microbiota is capable of quickly priming and maturing the immune system strongly enough to unchain a complex autoimmune reaction. The characterization of their cytokine profiling revealed a significant deficit in the frequency of Th17 cells in the lamina propria and in Peyer's patches of GF RR mice, suggesting a possible activation of MOG-specific T cells in the GALT (Berer et al., 2011).

As the gut microbiota harbors many ligands that are sensed by the immune system, there is a possibility that one, or more, of these ligands (microbial products) could provide autoreactive T cells with the necessary signals to contribute to CNS autoimmunity. It is known that microbial products play a relevant role in the development of EAE as the microbial products from the heat-killed *Mycobacterium tuberculosis* that are administered together with CFA are essential for the induction of EAE. Furthermore, since signals stemming from competent APCs are an important requirement for proper T cell priming in the context of autoimmunity, the relationship between MyD88-dependent pathways and EAE development has been explored. For instance, studies in MyD88 full knock-out mice revealed that these mice are able to resist EAE induction after immunization with MOG emulsified in CFA due to defects in the production of IL-6 and IL-23 by dendritic cells (Marta et al. 2008; Prinz et al. 2006). This deficiency was discovered to impair the priming of Th1 and Th17 responses that are known to drive the CNS autoimmunity in active EAE. Additionally, both studies demonstrated that TLR4 and TLR9 regulate severity in MOG-induced EAE.

In addition to activating innate immune cells, as described in the previous section, intrinsic TLR signaling within cells from the adaptive immune system can affect cell proliferation and differentiation; therefore, contributing to CNS autoimmunity. For instance, T cell expression of TLR2 regulates Th17 cell responses and a loss of TLR2 in CD4⁺ T cells ameliorated EAE (Reynolds et al. 2010). Similarly, TLR4 expression in CD4⁺ T cells is required for EAE development as the loss of TLR4 exclusively on CD4⁺ T cells almost completely abrogated disease symptoms (Reynolds et al. 2012). Furthermore, Tregs were found to exhibit higher expression levels of TLR2 in blood from MS patients when compared to those Tregs isolated from healthy controls (Nyirenda et al. 2015). Although these aforementioned studies nicely

illustrate a variety of effects that MyD88-dependent pathways exert in the development of EAE, the TLR-dependent signals within non-immune cells in the context of EAE has been rarely addressed.

TLRs expression is not only limited to cells of the immune system, but they can also be found in other cell types, such as fibroblasts and endothelial cells. As mentioned above, TLR-dependent signals within intestinal epithelial cells greatly contribute to the host-microbiota crosstalk. Expression of TLRs in these cells is essential to maintaining a healthy epithelial barrier that aids in spatially segregating gut microbiota and the host immune system to avoid unnecessary immune responses to gut microbes that lead to intestinal inflammation. Changes in the dynamic of the host-microbiota interactions are thought to expose the immune system to the local gut microbiota and such exposure is believed to contribute to the development of several autoimmune diseases. Evidence of the presence of microbial components outside gut tissues were reported in studies performed using brain tissue samples from MS and from non-human primate EAE models that revealed a high number of PGN-containing dendritic cells and macrophages with an enhanced expression of co-stimulatory molecules (Schrijver et al. 2001; Visser et al. 2006). Therefore, it is possible that TLR ligands derived from commensal bacteria or PGN play an important role in CNS autoimmunity, however, direct evidence is still lacking. Finally, the involvement of MyD88 in gut-derived tissues in the context of EAE are poorly understood, if not, yet to be described.

1.4 Activation of T lymphocytes

1.4.1 Calcium influx as an early marker for T lymphocyte activation

Calcium signaling is of vital importance to a wide array of immune responses. A controlled increase in cytosolic and organellar calcium concentrations in lymphocytes regulate complex and crucial effector functions such as metabolism, proliferation, differentiation, cytotoxicity, as well as antibody and cytokine secretion. In resting T lymphocytes cytosolic calcium concentration is known to maintained at a low concentration (between 50-100 nM) and engagement of their TCR with cognate antigen causes an increase in Ca^{2+} to about 1 μM (Joseph et al. 2014).

In order to become activated, a naïve T cell must become in contact with an APC carrying an antigen on its surface. The contact between these two cells leads to the formation of the immunological synapse at the T cell-APC contact site. This immunological synapse is a highly organized structure that involves the synchronized engagement of both the TCR and co-stimulatory molecules on the T cell side with the peptide conjugated to MHC complexes and co-stimulatory molecules on the APC side. Protein tyrosine kinases ZAP70 and LCK become activated upon antigen recognition by T cells and this activation led to the phosphorylation of adapter proteins LAT and SLP76 (Figure 1.4.1.1). This process allows the recruitment of the IL-2 inducible T cell kinase (ITK) and the activation of phospholipase C γ (PLC γ). In a similar manner, binding of G protein-coupled receptors activates of phospholipase C β (PLC β), both which in turn catalyzes the hydrolysis of phosphatidylinositol-4,5-bisphosphate (PtdIns(4,5)P₂) to produce second messengers inositol-1,4,5-trisphosphate (IP₃) and diacylglycerol (DAG) (Christo et al. 2015). IP₃ binds to its receptor in the endoplasmatic reticulum (ER) membrane thereby inducing the first release of calcium from the ER into the cytosol in a process known “store depletion”. (Feske 2007). The loss of calcium from the ER is sensed by the stromal interaction molecule 1 (STIM1), located in the ER membrane, through its EF-hand motifs and form oligomers via protein-protein interaction of SAM and ERM domains to form a discrete puncta. These STIM1 puncta interact directly with the pore-forming unit ORAI1 of CRAC channels present in the plasma membrane. ORAI1, which exists as a dimer in the plasma membrane, forms tetramers following STIM1 coupling and mediates the opening of the ORAI channels (Penna et al. 2008). Following the opening of ORAI channels, a continuous influx of extracellular calcium takes place, thereby promoting the binding of calcium to the four high affinity EF-hands of calmodulin (CaM). CaM binds and activates calcineurin (Cn), which in turn dephosphorylates the inactive nuclear factor of activated T cells (NFAT) transcription factor. The dephosphorylation of cytoplasmic NFAT results in the translocation of NFAT molecule into the nucleus and induces NFAT-

mediated gene transcription. However, as NFAT only weakly binds to the DNA, it must cooperate with other transcription factors to influence gene regulation efficiently (Macian 2005).

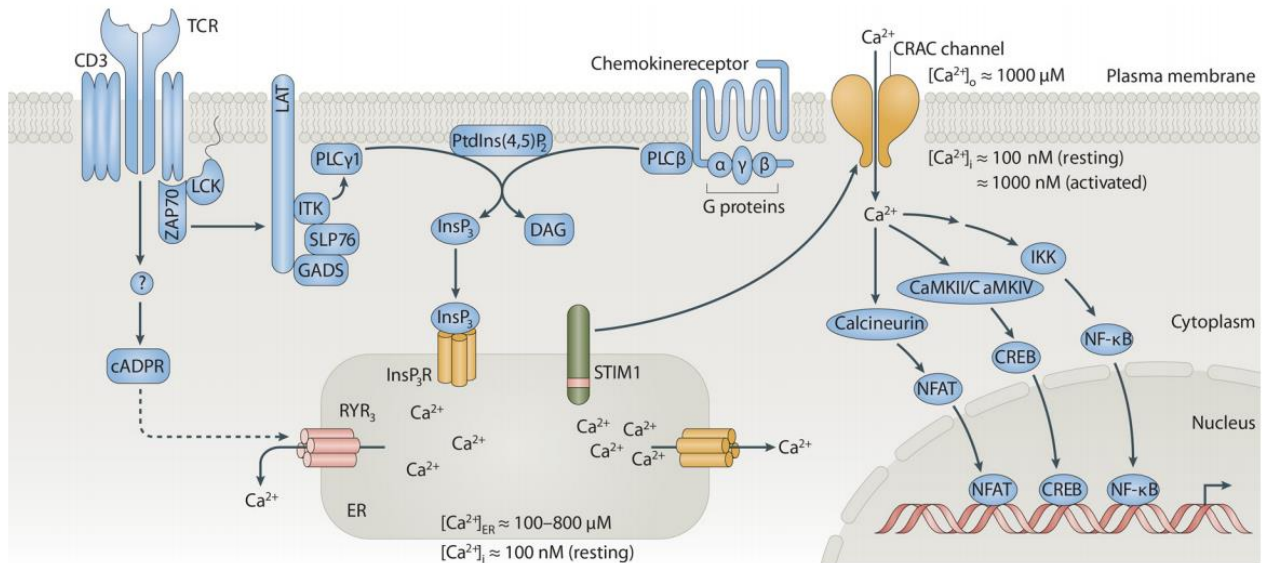


Figure 1.4.1.1. Scheme of the calcium-signaling cascade upon T cell activation.

Resting T cells are characterized by the presence of a sharp gradient in calcium concentrations between the cytoplasm and the extracellular space, as well as between the cytoplasm and the lumen of the ER. Typically, the intracellular calcium concentration in resting T cells oscillates around 100 nM. However, upon antigen recognition through the TCR of T cells, intracellular calcium concentration raises to around 1000 nM. This raise in calcium concentration leads to the activation of protein tyrosine kinases LCK and ZAP7. This event, in turn, leads to the phosphorylation of adaptor proteins SLP76 and LAT, which are then phosphorylated to recruit and activate ITK and PLC γ . Similarly, PLC β is activated through the binding of G protein-coupled chemokine receptors. Together, PLC β and PLC γ hydrolyze PtdIns(4,5)P₂ to IP₃ and DAG. Subsequently, IP₃ binds to and opens IP₃ receptors in the membrane of the ER, releasing calcium ions from the intracellular calcium stores. This decrease in calcium within the ER is sensed by STIM1, causing the activation of CRAC channels in the plasma membrane. The calcium influx through CRAC channels along with the elevated intracellular calcium concentration activates calcineurin. The dephosphorylation of calcineurin aids in the activation of transcription factors such as NFAT or NF- κ B through dephosphorylation events, allowing the translocation of these molecules into the nucleus to initiate transcription of target genes. (License number: 5112910981345. Adapted from Feske, 2007).

1.4.2 NFAT translocation as a visual marker of T cell activation

The NFAT transcription factors is a family of five proteins whose expression was initially to be thought to be only restricted to T cells. However, it was later discovered that the expression of NFAT proteins has not only been identified on T cells but also in non-immune cells, such as hepatocytes (Cai et al. 2021). A role for these proteins has been identified in several autoimmune diseases such as IBD and RA (Gerth et al. 2004; Sitara and Aliprantis 2010). The NFAT family consists of five members: NFAT1, NFAT2, NFAT3, NFAT4, and NFAT5, being NFAT1 and NFAT2 proteins the most-studied NFAT family members due to their high expression in T cells. From these NFAT five proteins, four of these proteins are regulated by calcium signaling.

As mentioned in the previous section, the activation of T cell leads to the dephosphorylation of NFAT by the phosphatase calcineurin enzyme. This process leads to the nuclear translocation of NFAT within minutes of its dephosphorylation and it initiates the transcription of NFAT-mediated genes. From the NFAT family, NFAT1 is commonly expressed in immune cells and is regulated by calcium signaling pathways (Fig. 1.4.1.1). The fast translocation of NFAT into the nucleus post T-cell activation has proven to be a useful quality of this protein in the investigation of T early translocation events. In her publication, Pesic and colleagues generated an activation sensor by removing the highly conserved DNA-binding domain of NFAT (Macian 2005). The resulting protein was then linked to a GFP-protein and labeled Δ NFAT-GFP. This GFP-truncated variant of NFAT-1 was used in experiments destined to visualize early T cell activation events within the spinal cord (Pesic et al. 2013). It has also been reported that the translocation of Δ NFAT-GFP into was observed in the nucleus of autoreactive T cells within the leptomeningeal area after interaction with perivascular phagocytes (Lodygin et al. 2013; Pesic et al. 2013). The observed signal was reported to occur within a few minutes after stimulation and it was concluded that it does not necessarily require a long-lasting contact. Finally, in this publication, it was also observed that T cells with nuclear NFAT have reduced motility and these T cells could make sequential contact with meningeal phagocytes.

An alternate method to visualize T cell activation is through the usage of NFAT transcriptional response elements that are placed upstream of EGFP (NFAT-TRE-sGFP) (Siewert et al. 2012). Upon NFAT translocation into the nucleus, the cell starts expressing GFP. This approach has the advantage that T cell activation can be analyzed simply through the expression of GFP. This was not possible for NFAT-GFP, which requires precise identification of signal in subcellular resolution. However, NFAT-TRE-sGFP has a time lag from T cell stimulation to GFP expression since GFP needs maturation time. Taking the

advantage of easy detection, we planned to use NFAT-TRE-sGFP sensor to detect T cell activation in this study.

Objectives

The gut microbiota has been the focus of study between several research groups that attempt to gain a deepened understanding of how these microorganisms influence the development of different autoimmune diseases. In the case of MS, studies performed on EAE models have identified the gut microbiota as a key player in the development and course of the disease, as the importance in the recolonization of these microorganisms in germ-free animals has shown to have a profound effect in EAE development. Despite of these findings, the exact mechanism on how the commensal gut microbiota contributes to EAE, and ultimately MS, development remains unclear.

One potential pathway that could aid in understanding the etiology of MS is by investigating the effect of the MyD88-dependent signaling pathway in EAE development. MyD88 is a key downstream adaptor molecule common to most Toll-like receptors (TLRs), a type of pattern-recognition receptors (PRRs) responsible for sensing bacteria that is not only expressed in immune cells but also on IECs. In the gut, TLRs form part of the first line of defense against invading-microorganism. Therefore, we attempt to investigate whether the MyD88-dependent pathway contributes to EAE development based on the involvement of the gut microbiota in EAE development.

Therefore, in an attempt to answer this question, the primary aim of the present study is to unravel the mechanism used by the commensal gut microbiota in influencing the etiology of EAE. This was attempted through cytokine profiling and evaluation of EAE development in conditional knock-out mice that lack MyD88 in relevant immune cells, such as such as CD4⁺ T cells, CD19⁺ B cells and in IECs from the intestinal epithelium. In addition, these conditional knock-out mice are crossbred with OSE mice, so they are subsequently evaluated for their development and severity of spontaneous EAE. To complement these experiments, the bacterial composition of tissue-specific MyD88 knock-out mice is evaluated through sequencing of their 16S rRNA of their stool and gut contents, to identify a potential dysbiosis of commensal microbes that could contribute to the potential altered cytokine profiling in mice suffering from EAE.

Lastly, molecular mimicry is a mechanism that tries to explain how autoreactive T cells could be activated and trigger MS pathogenesis. Several reports have linked infection with CMV and EBV to MS. We speculate whether the gut microbiota could also activate autoreactive T cells in the gut and initiate EAE pathogenesis. Therefore, an important aim of this study is to discover the commensal gut bacteria that are responsible for causing the activation of autoreactive T cells, key players in initiating EAE. To

this end, we attempt to establish an in-vivo and in-vitro screening assay using T-cell hybridomas to be able to identify potential microbial particles that could trigger the early events of MS.

2. Materials and Methods

2.1 Materials

2.1.1 Mice

Animals used for this study were bred and housed in animal facilities of the Max Planck Institutes of Biochemistry and Neurobiology. All animal procedures were conducted by following the guidelines provided by the committee on animals of the Max Planck Institute for Neurobiology and with the license of the respective German authorities (Regierung von Oberbayern).

Transgenic Mouse Lines (C57BL/6 background)

- **MyD88^{loxP/loxP} (Kleinridders et al., 2009)**

Transgenic mouse that contains a loxP sites on both side of exons 3-5 of the MyD88 gene. When bred to any mice that express a Cre recombinase the resulting offspring will have exons 3-5 deleted in the tissue that expresses the cre-recombinase.

- **MyD88KO**

Transgenic knockout mouse with a global deletion of MyD88 adaptor molecule. To generate these mice, the B6.C-Tg(CMV-cre)1Cgn/J mouse, in which a deletion of loxP-flanked genes occurs in all tissues due to the expression of Cre recombinase under the control of a CMV promoter, was bred with MyD88^{loxP/loxP} mice. The resulting mice were heterozygous for MyD88 gene expression (MyD88^{loxP/-}) and MyD88^{loxP/-} mice were intercrossed to obtain MyD88^{-/-} mice.

- **MyD88^{loxP/loxP} x villin-cre (Kleinridders et al., 2009, el Marjou et al., 2004)**

Tissue-specific knockout mouse with a targeted deletion of the MyD88 gene in epithelial cells of small and large intestines. To generate these mice, the B6.SJL-Tg(Vil-cre)997Gum/J strain, which is a transgenic mouse carrying a Cre recombinase under control of the intestinal epithelial-specific mouse Vil1 gene, was intercrossed with MyD88^{loxP/loxP} mice.

- **MyD88^{loxp/loxp} x CD4-cre (Lee et al., 2001)**

Tissue-specific knockout mouse with a targeted deletion of the MyD88 gene in CD4⁺ T cells. To generate this mice, the B6.Cg-Tg(Cd4-cre)1Cwi/BfluJ strain was intercrossed with MyD88^{loxp/loxp} mice. The B6.Cg-Tg(Cd4-cre)1Cwi/BfluJ mice is a transgenic line containing a CD4 enhancer, promoter and silencer sequences that drive the expression of a Cre-recombinase gene.

- **MyD88^{loxp/loxp} x CD19-cre (Rickert et al. 1997)**

Tissue-specific knockout mouse with a targeted deletion of the MyD88 gene in CD19⁺ B cells. To generate this mice, B6.129P2(C)-Cd19^{tm1(cre)Cgn}/J mice were intercrossed with MyD88^{loxp/loxp} mice. The B6.129P2(C)-Cd19^{tm1(cre)Cgn}/J mice is a transgenic line where the Cd19 promoter directs specific cre expression during both the earliest stages and throughout B-lymphocyte development and differentiation..

- **OT-II (Barnden et al., 1998)**

Ovalbumin-specific TCR transgenic mouse, where CD4⁺ T cells express a transgenic TCR recognizing OVA₃₂₃₋₃₃₉ peptide in the context of I-A^b.

- **2D2 (Bettelli et al., 2003)**

MOG-specific TCR transgenic mouse, where CD4⁺ T cells express a transgenic TCR that recognizes MOG₃₅₋₅₅ peptide in the context of I-A^b.

- **Th (Litzenburger et al., 1998)**

MOG-specific B-Cell receptor (BCR) knock-in mouse, where B cells express a rearranged Ig heavy chain of a MOG-specific antibody.

- **Actin-eGFP (Okabe et al., 1997)**

Transgenic mouse line with an "enhanced" GFP (EGFP) cDNA under the control of a chicken beta-actin promoter. This strain also features a cytomegalovirus enhancer that makes all tissues, apart from erythrocytes and hair, to appear green under light excitation.

2.1.2 Cell Lines

Cell line	Description	Reference
3T3	Mouse embryonic fibroblasts	ATCC® CRL-1658™
BW5147	Mouse lymphoma	ATCC® TIB-48™
HEK293T	Human embryonic kidney	ATCC® CRL-3216™
Phoenix eco	Retrovirus producer line based on HEK293 cells for the generation of helper free ecotropic retroviruses.	ATCC® CRL-3214

2.1.3 Buffers and Solutions

Phosphate Buffered Saline (PBS)

10 mM Na₂HPO₄, 1.8 mM KH₂PO₄, 140 mM NaCl, 2.7 mM KCl, pH 7.2.

Erythrocyte Lysis Buffer

0.83 % NH₄Cl

ACK buffer

150 mM NH₄Cl, 10 mM KHCO₃, 0.1 mM EDTA

Percoll Solutions (GE Healthcare)

- 100 % Stock Percoll: 9 parts (v/v) Percoll + 1 part (v/v) of 10x PBS.
- 80 % Percoll: 8 parts (v/v) 100 % Percoll + 2 parts (v/v) RPMI 1640.
- 40 % Percoll: 4 parts (v/v) 100 % Percoll + 6 parts (v/v) RPMI 1640.

Mouse Tail Lysis Buffer

100 mM Tris-HCl pH8, 5 mM EDTA, 0.5 % Tween20, 120 mM NaCl, 1 mg/mL Proteinase K

Cell Culture Media

RPMI 1640 or DMEM (Sigma-Aldrich) media were prepared by adding with 100 μM MEM non-essential amino acids, 1 mM sodium pyruvate, 50,000 units penicillin, 50 mg streptomycin, 2 mM L-glutamine (all

Gibco™) and 10 % or 20 % heat-inactivated fetal bovine serum (FBS) (Biochrom GmbH), 200 µM β-Mercaptoethanol. Prior to adding, FBS was inactivated for 30 minutes at 56°C. The medium was sterilized by filtration (pore size 0.2 µm) under a cell culture bench. Quantities listed are for the preparation of 500 mL of medium.

Trypan Blue Solution

3 mL of Trypan Blue Solution (Sigma-Aldrich) in 8 mL cell culture PBS. The solution was sterilized by filtration (pore size 0.2 µm) under a cell culture bench.

2x BES (pH 6.95)

50 mM N,N-bis(2-hydroxyethyl)-2-aminoethanesulfonic acid, 280 mM NaCl, 1.5 mM Na₂HPO₄

Flow Cytometry Buffers

- FACS staining Buffer: 1 % BSA, 0.1 % sodium azide in PBS.
- Foxp3 Fixation/Permeabilization Concentrate and Diluent (eBioscience).
- Permeabilization Buffer (10X) (eBioscience).

ELISA Buffers and Solutions

- 0.1 M Carbonate/Bicarbonate Buffer pH 9.5: 8.4 g NaHCO₃, 3.56 g Na₂CO₃ in 1 L deionized water, pH 9.5.
- ELISA Washing Buffer: 0.5 mL Tween-20 in 1 L of PBS.
- ELISA Blocking Solution: PBS complemented with 10 % FBS.
- ABTS Substrate Solution: 1 mM ABTS (Sigma-Aldrich) in 70 mM citrate-phosphate buffer, pH 4.2. Add 1 µl 30 % H₂O₂ solution per 1 mL ABTS prior ELISA development.
- 3,3',5,5'-Tetramethylbenzidine (TMB) High Sensitivity Substrate Solution (BioLegend).
- ELISA Stop Solution: 2N H₂SO₄.

Luria Bertani (LB) Medium

10 g tryptone (Sigma-Aldrich), 5 g yeast extract (Sigma-Aldrich), 10 g sodium chloride (Roth) in 1 L deionized water. 100 µg/mL ampicillin or 30 µg/mL kanamycin was added for selection.

LB Agar Selection Plates

LB Medium was prepared as above described and 15 g of agar was added to 1 L of medium. LB agar medium was poured into sterile bacterial petri dishes (Greiner Bio-One) after being autoclaved, let solidify and stored at 4°C until use.

Tris-acetate (TAE) Running Buffer

40 mM Tris-HCl, 1mM EDTA pH 8.0, 40 mM glacial acetic acid

DNA loading dye 10x

50 mM Tris-HCl, pH 7.6, 60 % glycerol, 0.05 % bromophenol blue, 0.05 % xylene cyanol FF

2.1.4 Antibodies

2.1.4.1 Flow Cytometry Antibodies

Antibodies are either directly labeled with eFluor® 450, FITC, PE, PerCP-Cy5.5, PE-Cy7, APC, APC-eFluor 780 or Alexa Fluor 647 fluorophores or are biotinylated and used in conjunction with streptavidin-coupled fluorophores.

Specificity	Clone	Antibody class	Dilution	Manufacturer
B220	RA3-6B2	Rat IgG2a, κ	1:200	BioLegend
CD3	145-2C11	Armenian Hamster IgG	1:200	BioLegend
CD4	RM4-5	Rat IgG2a, κ	1:200	BioLegend
CD11b	M1/70	Rat IgG2b, κ	1:200	BioLegend
CD11c	N418	Armenian Hamster IgG	1:200	eBioscience
CD25	PC61.5	Rat IgG1, λ	1:200	eBioscience
CD45	30-F11	Rat IgG2b, κ	1:200	eBioscience
CD69	H1.2F3	Armenian Hamster IgG1, λ3	1:200	BD Pharmingen™
CD80	16-10A1	Armenian Hamster IgG	1:200	eBioscience
Foxp3	FJK-16s	Rat IgG2a, κ	1:100	eBioscience
I-A	NIMR-4	Rat IgG2b	1:400	eBioscience
IFN-γ	XMG1.2	Rat IgG1, κ	1:100	eBioscience
IL-4	BVD6-24G2	Rat, IgG1, κ	1:100	eBioscience
IL-10	JES5-16E3	Rat IgG2b, κ	1:100	BioLegend
IL-17	TC11-18H10.1	Rat IgG1, κ	1:100	BioLegend
Ki67	B56	Mouse IgG1, κ		BD Pharmingen™
Ly6C	AL-21	Rat IgM, κ	1:200	BD Pharmingen™
Ly6G	1A8	Rat IgG2a, κ	1:200	BioLegend
TNFα	MP6-XT22	Rat IgG1, κ	1:100	BioLegend
Va2	B20.1	Rat IgG2a, λ	1:200	BD Pharmingen™
Va3.2	RR3-16	Rat IgG2b, κ	1:200	eBioscience
Vb5	MR9-4	Mouse IgG1, κ	1:200	BD Pharmingen™
Vb11	RR3-15	Rat IgG2b, κ	1:200	BD Pharmingen™
Streptavidin	-	-	1:1000	eBioscience

2.1.4.2 Purified Antibodies and Avidin

Specificity	Clone	Antibody class	Manufacturer
CD3	145-2C11	Armenian Hamster IgG1	BioXCell
CD28	PV-1	Armenian Hamster IgG	BioXCell
Avidin HRP	-	-	eBioscience

2.1.4.3 Antibodies for Enzyme-linked Immunosorbent Assay (ELISA)

Target	Capture Antibody	Detection Antibody (Biotinylated)	Standard	Manufacturer
IgM	Purified Rat anti-mouse IgM	rat anti-mouse IgM	Mouse IgM, κ	BD Pharmingen™
	Clone R35-72	Clone R35-118	Clone C38-2	
IgA	Purified Rat anti-mouse IgA	Rat anti-mouse IgA	Mouse IgA, κ	BD Pharmingen™
	Clone C10-3	Clone C10-1	Clone M18-254	
IgG	Mouse IgG total ELISA Ready-Set-Go!			eBioscience
IL2	Purified Rat Anti-Mouse IL-2	Rat Anti-Mouse IL-2	Recombinant mouse IL-2	BD Pharmingen™
	Clone JES6-1A12	Clone JES6-5H4		

2.1.5 Primers

2.1.5.1 Primers for Genotyping

Gene	Primer name	Oligo sequence (5' → 3')	DNA expected size
MyD88	Seq16	CAG TCT CAT CTT CCC CTC TGC C	Wildtype: 600 bp
	Seq19	GGG AAT GGC AGT CCT CTC CCA G	Flox gene: 700 bp
	MyD88R	GTC AGA AAC CAC CAT GC	Deletion: 400 bp
Vil1 internal positive control	Villin fwd	CAA GCC TGG CTC GAC GGC C	Wildtype: no band
	Cre-recombinase	GGT CGT GGC AGC CCG GAC	Transgenic: 326 bp
	oIMR 8744	CAA ATG TTG CTT GTC TGG TG	Control band: 206 bp
	oIMR 8745	GTC AGT CGA GTG CAC AGT TT	
V alpha 3.2 TCR	Va3.2-2D2-M	CCC GGG CAA GGC TCA GCC ATG CTC CTG	Wildtype: no band
	Ja18-2D2-M	GCG GCC GCA ATT CCC AGA GAC ATC CCT CC	Transgenic: 675 bp
CD4-cre internal control	AG-Cre 6	CCC AGA AAT GCC AGA TTA CG	Wildtype: no band
	AG-CD4 L6	CCC AAC CAA GAG CTC	Transgenic: ~550 bp
	oIMR 7338	CTA GGC CAC AGA ATT GAA AGA TCT	Control band 324 bp
	oIMR 7339	GTA GGC GGA AAT TCT AGC ATC C	
CD19-cre	CD19d (wt)	CCA GAC TAG ATA CAG ACC AG	Wildtype: 452 bp
	Cre7	TCA GCT ACA CCA GAG ACG G	Knock-in 700 bp
	CD19c (both)	AAC CAG TCA ACA CCC TTC C	

2.1.5.2 Primers for Real-Time quantitative PCR

Gene	Primer name	Oligo sequence (5' → 3')	Detection
Wild type IgH locus	Sense	ATT GGT CCC TGA CTC AAG AGA TG	ROX
	Anti-sense	TGG TGC TCC GCT TAG TCA AA	ROX
	Probe	CCT TGC ACC AGT CAG AGA CCA CAG GG	ROX
Knock-in IgH locus	Sense	TGA GGA CTC TGC CGT CTA TTA CTG T	ROX
	Anti-sense	GGA GAC TGT GAG AGT GGT GCC T	ROX
	Probe	CCA GTA TGG CAT GTT TAC CAT CGT ATT ACC	ROX
16S rRNA EUB	8F	AGA GTT TGA TCC TGG CTC AG	SYBR Green
16S rRNA EUB	338R	GCT GCC TCC CGT AGG AGT	SYBR Green
16S rDNA of SFB	SFB sense	GAC GCT GAG GCA TGA GAG CAT	SYBR Green
16S rDNA of SFB	SFB anti-sense	GAC GGC ACG GAT TGT TAT TCA	SYBR Green

2.1.5.3 Primers for Molecular Cloning

Target Sequence	Primer name	Oligo sequence (5' → 3')	Melting Temperature	Purpose
NFAT-TRE-sGFP	pCDNA6-NFAT sense #1	GCC AGA TCT CTG GAT CAG CCA TAT CAC ATT TGT A	54.9 °C	Insertion of BglII restriction site upstream of target sequence
	pCDNA6-NFAT anti sense #2	AAG GTC AGG AAC AGA TGG AAC	54.6 °C	Amplifies NFAT-TRE-sGFP

2.1.6 Plasmids

Name	Plasmid Type	References
pQCXIX	Retroviral	Clontech
pMSCV-puro-NFAT-GFP	Retroviral	Kyratsous, N., 2016
pMSCVneo-IRES2-GFP	Retroviral	Addgene
pQC-NFAT-TRE-sGFP	Retroviral	Described in this thesis
pCL-Eco	Retroviral	Mues, M., 2012
pcDNA6-NFAT-TRE-sGFP	Mammalian expression	Siewert et al., 2012.
pmaxGFP®	Mammalian expression	Lonza

2.1.7 Kits

Kit Name	Type	Manufacturer
X-fect	DNA Transfection Reagent	Clontech
TransIT 2020	Transfection Reagent	Mirus Bio LLC
Viromer® Yellow, Viromer® Red	mRNA and DNA Transfection Reagent	Lipocalix
Ecotropic Receptor Booster	Transduction booster	Clontech

2.2 Methods

2.2.1 Mouse Routine

2.2.1.1 Tail Genomic DNA Isolation and PCR Genotyping

Tail biopsies from mice were collected in a 1.5 mL Eppendorf tube. To isolate genomic DNA, biopsies were digested in 500 μ L tail lysis buffer overnight at 56°C degrees. DNA was isolated by phenol-chloroform extraction. In brief, 500 μ L phenol/chloroform/isoamylalcohol (Roth) was added to the overnight lysate, vortexed vigorously and centrifuged (13,000 r.p.m., 10 minutes, room temperature) to separate DNA from proteins. The aqueous phase was transferred into a new 1.5 mL Eppendorf tube and precipitated with 1 mL 100 % ethanol. After centrifugation (13,000 r.p.m., 10 minutes, 4°C), the DNA pellet was washed with 400 μ L 70 % ethanol and centrifuged at 13,000 r.p.m. at 4°C for 5 minutes. Finally, the pellet was resuspended in 300 μ L of 10 mM Tris.

Mice were genotyped by PCR using genomic DNA isolated from tail biopsies using the DreamTaq Green PCR Master Mix (2X) (Thermo Fisher Scientific) in combination with the transgene-specific primer set at a concentration of 10 μ M. For visualization of DNA bands, PCR amplicates were loaded together with the 1 kb DNA ladder (NEB) into a 2 % agarose gel containing 0.5 μ g/mL Ethidium Bromide (Roth) in TAE Buffer.

2.2.1.2 Leukocyte Isolation from Peripheral Blood

Anesthetized mice were bled by retro-orbital bleeding in order to collect 4-6 drops of blood into an Epi containing 100 μ L of 200 U/mL heparin (Sigma-Aldrich) dissolved in PBS. Erythrocytes were lysed by incubating the samples with 1 mL ACK buffer for 5 minutes in room temperature. Leukocytes were spun down at 500 rcf for 5 minutes at 4 °C. After repeating this last step once, the ACK incubation and spin down steps, leukocytes were finally resuspended in 150 μ L FACS buffer for further analysis.

2.2.1.3 Isolation of serum from total blood

Total blood was collected from anesthetized mice by retro-orbital bleeding into a 1.5 mL Eppendorf tube, careful avoiding red blood cells (RBCs) lysis. Blood samples were allowed to clot for one hour on ice and serum was separated into a new 1.5 mL Eppendorf tube after centrifuging samples (13,000 r.p.m., 20 minutes, 4°C). Isolated serum samples were stored at -20°C until use.

2.2.1.4 Mononuclear Leukocyte Isolation from Organs

Mice were euthanized via exposure to carbon dioxide (CO₂). Lymphoid organs, namely bone marrow, spleen, axillary, inguinal and mesenteric lymph nodes, as well as gut-associated tissues (GALT) (Peyer's patches, ileal and colonic lamina propria) were dissected and collected in complemented RPMI Medium.

Lymphoid organs

Single-cell suspensions were prepared from bone marrow, spleen, peripheral lymph nodes (axillary and inguinal), mesenteric lymph nodes and Peyer's patches through mechanical disruption by forcing the tissue through 40 µm cell strainers (Falcon). Spleen and bone marrow underwent RBCs lysis by resuspending and incubating cells in 0.83 % NH₄Cl for 3 min at room temperature. Cells were washed with RPMI, centrifuged (1200 r.p.m., 10 minutes, 4°C) and resuspended in complemented RPMI Medium.

Lamina propria lymphocytes (LPL)

For the isolation of lamina propria lymphocytes, small intestine and colon were collected in ice-cold HBSS (Gibco™) Medium complemented with 15 mM HEPES (Sigma-Aldrich). After collecting Peyer's patches and removing fatty tissue and fecal contents, the intestine was opened longitudinally and cut into small pieces. The resulted intestinal fragments were washed three times for 15 minutes with stirring (300 r.p.m.) in HBSS Medium containing 5 mM EDTA, 15 mM HEPES and 10 % FBS. Next, intestinal pieces were washed once for 5 minutes with stirring in RPMI Medium containing 15 mM HEPES and 10 % FBS. Afterwards, the clean intestinal pieces were incubated at 37 °C with stirring (500 r.p.m.) in RPMI Medium complemented 15 mM HEPES, 10 % FBS and 100 U/mL Collagenase D (Roche). The digested tissue was forced through a 100 µm cell strainer (Falcon) and washed twice in HBSS Medium containing 5 mM EDTA, 15 mM HEPES and 10 % FBS. Subsequently, the cell pellet was resuspended in 5 mL 40 % Percoll solution and was overlaid on 2.5 mL 80 % Percoll. The gradient was centrifuged at 2000 r.p.m., for 20 minutes at room temperature without breaks, and the interface containing the lamina propria lymphocytes, was collected into a 15 mL Falcon tube containing 10 mL complemented RPMI Medium. Finally, cells were centrifuged (1200 r.p.m., 10 minutes, 4°C) and resuspended in complemented RPMI Medium for further analysis.

2.2.1.5 Generation of bone marrow derived dendritic cells (BMDCs)

For the generation of BMDCs, wild-type C57BL/6 mice were euthanized and both femurs were dissected and collected in serum-free RPMI medium. Epiphyses of the femur were removed, and the bone marrow was flushed with cold serum-free RPMI medium. Next, the bone marrow was collected in a 50 mL tube (Falcon) and washed with serum-free RPMI medium by centrifugation (1200 r.p.m., 10 minutes, 4°C). Erythrocytes were lysed by incubation in 0.83 % NH₄Cl as previously described. Cell density was determined with Trypan blue solution. Cells were resuspended in complemented RPMI medium containing 1 mL of granulocyte-macrophage colony-stimulating factor (GM-CSF)-containing supernatant of hybridoma cell line (Karasuyama and Melchers 1988) and 2.5 x 10⁶ cells were plated per bacteriological petri dish (Greiner Bio-One). At day 3 and 6 of culture, medium was changed with complemented RPMI medium containing 2 mL of GM-CSF-containing hybridoma supernatant. Finally, on day 8 of culture, BMDCs were collected and frozen in freezing medium (10 % DMSO in FBS) at -80°C.

2.2.1.6 Adoptive cell transfer

Single-cell suspensions were prepared from spleens from OT-II or actin-eGFP mice as described in 2.2.1.4. Either B-cell depletion using the Dynabeads[®] Mouse Pan B (B220) kit (Thermo Fischer Scientific) or T cell isolation using the EasySep[™] Mouse T Cell Isolation Kit (STEMCELL Technologies) was performed following the manufacturer's instructions. Purity was as confirmed by flow cytometry. Subsequently, 18–25x10⁶ cells B-cell-depleted splenocytes or purified T cells were injected intravenously into wild-type C57BL/6 mice.

2.2.1.7 FITC-Dextran gavage

Intestinal permeability was evaluated via FITC-dextran (molecular mass 4 kDa; FD4, Sigma-Aldrich) gavage. To this end, FITC-dextran was dissolved in sterile PBS to a concentration of 100 mg/mL. Each mouse received a dose of 50 mg FITC-dextran per 100 g of body weight or PBS as a control. After 4 hours, whole blood was collected by retro-orbital bleeding into a 1.5 mL Eppendorf tube. Serum was obtained by centrifugation as described in 2.2.1.3. FITC-dextran levels in serum were determined by measuring sera samples and serially diluted FITC-dextran standard curve at excitation wavelength 485 nm and emission of 530 nm on a 96-well solid black (Costar[™]). Measurements were calculated against the standard curve and were recorded as nanograms of FITC-dextran per microliter of serum.

2.2.1.8 Ovalbumin gavage

First, splenocytes from OT-II mice were collected and their B-cells were depleted using the Dynabeads® Mouse Pan B (B220) kit (Thermo Fischer Scientific). Consequently, these B-cell depleted splenocytes were transferred onto wild-type C57BL/6 mice via tail vein injection. The next day, recipient mice were fed either with 20 mg ovalbumin (Roth) in 200 µL PBS, PBS or left untreated. Mice were sacrificed 3 days after OVA treatment and lymphoid organs and GALT were collected for FACS analysis.

2.2.1.9 Active induction of Experimental Autoimmune Encephalomyelitis (EAE)

EAE was induced by injecting mice subcutaneously into the flanks with 200 µl of emulsion containing 200µg MOG₃₅₋₅₅ peptide (MEVGWYRSPFSRVVHLYRNGK) emulsified along with 500 µg M. tuberculosis H37 Ra (Difco) in incomplete Freund Adjuvant oil (Difco). Additionally, mice received 400 ng pertussis toxin (PTX) (List Biological Laboratories) intraperitoneally (i.p.) on days 0 and 2 after immunization.

Clinical signs of EAE were assessed daily according to the following score scale: score 0 – no disease; score 0.5 – reduced tail tonus; score 1 – limp tail; score 1.5 – limp tail and ataxia; score 2 – limp tail, ataxia and hind limb weakness; score 2.5 – at least one hind limb paralyzed/weakness; score 3 – both hind limbs paralyzed/weakness; score 3.5 – complete paralysis of hind limbs; score 4 – paralysis until hip; score 5 – moribund or dead.

2.2.2 Flow Cytometry

Surface Staining

For detection of cell surface markers, cells were transferred into a 96-well V bottom plate (Nunc), spun down (1200 r.p.m., 10 minutes, 4°C) and washed with 150 µL FACS buffer. Next, cells were resuspended in 50 µL of FACS buffer containing a cocktail of fluorochrome-labelled monoclonal antibodies at optimized dilutions. After an incubation step of 20 minutes at 4°C in the dark, cells were washed twice in 150 µL FACS buffer. Whenever a biotin-conjugated antibody was used, a secondary staining using fluorescently-conjugated Streptavidin was performed following the same protocol.

Intracellular Staining

For intracellular cytokine staining, cells were activated with 50 ng/mL PMA (Sigma-Aldrich) and 500 ng/mL ionomycin (Sigma-Aldrich) in the presence of 5 µg/mL brefeldin A (Sigma-Aldrich) for 4 hours at 37°C. Foxp3 and Ki-67 staining required no PMA/ionomycin stimulation. After surface staining, cells were fixed and permeabilized in the dark for 45 minutes at 4°C in 100 µL Foxp3 Fixation/Permeabilization solution, followed by a staining with a cocktail of fluorochrome-labelled monoclonal antibodies at optimized dilutions. Finally, cells were washed twice in Permeabilization buffer and resuspended in 150 µl FACS buffer.

Acquisition and Data Analysis

Samples were acquired in the FACSVerse™ (BD). FACS data were analyzed using FlowJo 7.6.5 software (TreeStar).

Cell Sorting

After stimulation of BW5147 lymphoma cells for 4 hours with 50 ng/mL PMA (Sigma-Aldrich) and 500 ng/mL ionomycin (Sigma-Aldrich), cells were washed twice with PBS (1200 r.p.m., 10 minutes, 4°C), filtered through 100 µm filter (Falcon) and sorted for GFP expression using the FACS Aria Fusion Cell Sorter (BD).

2.2.3 Enzyme-linked Immunosorbent Assay (ELISA).

Sample preparation

Serum and fecal pellets were collected from age-matched mice. Fecal homogenates were prepared by homogenizing fecal pellets in PBS by bead beating (30 Hz, 10 seconds) using Fast Lysing Matrix D tubes (MP Biomedicals) after samples were incubated for 1 hour at 4°C. The total fecal protein content was quantified by means of the Pierce BCA Protein Assay Kit (Thermo Fisher Scientific) following the manufacturer's instructions. For ELISA, isolated fecal homogenates and serum samples were diluted 100-fold for IgA and IgM ELISA and 10,000-fold for IgG ELISA. For the detection of IL-2, BW5147 lymphoma supernatant was used undiluted.

ELISA

High-binding 96-well plates (Maxisorp, Nunc) were coated overnight at 4°C with 1 µg/mL capture antibody diluted in PBS for the quantification of immunoglobulins or in carbonate/bicarbonate buffer for IL-2 quantification. Next, plates were washed three times with ELISA washing buffer and blocked with 200 µL of ELISA blocking solution for 2 hours at room temperature. After washing six times, plates were incubated with 100 µL of diluted samples for 2 hours at room temperature. The standard curve was generated using two-fold serial dilutions of the corresponding standard. Afterwards, plates were washed six times and incubated with 1 µg/mL detection antibody for 1 hour at room temperature. Subsequently, plates were washed six times and incubated with HRP-coupled secondary antibody 1000-fold diluted in ELISA blocking solution for 30 minutes. After washing six times, the bound antibody was detected using 3,3',5,5'-tetramethylbenzidine substrate (TMB) at wavelength 450 nm for IgA ELISA or 2,2'-azino-bis-3-ethylbenzothiazoline-6-sulphonic acid (ABTS) at wavelength 405 nm for IL-2, IgG, IgM ELISA. Serum IgA and IgM were normalized to total serum IgG and fecal IgA was normalized to the total fecal protein content.

Acquisition and Data Analysis

ELISA samples were acquired in the EnSpire (PerkinElmer). ELISA data was consequently analyzed using GraphPad Prism 5 software (Software MacKiev™).

2.2.4 Fecal DNA extraction and 16S rRNA qPCR

DNA extraction was carried out according to a modified version of a QIAamp DNA stool kit (Qiagen). Following extraction and resuspension in H₂O, DNA quantification was performed with a NanoDrop ND-1000. Fecal DNA was used as the amplification template using (2X) ROX qPCR Master Mix and 2X Absolute SYBR Green ROX mix (both Thermo Fisher Scientific). Samples were run in the 7900HT Fast Real-Time PCR System and analyzed by SDS 2.3 software (both Applied Biosystems). Primers for the 16S rRNA of SFB, and Eubacterial (EUB) species used are listed in 2.1.6.2. SFB species levels were normalized to the total amount of EUB DNA.

2.2.5 16S ribosomal RNA (rRNA) gene sequence analysis

Frozen caecal samples from relevant mice strains were lysed by adding 600µl DNA stabilization solution (STRATEC biomedical), 400 µl Phenol:Chloroform:IsoAmyl alcohol (25:24:1; Sigma-Aldrich) and 500 mg autoclaved glass beads (0.1mm; Roth). Samples were shaken using a FastPrep®-24 (3 x 30 sec at maximum speed) (MP Biomedicals) fitted with a 24 x 2 mL cooling adaptor. Lysed samples were then boiled at 95°C for 5 minutes, and centrifuged at 15000xg for 5 minutes at 4°C. The resulting supernatants were transferred onto a new Epi and digested with RNase (0.1 µg/µl; Amresco) for 30 min at 37°C. The samples were then purified using gDNA columns (Macherey-Nagel) following the manufacturer's protocol. Finally, the concentration and purity of the isolated metagenomic DNA from each sample was determined using a NanoDrop® (Thermo Scientific). During library preparation, samples were stored at 4 °C and kept at -20 °C for long-term storage. Prior to sequencing, 12ng of metagenomic DNA from each sample was amplified for the V3/V4 region of 16S rRNA genes for 25 cycles using 341F and 785R primers. Then, samples were purified using the AMPure XP system (Beckmann), pooled together in an equimolar amount, and sequenced with the MiSeq system (Illumina Inc.) using the paired-end mode (PE275). Then, a library was prepared by using a final DNA concentration of 10 pM and 15 % (v/v) PhiX standard library. The resulting raw read files were demultiplexed and each sample was analyzed using USEARCH (Edgar 2010) platform following the UPARSE (Edgar 2013) approach. To this end, all reads were first trimmed to the position of the first base with quality score <3 and then paired. Then, only sequences with an assembled size of 380-440 nucleotides were kept. Next, paired reads with expected error greater than 3 were further excluded and the remaining sequences were again trimmed by 10 nucleotides on both sides in order to avoid GC bias and non-random base composition. The resulting sequences from each sample were dereplicated and

checked for chimeras using the UCHIME platform (Edgar et al. 2011). Next, sequences of all samples were combined, sorted by abundance, and operational taxonomic units (OTUs) with a threshold of 97 % similarity were selected. In order to create one OTU table for all samples, all sequences were mapped back to the representative sequences. Next, only the resulting OTUs with a relative abundance higher than 0.5 % total sequences per sample were retained. The final OTU counts were then normalized to the sample that contained the lowest number of sequences. A manual assignment of the final OTU taxonomy for each OTU was performed by following the most detailed taxonomic classification among Silva (Quast et al. 2013), RDP (Wang et al. 2007), and Greengenes (DeSantis et al. 2006). In cases where different predictions arose, the Silva taxonomic classification was used instead of the RDP, and the RDP instead of the Greengenes taxonomic classification. In the case of OTUs showing a significant differential abundance between groups, the EzTaxon classification (Chun et al. 2007) was used in order to identify the closest described species. When estimating the diversity within samples (alpha-diversity), the Shannon index was calculated and transformed to the corresponding effective number of species as described by Jost (Jost 2007). When performing comparisons across samples (beta-diversity), phylogenetic trees across all OTU representative sequences were constructed using the maximum likelihood method in Mega6 (Tamura et al. 2013) and used for calculation of samples distances with generalized Unifrac (package GUniFrac in R) (Chen et al. 2012). This experiment was partially supported with the help of Dr. Monika Schaubeck.

2.2.6 Cloning and Sequencing

For generating the pQC-NFAT-TRE-sGFP plasmid, NFAT-TRE-sGFP sequence was amplified from pcDNA6-NFAT-TRE-sGFP in six replicate by PCR using sequence-specific primers and the iProof™ High-Fidelity DNA Polymerase (Bio-Rad) following the manufacturer's instructions. Next, PCR products were combined; purified using the MinElute PCR Purification Kit (Qiagen) and DNA was quantified with a NanoDrop ND-1000. Both the purified PCR product and pQCXIX vector were digested with restriction enzymes BglIII and NotI (New England BioLabs) overnight at 37°C in NEB buffer 3.1. Next, the digested pQCXIX vector, and the desired DNA fragment was isolated using the QIAquick Gel Extraction kit (Qiagen) following the instructions supplied by the manufacturer. Similarly, the digested insert PCR product was purified using the MinElute PCR Purification kit (Qiagen). Following estimation of DNA concentration by Nanodrop ND-1000 measurement, vector backbone and insert were mixed in molar ratios of 1:3 and 1:5 vector to insert. Fragments were ligated in a total volume of 20 µl T4 DNA ligase

buffer using 400 units T4 DNA ligase (New England BioLabs) overnight at 16°C. NEB 5-alpha competent *Escherichia coli* cells (New England BioLabs) were transformed with the plasmid DNA following manufacturer's instructions. Transformed cells were spread on LB-agar selection plates with 100 µg/mL ampicillin and incubated overnight at 37°C. 10-20 colonies were picked and further cultured in 5 mL of LB Medium containing ampicillin 100 µg/mL at 37°C for 18 hours. Plasmid DNA was isolated from mini cultures using the QIAprep Spin Miniprep kit (Qiagen). Plasmid DNA was sent for a "cycle, clean & run" sequencing service at the Genomics Service Unit at the Ludwig Maximilians University (LMU) using a pCDNA6-NFAT sense 1 primer.

2.2.7 Tissue histology and immunofluorescence microscopy.

Dissected terminal ileum and colons were cut lengthwise and fixed in 4 % buffered formalin. Sections of formalin-fixed, paraffin-embedded colon tissues were stained with hematoxylin and eosin using standard protocols. Sections were imaged on a Bright-field microscope (Nikon).

2.2.8 Cell Culture

Cultivation of Mammalian Cells

Adherent cells, HEK293T and 3T3, and BW5147 lymphoma cells were cultivated in complemented DMEM medium in 10 cm cell culture-treated dishes (Falcon) in a humidified incubator (Heraeus) at 37°C and 10 % CO₂. Lymphoma cells growing in suspension were harvested by repeated pipetting, and adherent cells were detached with Trypsin-EDTA (Sigma-Aldrich) for 3-5 minutes at 37°C. Cell density and viability were determined using a Neubauer hemocytometer (Neubauer) by staining dead cells with Trypan blue solution. Cells were pelleted by centrifugation (1200 r.p.m., 10 minutes, 4°C) and were kept subconfluent by regular dilution with fresh DMEM medium.

Freezing and Thawing of Cell Stocks

For preparation of long-term stocks, 20-30×10⁶ cells were harvested and resuspended in 1.5 mL of freezing medium. For the freezing of stocks, samples were placed in a Freezing Container (Thermo Fisher Scientific) at -80°C and subsequently stored in liquid nitrogen. For thawing of cells, stocks were transferred to 37°C and washed once with 10 mL of DMEM Medium to remove DMSO, before resuspending in 10 mL of warm medium prior to culture.

Generation of a MOG-specific Mouse T cell Hybridoma

The production of a T cell hybridoma bearing a $V\alpha_{3.2}V\beta_{11}$ T cell receptor (TCR) was performed by polyethylene glycol (PEG)-mediated fusion. A day prior to the fusion, BW5147 lymphoma was split to achieve an exponential growth phase. Additionally, isolated splenocytes from a 2D2 mouse were activated with 0.5 $\mu\text{g}/\text{mL}$ anti-CD3 and anti-CD28 cocktail in complemented RPMI overnight at 37°C. On the day of the fusion, BW5147 lymphoma cells and splenocytes were washed twice with DMEM to remove all traces of FBS. The cell density was determined by using a Neubauer hemocytometer after staining with Trypan blue solution. Subsequently, cells were mixed in a ratio 2:1 splenocytes to lymphoma cells and were centrifuged (1200 r.p.m., 10 minutes, 4°C). After removing all media, 500 μL of 50% (w/v) PEG 1500 was pipetted dropwise over one minute followed by incubation at 37°C for one minute. Next, 1 mL of pre-warmed serum-free RPMI was pipetted over one minute followed by incubation at 37°C for one minute. Subsequently, 3.5 mL of pre-warmed serum-free RPMI was added and the cell mixture was incubated for 20 minutes at 37 °C. Finally, cells were centrifuged (1200 r.p.m., 10 minutes, 4°C), resuspended in fresh hypoxanthine-aminopterin-thymidine (HAT) Medium (Sigma-Aldrich) at a concentration of $1\text{-}2 \times 10^6$ cells/mL, plated in a 96-well flat bottom plate and incubated for 7 days incubated in a humidified incubator (Heraeus) at 37°C and 10 % CO_2 . Growing clones were screened for $V\alpha_{3.2}V\beta_{11}$ T cell receptor by FACS staining. These processes are illustrated in Figure 2.2.9.1.

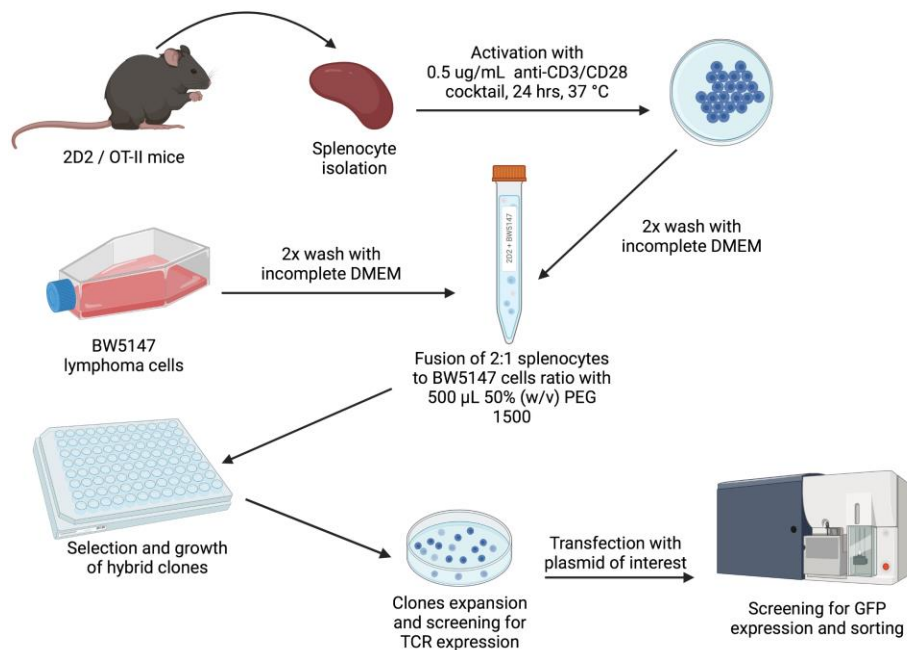


Figure 2.2.9.1. Schematic workflow PEG-mediated T cell-hybridoma generation.

To generate MOG-specific T cell hybridoma, splenocytes from 2D2 mice were pre-activated with anti-CD3/CD28 cocktails overnight. The day after, splenocytes were fused with fusion partner BW5147 by using PEG. Clones were selected and grew in selective HAT media containing 20% FCS. After 7 days of incubation, growing clones were screened by FACS for the expression of $V\alpha_{3.2}V\beta_{11}$ T cell receptor. Positive clones were transfected with NFAT-TRE-sGFP reporter gene and screened for GFP expression after activation with PMA/Ionomycin via FACS. (Created with Biorender.com by Veronica Solis).

Activation Assay of MOG-specific T cell hybridoma cells

A day prior the assay, freshly generated BMDCs were activated overnight with 1 $\mu\text{g}/\text{mL}$ LPS from *Escherichia coli* 0111:B4 (Sigma-Aldrich) in complemented RPMI containing 1 mL of GM-CSF producing hybridoma-conditioned medium. On the day of the experiment, BMDCs and MOG-specific mouse T cell hybridoma were collected in a 15 mL Falcon tube and washed by centrifugation (1200 r.p.m., 10 minutes, 4°C). After cell density was determined by using a Neubauer hemocytometer after staining with Trypan blue solution, 5×10^4 MOG-specific T cell hybridoma cells and 1×10^4 BMDCs were plated per

well in a 96-well plate (Falcon). The activation of MOG-specific T cell hybridoma cells was evaluated against peptides OVA323-339 (ISQAVHAAHAEINEAGR), NF-m18-30 (TETRSSFSRVSGS), MOG35-55 (MEVGWYRSPFSRVVHLYRNGK) at concentrations 20, 2, 0.2 and 0.02 $\mu\text{g}/\text{mL}$. These peptides were synthesized by BioTrend or by the core facility of Max Planck Institute of Biochemistry. Furthermore, activation against recombinant MOG (rMOG) purified from bacterial inclusion bodies, ovalbumin (Sigma-Aldrich) was analyzed. As a positive control for their activation, MOG-specific hybridomas were stimulated with anti-CD3 antibody. Finally, Cells were incubated at 37°C and 10 % CO₂ for 24 hours and its activation state was quantified detecting IL-2 production by ELISA.

Transfection of Mammalian Cells

A day prior transfection, $0.5\text{-}2 \times 10^5$ adherent cells were plated on a 6-well plate (Falcon) in 2 mL of complemented DMEM medium so that cells will be 70-90 % confluent at the time of transfection. In the case of suspension cells, $4\text{-}8 \times 10^5$ cells were plated on a 6-well plate in 2 mL of complemented DMEM medium just prior the preparation of transfection complexes. Transfection was performed the following day using different transfection reagents, as listed in 2.1.8. Transfection protocols were followed as manufacturers' instructions. Transfection efficiency was assessed 48 hours after by flow cytometry.

Electroporation of Mammalian Cells

A day prior electroporation, cells were cultured at a density of 1×10^6 cells/mL. The following day harvested cells were washed with PBS and were resuspended in 800 μL serum-free DMEM and 10 μg plasmid DNA. Next, cells were transferred onto a 0.4cm Gene Pulser / MicroPulser Electroporation cuvettes (Bio-Rad) and incubated on ice for 10 minutes. Cells were pulsed at 280 V, 960 microF with the Gene Pulser Electroporation System (Bio-Rad) and incubated for 10 minutes on ice. Alternatively, cells were also electroporated using the Neon Transfection System (Thermo Fischer Scientific) following the manufacturer's instructions. Finally, cells were transferred onto a 10 cm cell culture-treated dish containing 10 mL of pre-warmed complemented DMEM. Cells were cultured at 37°C and 10 % CO₂. Electroporation efficiency was assessed 48 hours after by flow cytometry.

Calcium Phosphate Transfection of Phoenix cells

2×10^6 Phoenix cells were seeded per 10cm culture dish in 10 mL complemented DMEM 24 hours before transfection. Prior to transfection, 25 μ M chloroquine (Sigma-Aldrich) was added to the medium. The transfection complex was generated by diluting 12 μ g of DNA in 438 μ L H₂O, mixing in 62 μ L 2 M CaCl₂ and adding 500 μ L 2x BES drop by drop with constant vortexing. After 20 minutes of incubation at 37°C, the calcium phosphate-DNA co-precipitate was transferred dropwise onto the Phoenix cells. After incubating Phoenix cells overnight, culture medium was replaced to detoxify cells from transfection reagents.

Retrovirus collection and concentration

The supernatant of transfected Phoenix cells was collected on day 2 and 3 after the calcium phosphate transfection took place and filtered with a 0.45 μ m filter. Then, the filtered supernatant was concentrated (to approximately 50x) using an Amicon Ultra-15 mL (100 kDa MWCO) Centrifugal Filter Units (Merck Millipore) through centrifugation at 4000g for 20 min at 4 °C. Finally, the virus was aliquoted by pipetting 500 μ L per Epi, snap frozen and stored at -80 °C until usage.

Retroviral transduction of mouse MOG-specific T cell hybridoma and primary T cells

CD4⁺ T cells were purified from C57BL/6 wildtype mouse spleens using the EasySep™ Mouse T Cell Isolation Kit. Next, 2×10^6 cells T cells were added per well in a 6-well plate and stimulated with 0.5 μ g/mL anti-CD3 and anti-CD28 antibodies. For some cases, 20×10^6 total splenocytes per well in 2 mL warm complete RPMI were used without previous purification step and stimulated under equal conditions. In both cases, after 24 hours of stimulation, cells were supplemented with 10 ng/mL IL-2 and incubated for further 24 hours. The next day, stimulated T cells were collected and resuspended in fresh complete RPMI medium containing the retroviral particles, 8 μ g/mL polybrene (Sigma-Aldrich) and 10 ng/mL IL-2. 2×10^6 per well in 1 mL were plated in a 6 well-plate and cells were spun down at 2,000 g for 90 minutes at room temperature. After centrifugation, 500 μ L of fresh complete RPMI medium complemented with 10 ng/mL of IL-2 was carefully added to each well. Cells were then incubated at 37 °C overnight before assessed for transduction efficiency through FACS.

In the case of MOG-specific hybridomas, due to their high cell-division rate, these cells did not require stimulation prior retroviral transduction. Therefore, cells were resuspended in complete DMEM medium

containing retroviral particles, 8 $\mu\text{g}/\text{mL}$ polybrene (Sigma-Aldrich). 1×10^5 MOG-specific T cell hybridoma per well in 1 mL were plated in a 6 well-plate and spun down under equal conditions as described for stimulated T cells. After centrifugation, cells were fed with an additional 500 μL of complete DMEM medium. In some cases, MOG-specific T cell hybridoma cells were pretreated with an Ecotropic Receptor Booster (Clontech) following manufacturer's instructions prior retroviral transduction to aim for higher efficiency. 48 hours after transduction transgene expression was estimated by flow cytometry.

3. Results

3.1 The Interplay between the Gut Microbiota and MyD88-dependent Pathways in the Development of EAE

3.1.1. Deletion of MyD88 in intestinal epithelial cells (IECs) leads to severe EAE

The involvement of MyD88-dependent pathways in the pathogenesis of EAE has been outlined when a protective effect was observed in MyD88 full knockout (MyD88^{KO}) mice after immunization with MOG₃₅₋₅₅ in CFA (Prinz et al. 2006). The aim of this study was to unravel the mechanism in that intestinal innate immune responses, through the common adaptor molecule MyD88, shapes the course of EAE. To this end, the following studies were performed in tissue-specific knockout mice where MyD88 was deleted by using the gene-editing technology known as the Cre-lox system. To understand how the microbial-host crosstalk mediated by MyD88-dependent pathways influences EAE, tissue-specific MyD88 knockout mice were immunized with MOG₃₅₋₅₅ in CFA (Figure 3.1.1.1).

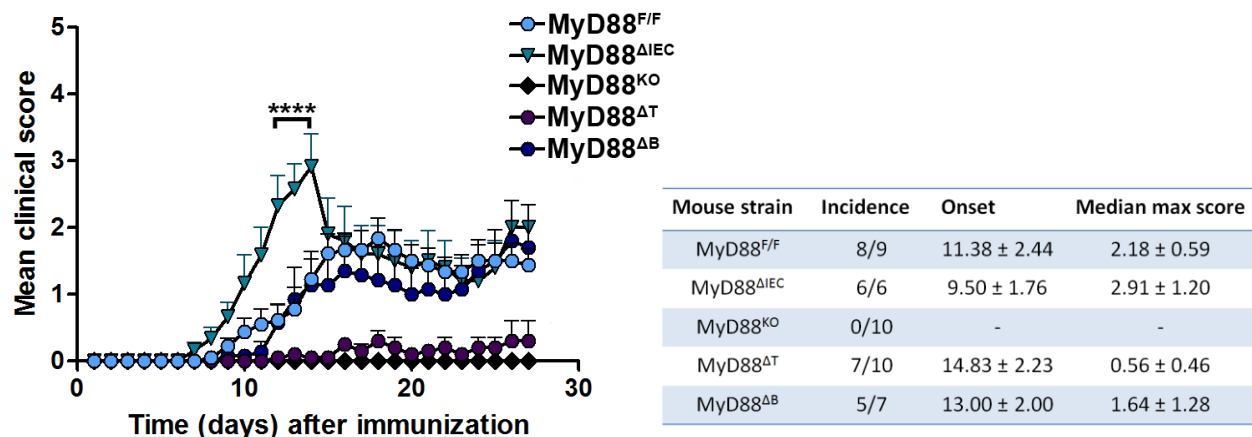


Figure 3.1.1.1. Deletion of MyD88 in Intestinal Epithelial Cells (IECs) exacerbates the severity of active EAE.

Tissue-specific MyD88-deficient mice were immunized with MOG₃₅₋₅₅ in CFA and PTX was given i.p. on days 0 and 2 after immunization. Each data point represents the mean ± SEM. (n= 6-10 mice per group aged 1,5 - 4 months old, pooled data from two independent experiments, *P < 0.0001, two-way ANOVA between MyD88^{ΔIEC} and MyD88^{F/F} groups).

In agreement with the aforementioned study, MyD88^{KO} mice remains fully protected from EAE after immunization when compared to MyD88-sufficient mice (MyD88^{F/F}). Furthermore, a protective effect on the course and severity of EAE was observed in mice where MyD88 was knocked-out in T cells (MyD88^{ΔT}); whereas mice with a deletion of MyD88 in B cells (MyD88^{ΔB}) has no effect in the EAE development compared to control mice. However, mice in that MyD88 were deleted in IECs (MyD88^{ΔIEC}) developed a more severe EAE when compared to littermates, suggesting a modulatory role for MyD88-dependent pathways in the disease pathogenesis.

Although EAE induction by immunization is the oldest and most frequently used model system to study MS in laboratory animals, the adjuvant used in the immunization process creates an inflammatory environment that is so extreme on the cellular level that the triggered condition differs in crucial ways from the actual disease pathogenesis. Therefore, to bypass the strong effect that the adjuvant exerts in the immune system, tissue-specific MyD88-deficient mice were crossbred with our spontaneous EAE model (Figure 3.1.1.2): a double-transgenic mouse that exhibits a basal EAE incidence between 40-60 % (Krishnamoorthy et al. 2006) known as opticospinal EAE [OSE] mouse. When compared to MyD88-sufficient OSE mice (OSE x MyD88^{F/F}), OSE mice crossed with MyD88^{ΔIEC} (OSE x MyD88^{ΔIEC}) exhibit an EAE incidence of about 80%.

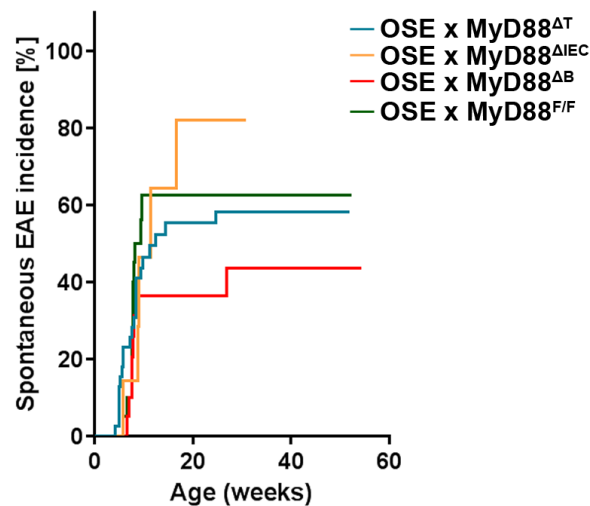


Figure 3.1.1.2. Lack of MyD88-dependent pathways in IECs play increases the incidence of spontaneous EAE.

Incidence of spontaneous EAE in a cohort of tissue-specific MyD88-deficient OSE mice housed in SPF conditions. (OSE x MyD88^{F/F} = 20; OSE x MyD88^{ΔIEC} = 7; OSE x MyD88^{ΔT} = 39; OSE x MyD88^{ΔB} = 20).

In summary, these observations suggest that MyD88-dependent pathways in IECs play a relevant role in the course and severity of EAE.

3.1.2 The effect of IECs MyD88-dependent pathways in epithelial barrier function

Our previous observations raised the question on how intestinal MyD88-dependent signals mediate the disease exacerbation observed in MyD88^{ΔIEC} mice. As earlier mentioned, MyD88-dependent pathways in the gut mediate the expression of gene products that favor epithelia barrier function and the development of innate immune responses. Therefore, we explored whether physical changes in the epithelial wall could contribute to those observations. To this end, formalin-fixed terminal ileum sections were stained with hematoxylin and eosin dyes and examined for the presence of pathologies that might endanger the integrity of the epithelial wall. When examining histological samples of steady-state MyD88^{ΔIEC} mice, we did not observe histological signs of intestinal inflammation or presence of obvious tissue disruption at 8 weeks of age (Figure 3.1.2.1).

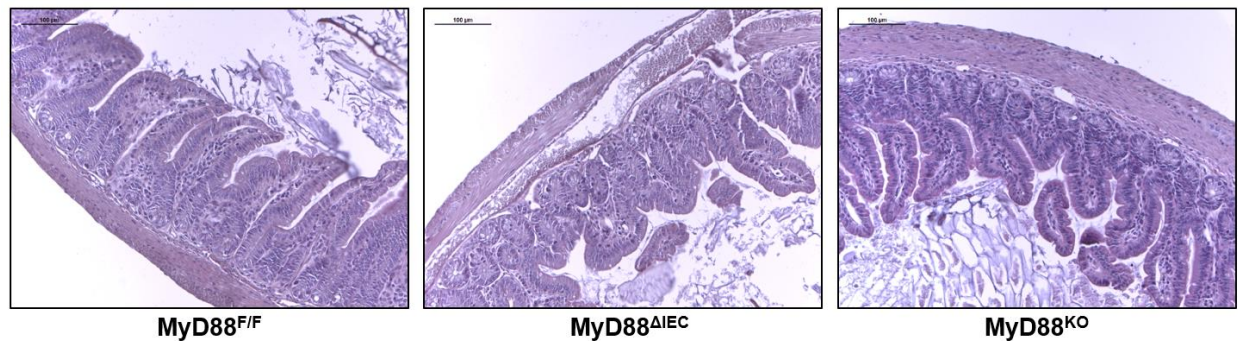


Figure 3.1.2.1. Epithelia cell wall and intestinal tissues remain intact regardless of MyD88 deficiency in IECs.

Representative H&E staining of formalin-fixed terminal ileum sections of 8-week-old MyD88^{ΔIEC} and MyD88^{KO} mice compared to control mice. Scale bar: 100 μm.

Not having observed any visible disruption in the epithelial barrier, we decided to explore the effect of MyD88-dependent signaling in the segregation of the gut microbiota to the epithelial wall. MyD88-dependent signaling in IECs is known to be important for the maintenance a physical separation of microbiota from the intestinal surface (Vaishnav et al. 2011). This physical separation is the result of the synthesis of antimicrobial proteins by gut epithelial cells that keep luminal bacteria at distance. A decrease in the abundance of these molecules is known to promote an approximation of the luminal bacteria to the small intestinal epithelial surface (Vaishnav et al. 2008). Therefore, to evaluate whether gut bacteria can translocate to gut-derived tissues in MyD88^{ΔIEC} mice and to aggravate the severity of EAE, endotoxin A levels were measured in serum of these mice by using the Pierce™ LAL Chromogenic

Endotoxin Quantification kit (ThermoFisher Scientific). Furthermore, a preliminary real-Time PCR for quantifying the presence of 16S rRNA in peripheral organs was performed by using universal primers pairs 8F and 338R that amplify V1-V2 regions of the 16S rRNA gene (Figure 3.2.1.2).

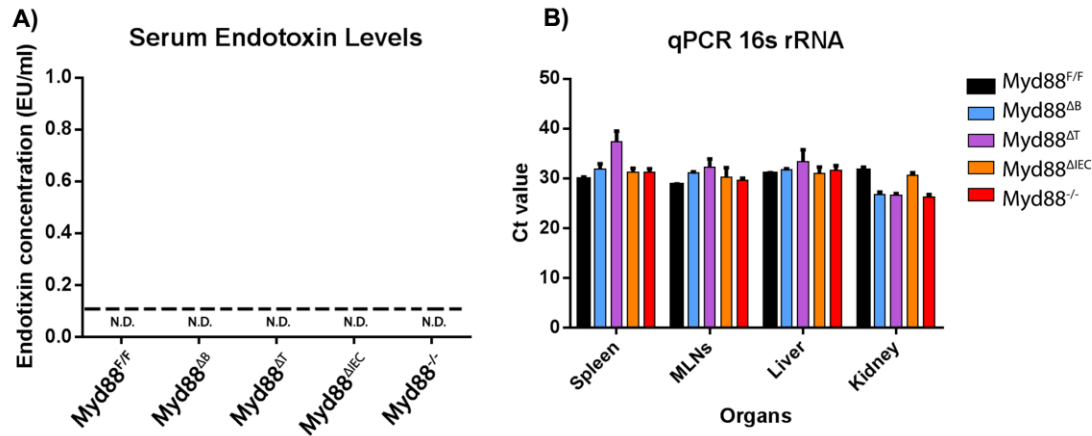


Figure 3.1.2.2. MyD88 deficiency in IEC does not promote bacteria colonization of peripheral or gut-derived organs.

A) Endotoxin A in serum was measured by LAL assay. Horizontal dotted line indicates detection limit of the assay, N.D.: non-detectable (N.D). $n = 4$ mice per genotype, aged 6–8 weeks old. Dashed line indicates detection sensitivity of 0.1 EU/mL. **B)** Preliminary real-Time PCR quantification of 16S rRNA in peripheral organs of mice aged 6-8 weeks old.

Based on these observations, it was concluded that peripheral tissues of steady-state mice remain free of bacteria despite of the lack MyD88-signaling in IECs; suggesting that a translocation of luminal bacteria into the gut-derived (intestinal lamina propria, mesenteric lymph nodes) tissues is highly unlikely. Yet, an increased intestinal permeability is known to promote proinflammatory events that may trigger autoimmune responses (Buscarinu et al. 2018; Nouri et al. 2014; Tajik et al. 2020). Therefore, to evaluate whether MyD88^{ΔIEC} mice has an increased intestinal permeability that might favor EAE development, mice received an oral dose of 50 mg of 4 kDa FITC-Dextran per 100 g body weight and the detection of leaked FITC-Dextran in serum was measured by spectrometry 4 hours after oral gavage (Figure 3.1.2.3).

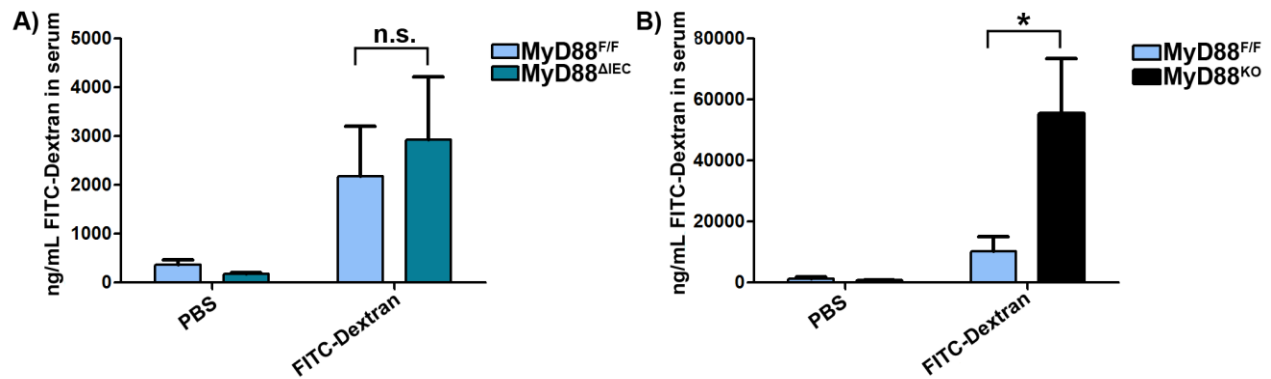


Figure 3.1.2.3. Effect of epithelial MyD88-dependent signaling in the intestinal permeability of MyD88^{ΔIEC} mice

(A) In vivo intestinal permeability was determined in serum 4 hours after FITC-dextran gavage. MyD88^{ΔIEC} and littermates (n=4). Graph is representative of 3 independent experiments. **(B)** Epithelial permeability in the intestines of control mice and mice lacking MyD88 (n=3) was evaluated. Graph is representative of 2 independent experiments. Bars depict mean ± SEM. (n.s. = not significant, *P<0.05, Student's t-test).

Based on these observations, a slight, yet not significant, increase of serum levels of FITC-Dextran was detected in mice where IEC MyD88-dependent signals pathways were knocked-out (Figure 3.1.2.3.a). Furthermore, a role of MyD88 in intestinal permeability was confirmed when a 5-fold increase of serum levels of FITC-Dextran was observed in MyD88^{KO} when compared to control mice (Figure 3.1.2.3.b).

Altogether, these findings suggest that although MyD88-dependent signals are crucial for maintaining the permeability of the gut epithelial cell wall, MyD88 signals through gut epithelial cells alone are not sufficient to significantly impair the epithelial barrier function of gut tissues.

3.1.3. The effect of intestinal MyD88-dependent pathways in adaptive immune responses

MyD88-dependent pathways are actively involved in the maintenance of the mucosal immune homeostasis not only by controlling innate immune responses or promoting the physical separation between the gut microbiota and the intestinal surface, but also by modulating the initiation of local adaptive immune responses in the GALT. The events that shape the course of EAE are known to be mediated by adaptive immune responses that require the presence of the commensal gut microbiota, as the incidence of spontaneous EAE in germ-free RR mice is severely reduced when compared to the mice housed in SPF condition (Berer et al. 2011). To determine the potential influence of MyD88-dependent pathways on adaptive immune responses, the production of relevant Th1 and Th2 cytokines from resident CD3⁺CD4⁺ T cells in spleen and GALT was quantified by flow cytometry after stimulation with 50 ng/mL PMA and ionomycin for 4 hours (Figures 3.1.3.1 and 3.1.3.2).

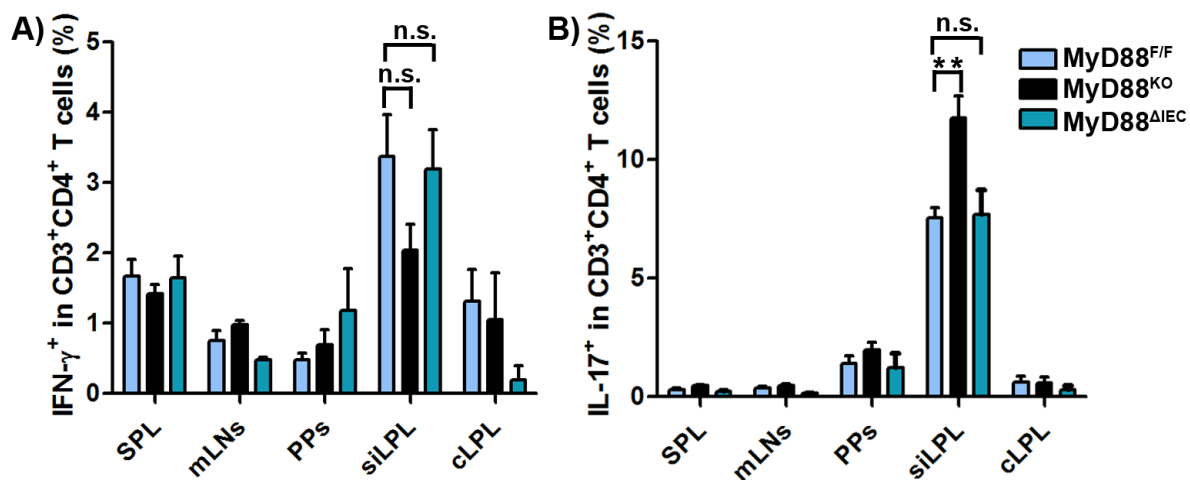


Figure 3.1.3.1. Effect of epithelial MyD88 on Th1/Th17 cells in lymphoid organs and GALT.

Frequencies of IFN- γ (A) and IL-17 (B) producing CD3⁺CD4⁺ T cells from the indicated organs of steady-state tissue-specific MyD88-deficient mice are shown. SPL, spleen; mLNs, mesenteric lymph nodes; PPs, Peyer's patches, siLPL, small intestinal lamina propria; cLPL, colonic lamina propria. n = 3–11 mice per group aged 4 – 8 weeks of age. Data were pooled from nine independent experiments. Bars represent mean \pm SEM. (**P < 0.01, n.s. = not significant, one-way ANOVA).

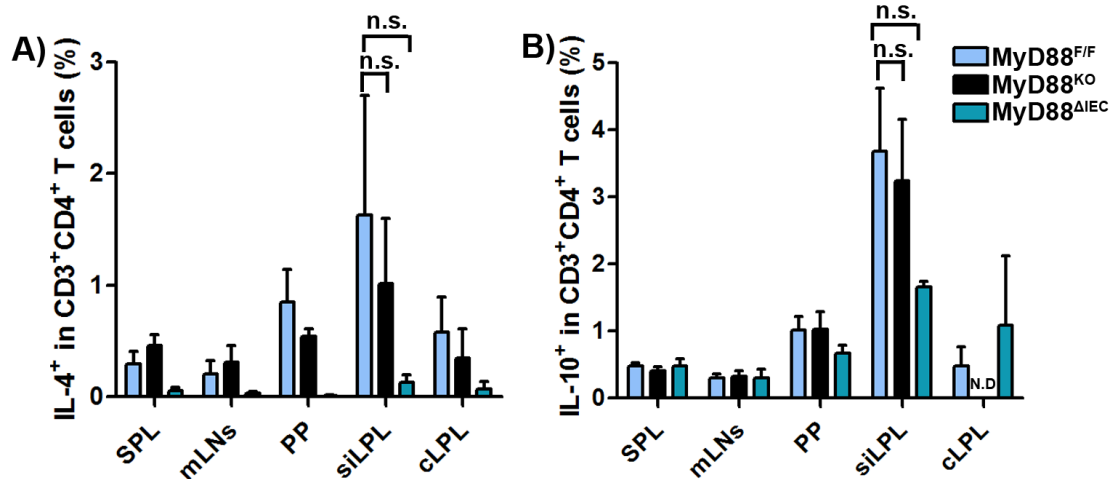


Figure 3.1.3.2. Effect of epithelial MyD88 on Th2 cytokines of lymphoid organs and GALT.

Frequencies of IL-4 (A) and IL-10 (B) producing CD3⁺CD4⁺ T cells from the indicated organs of steady-state tissue-specific MyD88-deficient mice are shown. SPL, spleen; mLN, mesenteric lymph nodes; PP, Peyer's patches; siLPL, small intestinal lamina propria; cLPL, colonic lamina propria. n = 3–11 mice per group aged 4 – 8 weeks of age. Data were pooled from nine independent experiments. Bars represent mean ± SEM. (N.D., not done, n.s., not significant, one-way ANOVA).

Based on these experiments, it was concluded that MyD88-dependent signaling in IECs has no significant effect on the ability of resident CD3⁺CD4⁺ T cells to produce IFN-γ and IL-17 in neither the GALT nor the spleen. Likewise, no significant differences in these cytokines were observed in the lamina propria of the small intestine or colon of MyD88^{ΔIEC} mice, indicating that MyD88 signals within IEC have no influence in the ability for local CD3⁺CD4⁺ T cells to produce these cytokines. Additionally, a slight reduction on Th2 cytokines IL-4 and IL-10 production was observed in the small intestinal lamina propria of MyD88^{ΔIEC} mice when compared to littermates; however, none of these findings is significant. On the other hand, MyD88-dependent pathways are confirmed to influence the production intestinal IL-17 as MyD88^{KO} mice show a significant increase in the frequency of IL-17⁺CD3⁺CD4⁺ T cells in the small intestinal lamina propria when compared to MyD88-sufficient mice.

Since intestinal MyD88-dependent pathways are known to maintaining the balance between anti- and pro-inflammatory responses in gut tissues (Araki et al. 2005; Gibson et al. 2008; Malvin et al. 2012; Rakoff-Nahoum et al. 2004), it was investigated whether local FoxP3⁺ regulatory T cells are influenced by the deficiency of MyD88 signaling in IECs (Figure 3.1.3.3). To this end, frequencies of FoxP3⁺ T cells were

quantified by flow cytometry in the spleen and GALT of steady-state MyD88 tissue-specific knockout mice.

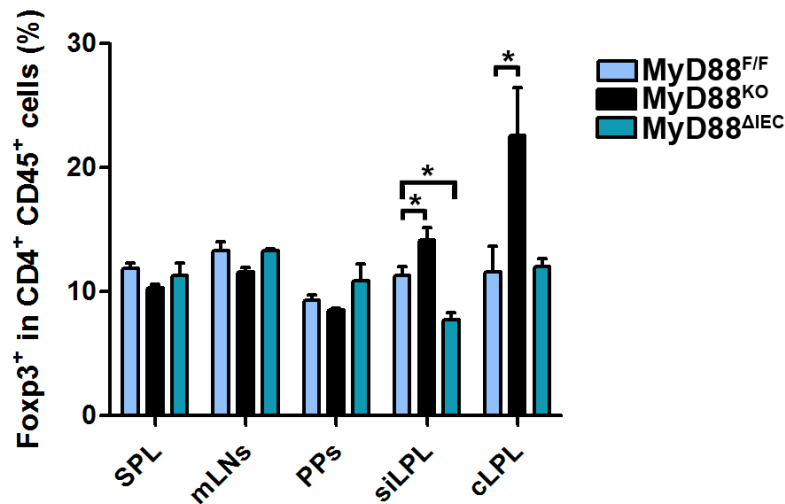


Figure 3.1.3.3. Effect of epithelial MyD88 on FoxP3⁺ regulatory T cells of lymphoid organs and GALT.

Frequencies of FoxP3⁺ producing CD4⁺CD45⁺ T cells from the indicated organs of steady-state tissue-specific MyD88-deficient mice are shown. SPL, spleen; mLN, mesenteric lymph nodes; PPs, Peyer's patches; siLPL, small intestinal lamina propria; cLPL, colonic lamina propria. n = 3–11 mice per group aged 4 – 8 weeks of age. Data were pooled from nine independent experiments. Bars represent mean ± SEM. (*P<0.05, one-way ANOVA).

We observed that frequencies of FoxP3⁺ regulatory T cells were influenced by signals mediated through MyD88 adaptor molecule as MyD88^{KO} mice show significant increased frequencies of Tregs in both small intestinal and colonic lamina propria when compared to littermates. In contrast, significantly lower frequencies of Tregs were found in the small intestinal lamina propria of MyD88^{ΔIEC} mice, suggesting that intestinal epithelial MyD88-dependent pathways aid in regulating the Treg population in the small intestine but not in the colon.

As MyD88-mediated signals are also necessary for the recruitment of myeloid cells into gut tissues to aid in early innate immune responses (Jarchum et al. 2012), frequencies of monocytes and neutrophils in the spleen and GALT were quantified by flow cytometry (Figure 3.1.3.4). It has been observed that the hematopoietic differentiation of monocytes and neutrophils in the bone marrow remain intact in tissue-specific MyD88-knockout mice as frequencies of these myeloid cells in the bone marrow of MyD88^{KO} and MyD88^{ΔIEC} mice do not differ to those of control mice. Likewise, no significant differences in

frequencies of monocytes and neutrophils were found in spleen or GALT of steady-state tissue-specific MyD88 knockout mouse.

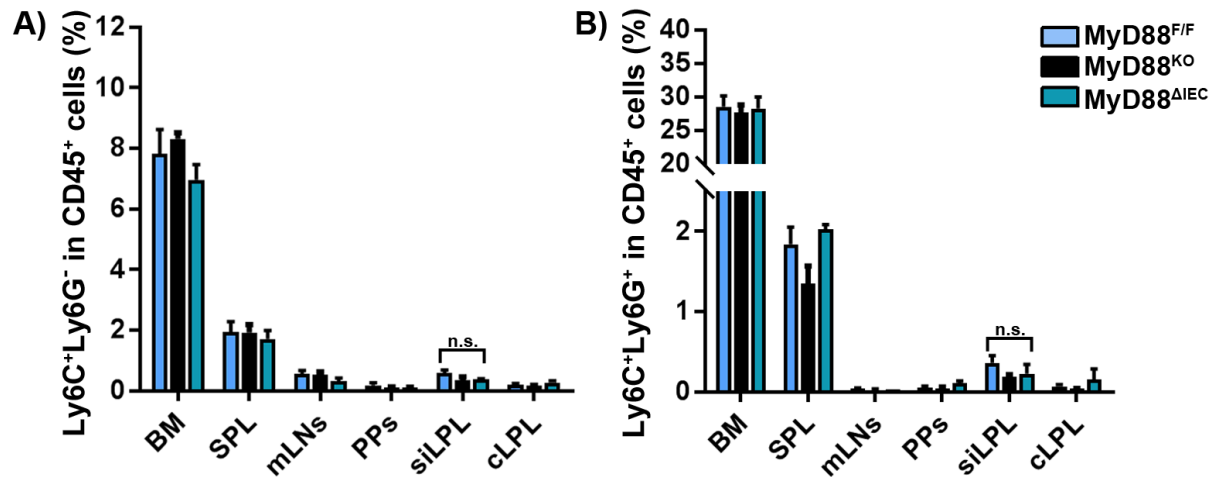


Figure 3.1.3.4. Effect of epithelial MyD88 on the generation and recruitment of myeloid cells in spleen and GALT. Frequencies of Ly6C⁺Ly6G⁻ monocytes (A) and Ly6C⁺Ly6G⁺ neutrophils (B) in CD45⁺ cell compartment from the indicated organs of steady-state tissue-specific MyD88-deficient mice are shown. BM, bone marrow, SPL, spleen; mLNs, mesenteric lymph nodes; PPs, Peyer's patches; siLPL, small intestinal lamina propria; cLPL, colonic lamina propria. n = 3–10 mice per group aged 4 – 8 weeks of age. Data were pooled from nine independent experiments. Bars represent mean ± SEM. (n.s., not significant, one-way ANOVA).

Next, we explored the potential effect of MyD88-dependent signals in the concentration of secretory IgA (sIgA) antibody, as these signals are essential for the transport of sIgA from the GALT into the intestinal lumen. The production of sIgA is reported to be the first line of defense in protecting the intestinal epithelium from enteric toxins and pathogenic microorganism (Frantz et al., 2011). As sIgA plays an important role in keeping luminal bacteria at distance, we hypothesized whether a possible role of this immunoglobulin in MyD88^{ΔIEC} mice would hint to explaining the severe EAE phenotype observed in these mice.

To determine if sIgA antibody levels are influenced by the loss of intestinal epithelial MyD88-mediated signals, the amount of sIgA in fecal pellets of tissue-specific MyD88-knockout mice was quantified by ELISA and normalized to the total fecal protein content (Figure 3.1.3.5). Our findings are in line with previous reports that demonstrate that MyD88 signaling plays a role in regulating sIgA levels in the gut as the abundance of fecal sIgA in MyD88^{KO} mice is reduced when compared to that of control mice.

However, a deletion of epithelial MyD88 is not enough to alter sIgA levels as fecal samples from MyD88^{ΔIEC} mice do not differ in its amount when compared to control mice. In addition, when evaluating by ELISA the general serum immunoglobulin abundance of these mice (Figure 3.1.3.6), serum IgA levels, but not IgG nor IgM, were significantly reduced in MyD88^{KO} but not in MyD88^{ΔIEC} when compared to those of control mice.

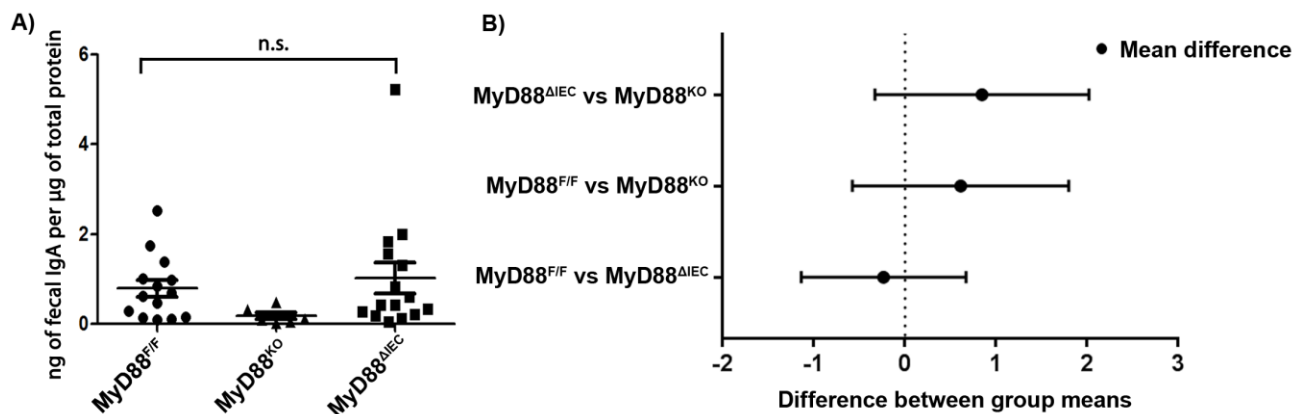


Figure 3.1.3.5. The abundance of fecal IgA does not depend on gut epithelial MyD88 signaling.

(A) The amount of fecal IgA from tissue-specific MyD88-deficient mice was quantified by ELISA and normalized to total fecal protein content. (B) Differences of sample means depicted with 95% confidence interval. (n = 6-15 mice per group aged 6-8 weeks old; n.s, not significant, Bonferroni correction after one-way ANOVA).

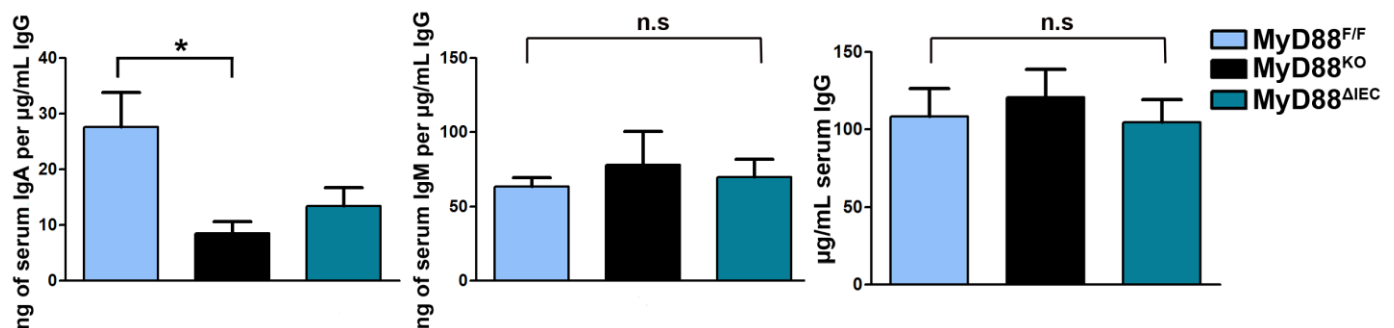


Figure 3.1.3.6. Effect of epithelial MyD88 on the abundance of serum immunoglobulins IgA, IgM and IgG.

The amount of serum IgA, IgM and IgG from tissue-specific MyD88-deficient mice was quantified by ELISA and normalized to total serum IgG content. Bars depict mean ± SEM. (n = 8-14 mice per group aged 6-8 weeks old; n.s, not significant, one-way ANOVA).

Taken altogether, intestinal epithelial-specific MyD88 signals are not sufficient to cause significant differences in adaptive immune responses of healthy mice, as frequencies of proinflammatory cytokines IFN γ and IL-17 remain intact in MyD88 Δ^{IEC} mice. Furthermore, in these mice, fecal IgA levels are similar to those of control mice and only an intermediate reduction of IgA in serum was observed. MyD88-mediated signals play no role in the hematopoietic differentiation of myeloid cells and the recruitment of these cells into gut tissues was not affected in steady-state mice. However, a significant reduction in the frequencies of FoxP3 $^+$ Tregs of the small intestinal, but not colonic, lamina propria of MyD88 Δ^{IEC} mice was observed, suggesting that epithelial MyD88-dependent signals help in regulating the Treg population in this compartment.

3.1.4. The Effect of epithelial-specific MyD88 signaling in the composition of the gut microbiota

The intimate relationship between the immune system and the host gut microbiota is a complex interplay in which a delicate balance between physiological and excessive Toll-like Receptor signaling defines amid initiating anti- or proinflammatory immune responses. Cross-talk between the gut microbiota and intestinal epithelial cells is mediated by pattern recognition receptors, including the Toll-like receptor (TLR) family. Due to this close link between host gut microbiota and the immune system, the effect of epithelial-specific MyD88 signaling in the composition of the gut microbiota was assessed.

First, the relative abundance of segmented filamentous bacteria (SFB), potent inducers of lamina propria Th17 cells, was quantified from DNA isolated from fecal samples by Real-Time PCR and its abundance was normalized to total Eubacteria (Figure 3.1.4.1).

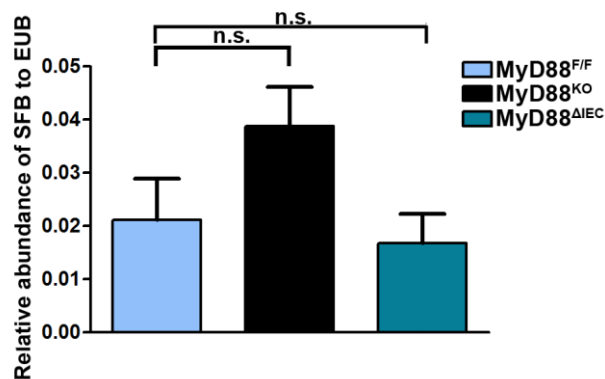


Figure 3.1.4.1. Effect of epithelial MyD88 on segmented filamentous bacteria (SFB) abundance in fecal pellets.

The abundance of SFB in fecal pellets was quantified in fecal pellets from tissue-specific MyD88-deficient by Real-Time PCR and normalized to total Eubacteria. Bars depict mean ± SEM. (n= 11-19 mice per group aged 6-8 weeks old; n.s, not significant, one-way ANOVA).

As observed in Figure 3.1.4.1, there were no significant differences detected in fecal samples from MyD88^{ΔIEC} mice when compared to control mice, suggesting that epithelial-specific MyD88 signals are not enough to modify the abundance of SFB. This observation is supported by the normal frequencies of local IL-17-producing T cell found in both the small intestinal and colonic lamina propria of these mice (Figure 3.1.3.1). It rather seems that MyD88 signals do not influence the abundance of SFB, as MyD88^{KO} mice show no significant difference when compared to MyD88-sufficient mice.

Next, to assess whether epithelial-specific MyD88 signals impact the overall microbiota composition, DNA from caecal luminal content from tissue-specific MyD88 knockout mice was isolated and regions V3/V4 of the 16S rRNA gene sequences were amplified and pyrosequenced to determine and compare the phylogenetic profile of the microbiota within each genotype (Figure 3.1.4.2).

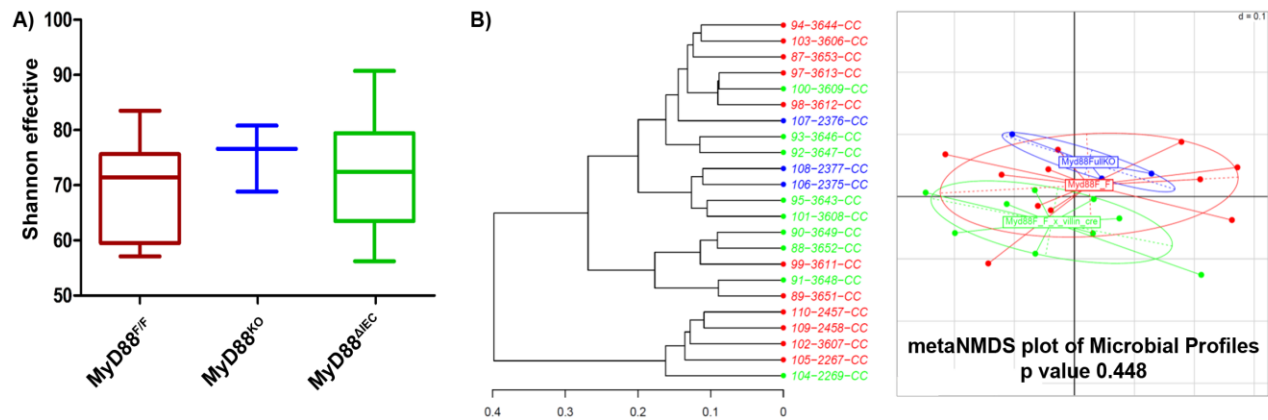


Figure 3.1.4.2. Effect of epithelial MyD88 signaling on caecal luminal microbiota.

(A) Alpha diversity in the caecal luminal microbiota. Bars depict mean \pm SEM. **(B)** Beta diversity illustrated by Phylogram and NMDS plot of microbial profiles in the caecal luminal content. (n= 3-12 mice per genotype aged 6-8 weeks old, one-way ANOVA). Analysis performed by Monika Schaubeck.

Based on these results, no significant differences between groups in the alpha or the beta diversity in the composition of caecal luminal microbiota was observed, suggesting that the microbiota composition of steady-state mice is not affected by the absence of MyD88-specific signals originated from intestinal epithelial cells.

Further analysis of the caecal microbiota at the order level demonstrated the presence of two dominant taxonomic orders within all groups: the Clostridiales order and the Bacteroidales order (Figure 3.1.4.3). Within these, the *Lachnospiraceae* and *Porphyromonadaceae* families were the main representatives identified for the Clostridiales and Bacteroidales order, respectively. When comparing the groups, however, no significant differences were observed.

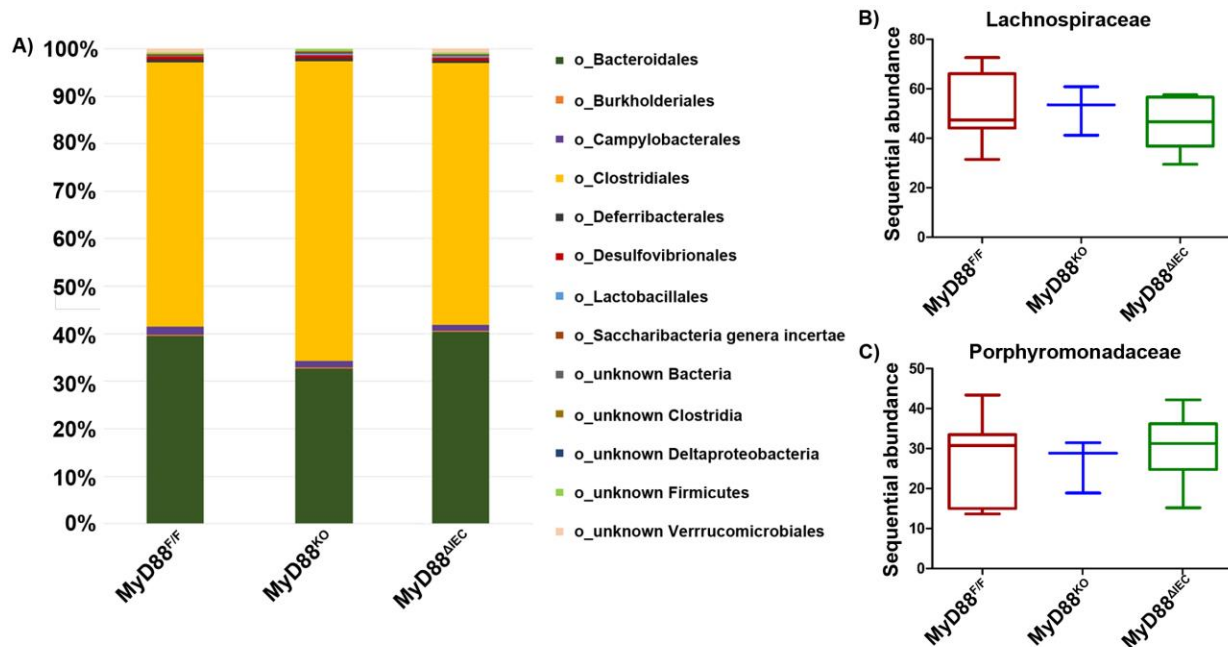


Figure 3.1.4.3. Effect of epithelial MyD88 signaling on taxonomical order of caecal luminal microbiota.

(A) Taxonomic order in the caecal luminal microbiota. Sequential abundance of Lachnospiraceae (**B**) and Porphyromonadaceae (**C**) in the caecal luminal content of tissue-specific MyD88 knock-out mice. (n= 3-12 mice per genotype aged 6-8 weeks old, one-way ANOVA). Analysis performed by Monika Schaubeck).

Based on these observations, we conclude that the deficiency of MyD88-dependent signals in the gut is not sufficient to exert a significant effect in the composition of the gut microbiota in MyD88^{ΔIEC} mice. These observations are found to be in line with previous experiments that show that steady-state MyD88^{ΔIEC} mice show no alteration in their adaptive immune profile discussed in section 3.1.3.

3.2 Establishing Tools to Identify Molecular Mimicry Events in Gut Tissues as a Trigger Mechanism for EAE

3.2.1 Generation a MOG-specific T cell Hybridoma as an antigen-screening In-Vitro Tool.

The concept that commensal gut bacteria play a relevant role in brain autoimmunity is supported by studies performed by Berer and her team in the relapsing-remitting model of EAE (Berer et al. 2011). In this study, the incidence of spontaneous EAE in germ-free RR mice was severely reduced. However, upon recolonization with SPF-derived fecal material, these mice promptly developed spontaneous disease. These observations led to the conclusion that the encephalitogenic immune response observed in these mice is mediated by the intestinal microbiota. However, the identity of the pathogen and the mechanism that triggers the early events of EAE pathogenesis remain elusive.

Based on these observations, it was hypothesized whether EAE autoimmunity could be initiated in the gut tissues through molecular mimicry. To test this hypothesis, we designed a screening strategy in which a stable MOG-specific T-cell hybridoma carrying the reporter sequence NFAT-TRE-sGFP (figure 3.2.1.1) would be used as an in-vitro tool to survey for potential MOG-like antigens contained in mice fecal pellet lysates. In this section, we describe the different approaches used to generate this cell line.

First, the plasmid pQC-NFAT-TRE-sGFP was cloned by inserting the target sequence NFAT-TRE-sGFP into the pQCXIX backbone by cut-and-paste-based cloning strategy by means of enzymes BglIII and NotI (Figure 3.2.1.1).

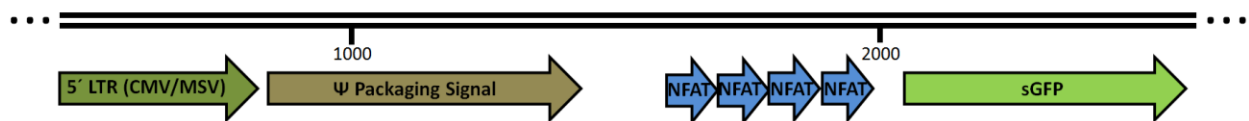


Figure 3.2.1.1. pQC-NFAT-TRE-sGFP retroviral construct diagram.

Representative diagram of the key elements of the pQC-NFAT-TRE-sGFP retroviral construct are shown. This sequence shows four NFAT transcriptional response elements (TRE) where NFAT molecules bind upon following antigen recognition. Binding of NFAT to this TRE induces the transcription of GFP that can be quantified by FACS.

Next, to generate a MOG-specific T-cell hybridoma, BW5147 lymphoma cells were fused with pre-activated $V\alpha 3.2^+V\beta 11^+$ splenocytes obtained from 2D2 mice via PEG-mediated fusion. Fused cells were screened for their surface expression of $V\alpha 3.2V\beta 11$ T cell receptor via FACS staining (Figure 3.2.1.2) after being cultured for 7 days under selective conditions. Positive clones that exhibited highest expression levels of $V\alpha 3.2^+V\beta 11^+$ TCR were further cultured to ensure their viability and the stability of the TCR expression under prolonged culture.

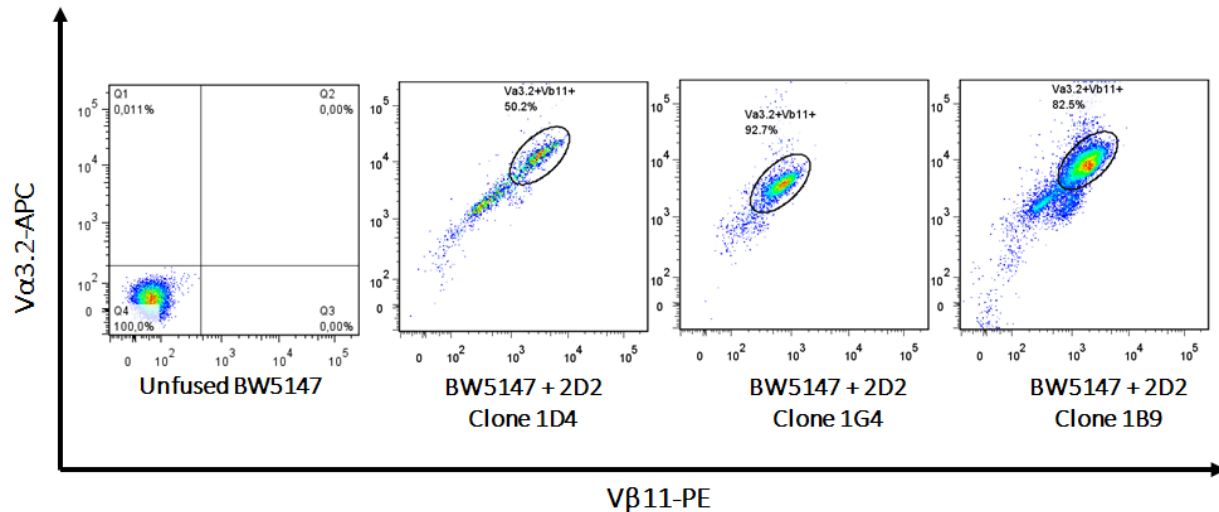


Figure 3.2.1.2. Screening of MOG-specific T cell hybridoma positive clones by FACS Staining.

Representative FACS staining of MOG-specific T cell hybridoma screening. Successful fusion of lymphoma BW5147 and $V\alpha 3.2V\beta 11$ splenocytes lead to the generation of MOG-specific T cell hybridoma cells that express $V\alpha 3.2V\beta 11$ on their surface. Positive clones are screened by FACS. (Data is representative of 5 independent experiments).

Subsequently, selected clones were screened for their selective reactivity to MOG_{35-55} antigen by quantifying their IL-2 production upon cognate presentation by professional antigen presenting cells (APCs). To this end, positive MOG-specific T cell hybridoma clones were activated with either ovalbumin (OVA) or MOG_{35-55} antigens in the presence of BMDCs or with anti-CD3 antibody for 24 hours. The IL-2 concentration was measured from the supernatant via ELISA. As shown in figure 3.2.1.3, only the MOG-specific T cell hybridoma 1B9 clone reacted to MOG_{35-55} antigen and CD3 stimulation but not to OVA. Clones 1D4 and 1G4 showed no reactivity to MOG_{35-55} ; however, clone 1G4 only reacted to CD3. The response of 1G4 and 1B9 clone to anti-CD3 antibody confirms that a hybridoma cell line could potentially have a functional TCR post-fusion with PEG. Based on these results, the only reactive MOG-specific T cell hybridoma that responds to MOG_{35-55} presented by APCs and to CD3 activation is clone

1B9. This clone was further expanded, used for further experiments and will be referenced from this point on as “TCH-2D2-B9 hybridoma”.

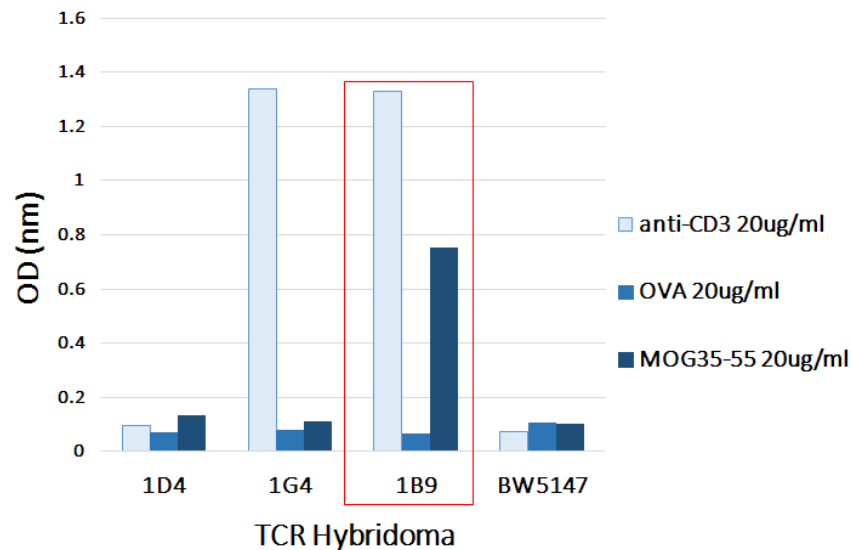


Figure 3.2.1.3. Antigen-specific IL-2 production of reactive MOG-specific T cell hybridoma clones.

Analysis of IL-2 secretion by MOG-specific T cell hybridoma clones in response to recognition of antigen presented by bone marrow–derived dendritic cells (BMDCs) through ELISA. OVA, ovalbumin; MOG, myelin oligodendrocyte glycoprotein. Data is representative of 3 independent experiments.

Then, TCH-2D2-B9 hybridoma cells were infected with pQC-NFAT-TRE-sGFP retroviral supernatant via spin-infection method either in the presence or absence of an ecotropic receptor booster mCAT-1. To quantify the transduction efficiency, control 3T3 and HEK cells were infected with pQC-NFAT-TRE-sGFP supernatant along with TCH-2D2-B9 hybridoma (Figure 3.2.1.4). Based on this experiment, it was observed that no GFP expression after PMA/Ionomycin stimulation could be detected for TCH-2D2-B9 hybridoma cells when pre-treating them with the ecotropic receptor booster. However, the retroviral transduction was confirmed to be successful as GFP expression was detected in both 3T3 and HEK293T cells. After performing this experiment several times, it was concluded that TCH-2D2-B9 hybridoma cells were resistant to retroviral infection with pQC-NFAT-TRE-sGFP and the presence of ecotropic receptor booster did not significantly improve the efficiency of the retroviral infection in TCH-2D2-B9 hybridoma cells.

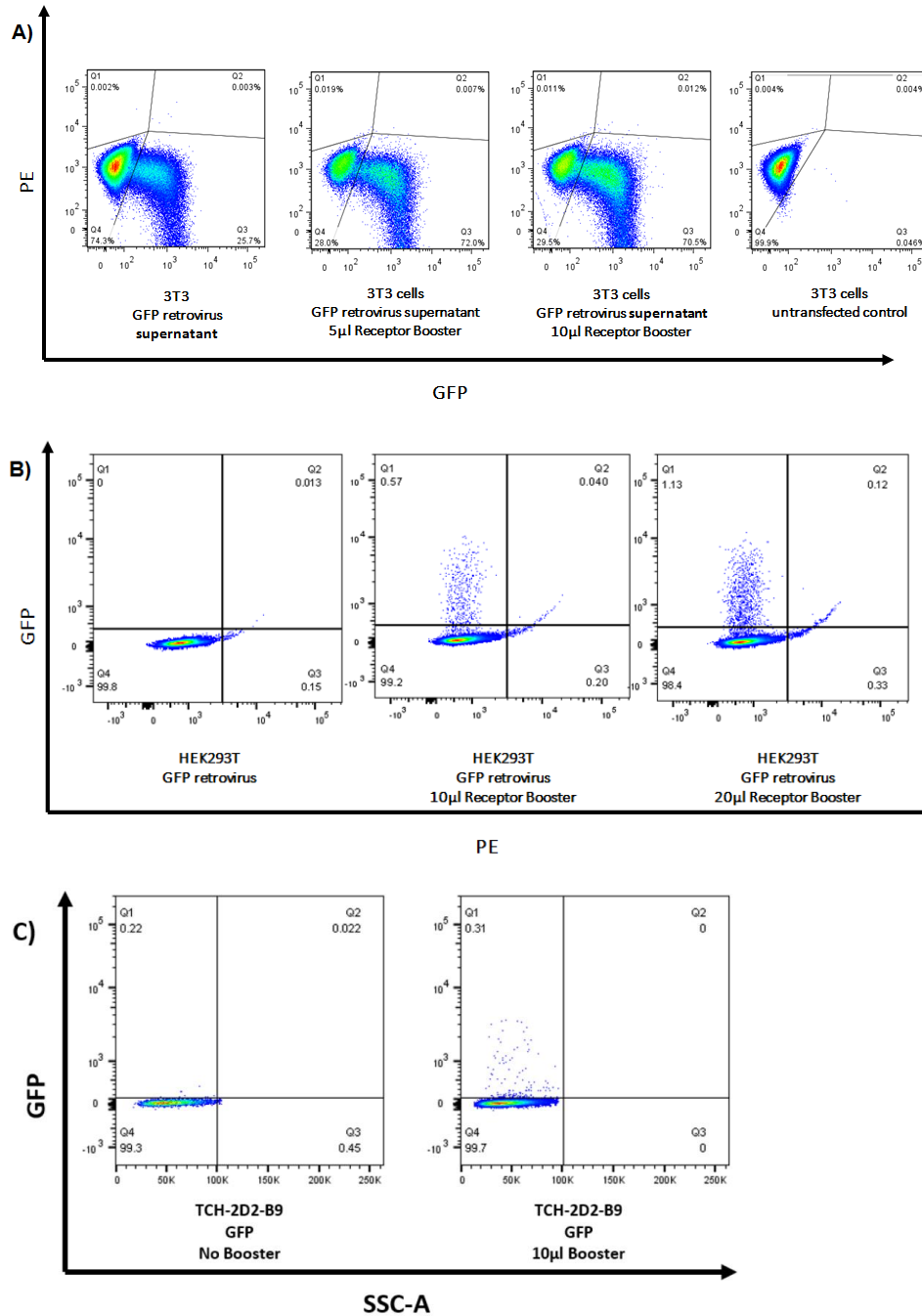


Figure 3.2.1.4. Screening of MOG-specific T cell hybridomas expressing NFAT-TRE-sGFP plasmid by FACS after being pre-treated with an ecotropic receptor booster treatment and stimulation with PMA/ionomycin.

Representative FACS screening of 3T3 cells (**A**), HEK cells (**B**) and TCH-2D2-B9 hybridoma (**C**) for GFP expression. Cells were first pre-treated with mCAT-1 ecotropic booster (Clontech) following the manufacturer's instructions. Subsequently, cells were transduced with pQC-NFAT-TRE-sGFP viral supernatant via spin-infection at 2000rpm for 90 minutes at RT and cultured for 48 hours. Finally, cells were stimulated with PMA/ionomycin cocktail for 4 hours before screened for GFP expression by FACS. (Data is representative of 5 independent experiments).

Having encountered difficulties to introduce the target sequence NFAT-TRE-sGFP using retroviral transduction into TCH-2D2-B9 hybridoma cells, we considered transfection as an alternative approach to introduce the desired sequence into our target cells using different transfection reagents. To this end, the plasmid pcDNA6-NFAT-TRE-sGFP was used to transfect TCH-2D2-B9 hybridoma cells by using Viromer Yellow (lipocalyx), Xfect (clontech) and TransIT 2020 (Mirus Bio) transfection reagents. Additionally, plasmid pMAX-GFP was used as a positive control for GFP expression (Figure 3.2.1.5 and 3.1.2.6). When transfecting TCH-2D2-B9 hybridoma cells with the above-mentioned reagent, we observed a lack of GFP expression after stimulation with PMA/Ionomycin cocktail. This led to the conclusion that none of these transfection reagents successfully introduced target sequence NFAT-TRE-sGFP into the genomic DNA of TCH-2D2-B9 hybridoma cells. Additionally, a control transfection of TCH-2D2-B9 cells with plasmid pMAX-GFP also resulted to be unsuccessful.

Similar results were obtained when electroporating TCH-2D2-B9 cells with pcDNA6-NFAT-TRE-sGFP (Figure 3.2.1.7A) as these cells do not express GFP after 4 hours of stimulation with PMA/Ionomycin. Interestingly, electroporation of unfused BW5147 lymphoma cells with pcDNA6-NFAT-TRE-sGFP showed to be successful, as a GFP signal was detectable via FACS after stimulation under the same conditions. However, the frequency of BW5147 cells carrying NFAT-TRE-sGFP was lower when compared to those transfected with control plasmid pMAX-GFP. Along with this experiment, a retroviral transduction of TCH-2D2-B9 cells and unfused BW5147 lymphoma cells was performed using pQC-NFAT-TRE-sGFP and pMSCV-GFP retroviral supernatant. Similar to the results observed in Figure 3.2.1.7A, quantification of the GFP expression after stimulation with PMA/Ionomycin cocktail revealed that TCH-2D2-B9 hybridoma is not capable to take up NFAT-TRE-sGFP as efficiently as the BW5147 lymphoma (Figure 3.2.1.7B).

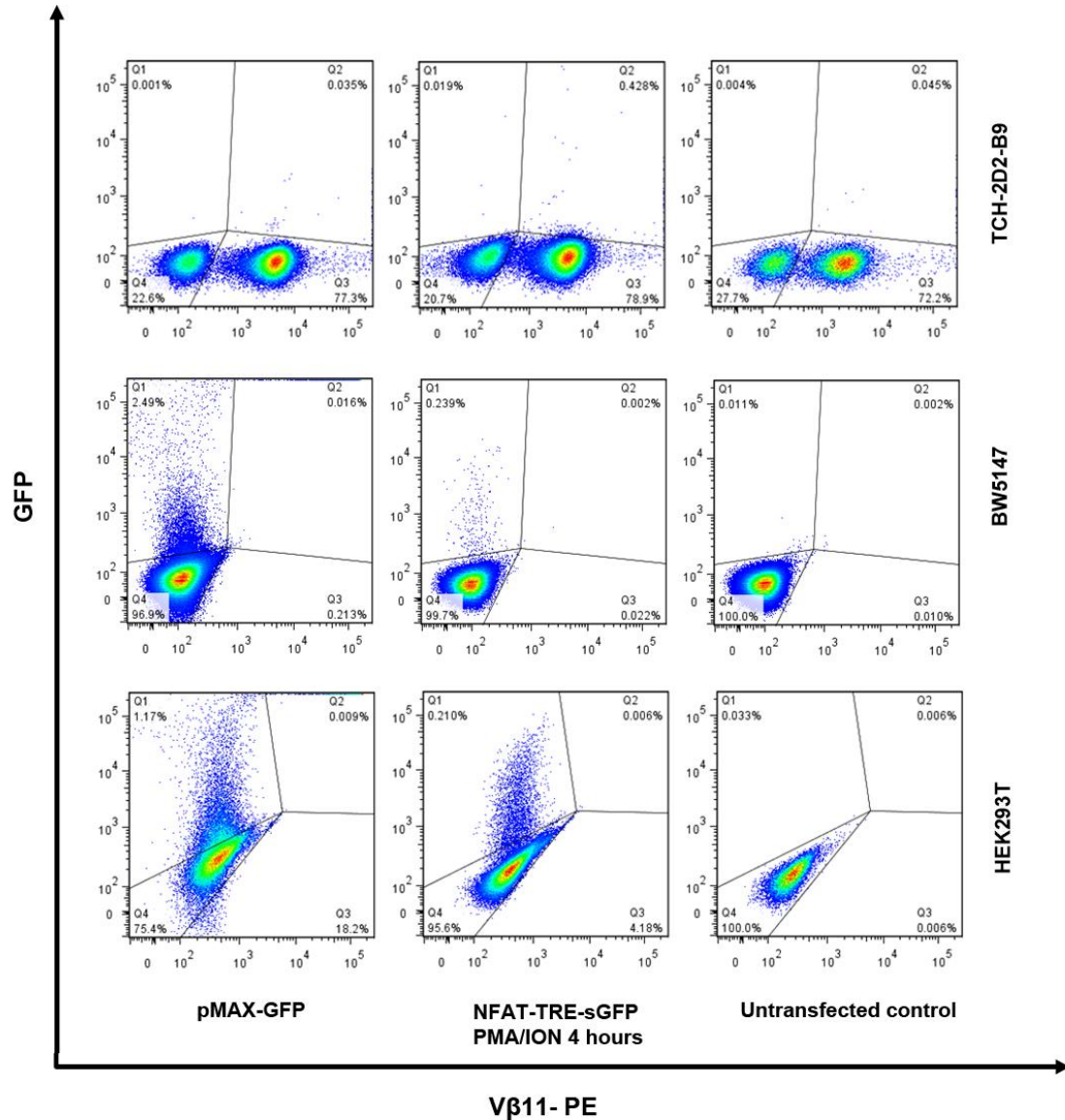


Figure 3.2.1.5. TCH-2D2-B9 T cell hybridoma cells don't incorporate pcDNA6-NFAT-TRE-sGFP plasmid efficiently. Representative FACS plots of TCH-2D2-B9 MOG-specific T cell hybridoma screened by FACS after transfection with pcDNA6-NFAT-TRE-sGFP plasmid using Viromer Yellow reagent. After culturing cells for 48 hours, cells were stimulated with PMA/Ionomycin cocktail for 4 hours before performing FACS Staining. (Data is representative of 4 independent experiments).

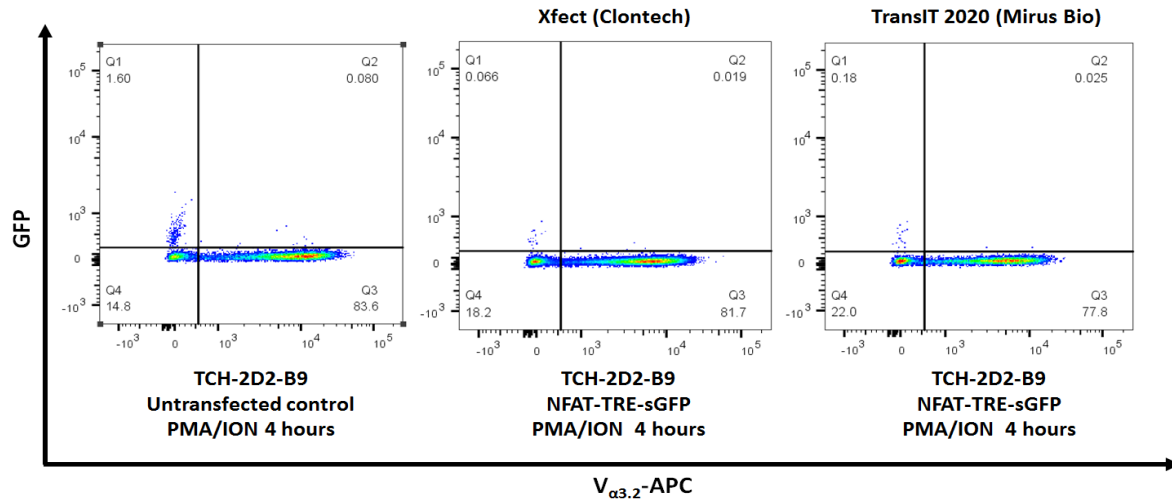


Figure 3.2.1.6. TCH-2D2-B9 T cell hybridoma appears to be resistant to transfection with different reagents.

Representative FACS plots of TCH-2D2-B9 MOG-specific T cell hybridoma screened by FACS after being transfected with pcDNA6-NFAT-TRE-sGFP plasmid using Xfect (Clontech) and TransIT2020 (Mirus Bio) reagents. Cells were stimulated with PMA/Ionomycin cocktail for 4 hours before performing FACS Staining. (Data is representative of 2 independent experiments).

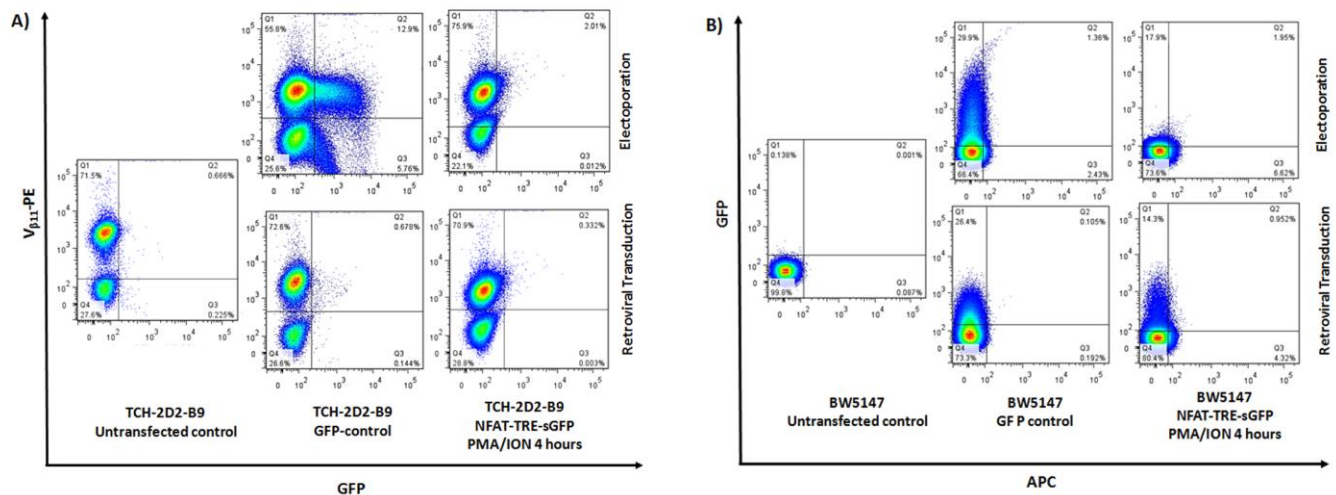


Figure 3.2.1.7. BW5147 lymphoma cells efficiently incorporate NFAT-TRE-sGFP via retroviral transduction.

Representative FACS plots of TCH-2D2-B9 MOG-specific T cell hybridoma (A) and BW5147 (B) screened by FACS after being electroporated with pcDNA6-NFAT-TRE-sGFP plasmid or infected with NFAT-TRE-sGFP retroviral supernatant. pMAX-GFP vector was used as a control for electroporation and pMSCV-GFP retroviral vector was used as control for transduction. Cells were stimulated with PMA/Ionomycin cocktail for 4 hours before screening for GFP expression via FACS. (Data is representative of 2 independent experiments).

Based on the observation that unfused BW5147 hybridoma cells can incorporate target sequence NFAT-TRE-sGFP more efficiently than TCH-2D2-B9 T cell hybridoma, the approach to generate this cell line was reversed. To this end, BW5147 lymphoma cells were first infected with NFAT-TRE-sGFP retroviral supernatant and screened for their expression of GFP after PMA/Ionomycin stimulation for 4 and 24 hours (Figure 3.2.1.8). Similarly, to previous experiments, GFP expression was detected by FACS in both culture conditions.

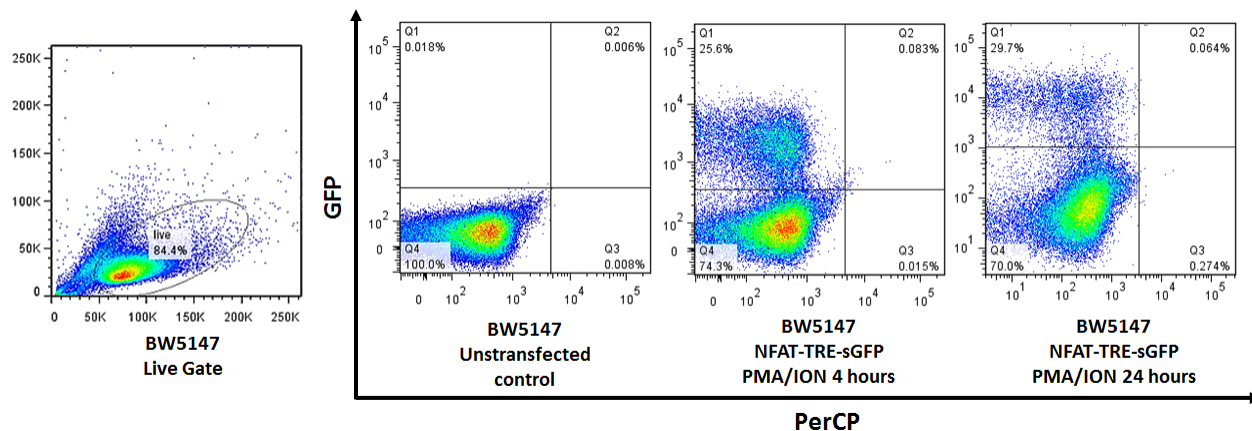


Figure 3.2.1.8. GFP expression by BW5147 lymphoma cells confirms stably expression of NFAT-TRE-sGFP.

Representative FACS screening of BW5147 lymphoma cells after retroviral transduction with pQC-NFAT-TRE-sGFP retroviral supernatant. These cells were stimulated with PMA/Ionomycin cocktail for 4 and 24 hours and the GFP expression was quantified by FACS. (Data is representative of 2 independent experiments).

Ultimately, a fresh batch of BW5147 lymphoma cells was infected with pQC-NFAT-TRE-sGFP retroviral supernatant and sorted for their GFP expression after PMA/Ionomycin stimulation for 4 hours. Subsequently, sorted cells were cultured, further expanded and fused with pre-activated $V\alpha 3.2^+V\beta 11^+$ splenocytes via PEG. Screening of fused cell with a microscope revealed that no clone survived when cultured in selective media (data not shown) suggesting that the fusion was not successful.

3.2.2 Establishing an in-vivo system for assessing T cell activation events in the gut.

As mentioned in the previous section, there is strong evidence suggesting that the activation of autoreactive T cells during early EAE pathogenesis are favored by events that occur in gut tissues that require the presence of the gut microbiota. Based on this, in parallel to generating an in-vitro tool using a MOG-specific T-cell hybridoma, we decided to set up an in-vivo system for assessing T-cell activation events in gut-derived tissues. To achieve this, the below strategy was planned (Figure 3.2.2.1).

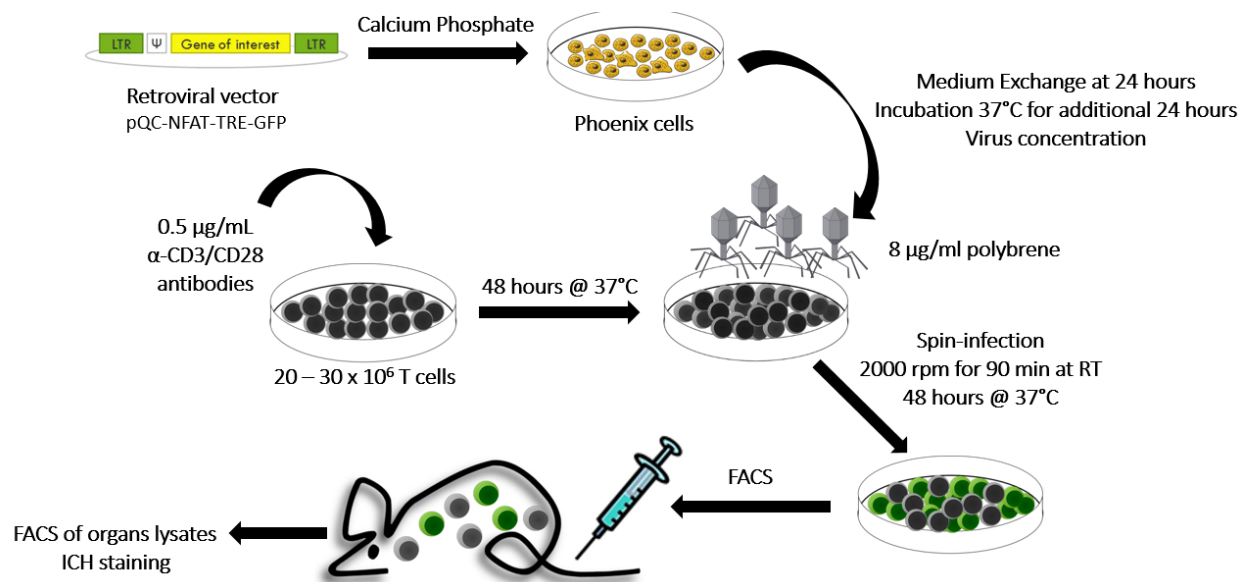


Figure 3.2.2.1. Schematic workflow of adoptive transfer of cells into mouse recipient.

Phoenix packaging cells were transfected with the corresponding vector (pQC-NFAT-TRE-GFP) using calcium phosphate. After overnight incubation, medium was replaced to detoxify cells from transfection reagents and incubated for further 24 hours at 37°C. Next, the transfection supernatant was collected, and the virus was concentrated by centrifuging through Amicon Ultra-15 mL centrifugal filter units at 4,000g until a final volume of 1 mL. Retroviral particles were resuspended and supplemented with 8 µg/mL polybrene. Prior to the spin-transfection, target cells were activated with 0.5 µg/mL α-CD3/CD28 cocktail for 48 hours at 37°C. Then, stimulated target cells were spin-infected for 90 minutes at room temperature and incubated for 48 hours at 37°C. Positive cells were then screened and sorted by FACS and transferred to recipient mice through tail-vein injection. Finally, target organs are recovered at different time points and the presence of the transferred cells was assessed by FACS.

The first step taken into establishing this approach was to determine the amount of cells required to transfer onto recipient mice in order to obtain a detectable number of transferred cells from organ lysates derived from gut tissues (Figure 3.2.2.2).

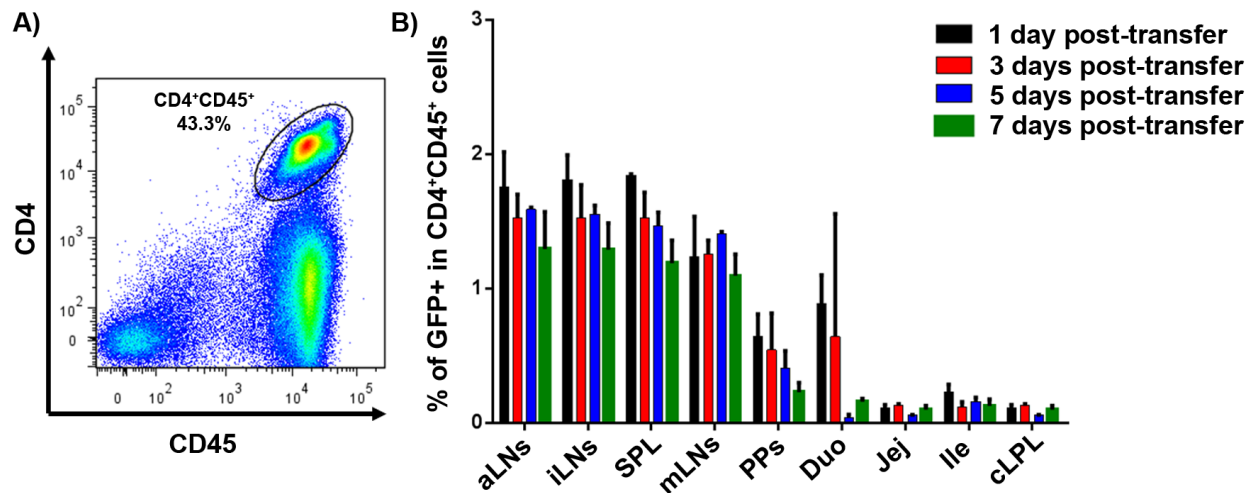


Figure 3.2.2.2. Frequencies of transferred B-cell depleted actin-GFP splenocytes recovered after 1, 3, 5 and 7 days post-transfer from different organs from C57BL/6 mice.

A) Purity of T cells in single-cell suspension assessed by FACS staining of surface markers CD4 and CD45 after depletion of B220⁺ B cell population using Dynabeads[®] Mouse Pan B (B220) kit (Thermofisher). **B)** Frequencies of GFP⁺CD4⁺CD45⁺T cells recovered in harvested organs at 1, 3, 5 and 7 days post-transfer. aLN: axillary lymph nodes, iLN; inguinal lymph nodes, SPL, spleen; mLN, mesenteric lymph nodes; PPs, Peyer's patches; Duo, duodenum; Jej, jejunum; Ile, ileum; cLPL, colonic lamina propria. n = 2 mice per group. Bars represent mean ± SEM (Pooled data of 2 independent experiments).

To this end, single-cell suspensions were prepared from spleens of actin-GFP mice and B cells were depleted using the Dynabeads[®] Mouse Pan B (B220) kit in order to enrich the CD4⁺ T cell population. The purity of the cell suspension was then assessed by FACS (Figure 3.2.2.2A) and it was determined that 43.3% of cells present in the suspension are GFP⁺CD4⁺CD45⁺T cells. Next, 20 × 10⁶ B-cell depleted splenocytes were adoptively transferred onto C57BL/6 mice and organs were harvested at 1, 3, 5 and 7 days post-injection to identify the day post-transfer in which most of the GFP⁺CD4⁺CD45⁺T cells are recovered from gut-derived tissues. The frequencies of transferred GFP⁺CD4⁺CD45⁺T cells present in all harvested organs was assessed for their GFP expression using FACS for all time points (Figure 3.2.2.2B). Based on this experiment, it was observed that for all time points the frequencies of GFP⁺CD4⁺CD45⁺T

cells was below 1% for all gut-derived tissues; namely PPs, duodenum, jejunum and ileum and in the colonic lamina propria. Furthermore, as only 43.3 % of transferred cells correspond to GFP⁺CD4⁺CD45⁺T cells, the observed frequencies of CD4⁺CD45⁺ T cells in these tissues are much lower. Additionally, as no difference in the frequency of recovered GFP⁺CD4⁺CD45⁺T cells was observed in all tested time points, day 3 post-injection was selected for further experiments. This is based on the expression pattern of T cell activation markers required for further experimentation such as CD69, whose detection is known to be short-lived

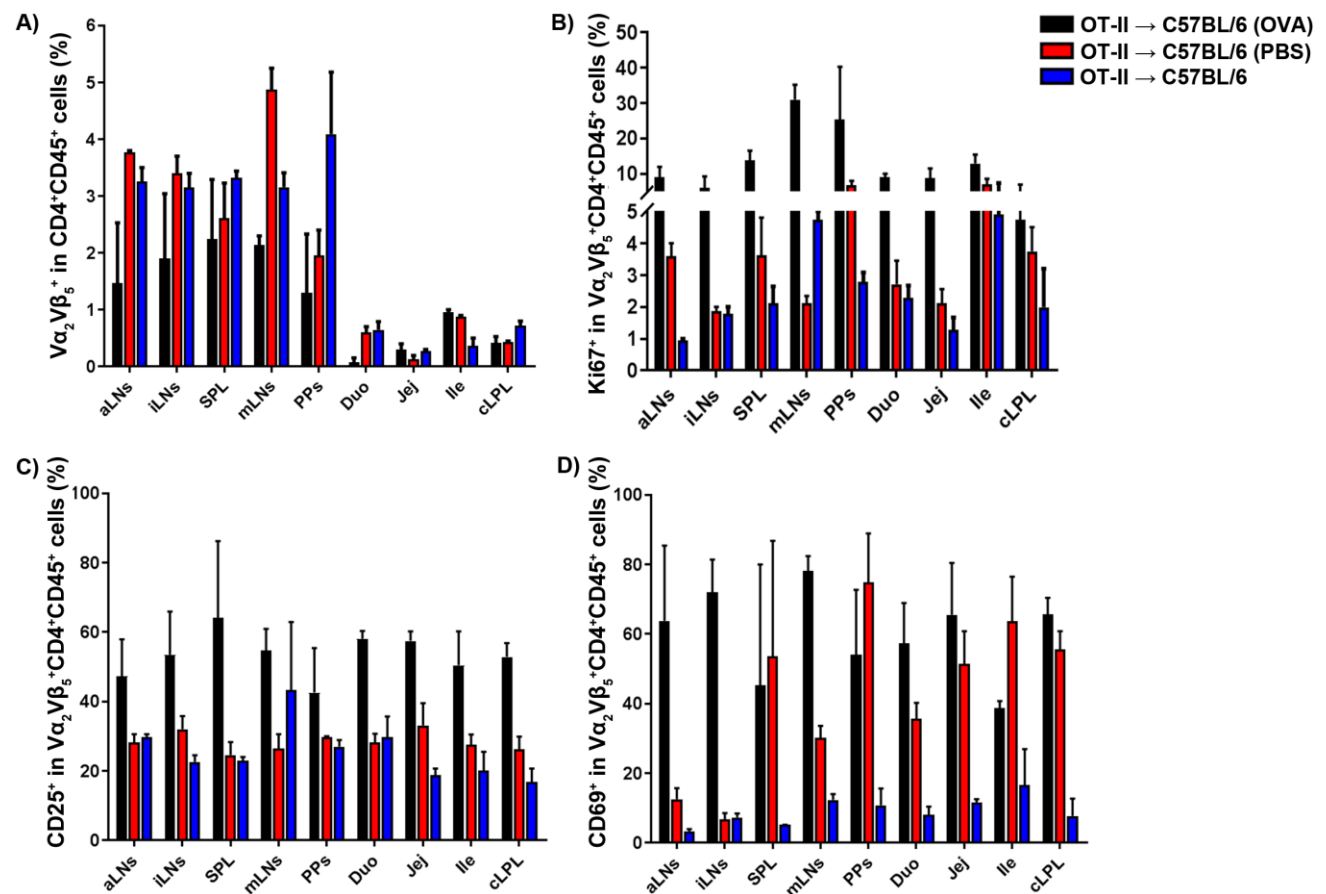


Figure 3.2.2.3. Frequencies of $V\alpha_2^+\beta_6^+$ cells recovered 24 hours after oral gavage with ovalbumin at 3 days post-transfer from different organs from recipient C57BL/6 mice.

(A) Frequencies of $CD4^+CD45^+V\alpha_2^+\beta_6^+$ T cells recovered from harvested organs 24 hours after oral gavage with 20 mg Ovalbumin, PBS or no gavage in C57BL/6 mice. **(B)** Frequencies of proliferation marker Ki67 and activation markers CD25 **(C)**, CD69 **(D)** in $CD4^+CD45^+V\alpha_2^+\beta_6^+$ T cells recovered from harvested organs 24 hours after oral gavage with 20 mg Ovalbumin or PBS and untreated C57BL/6 mice. aLNs: axillary lymph nodes, iLNs; inguinal lymph nodes, SPL, spleen; mLNs, mesenteric lymph nodes; PPs, Peyer's patches; Duo, duodenum; Jej, jejunum; Ile,

ileum; cLPL, colonic lamina propria. n = 2 mice per group. Bars represent mean \pm SEM (Representative data of 2 independent experiments).

Although the numbers of GFP⁺CD4⁺CD45⁺T cells recovered from gut-derived tissues was below 1% (Figure 3.2.2.2) , we assessed whether transferred cells would increase to higher frequencies upon activation throughout recognition of their cognate antigen. To this end, 25×10^6 B-cell depleted splenocytes from OT-II mice were transferred onto C57BL/6 mice via tail-vein and gavaged with 20 mg ovalbumin or PBS as control 48 hours after adoptive transfer of B-cell depleted splenocytes. In line with observations pictured in figure 3.2.2.1, we observed that frequencies of CD4⁺CD45⁺ V α 2⁺V β 6⁺ T cells remained below 1% for gut-derived tissues duodenum, jejunum, ileum and colonic lamina propria. An improvement in the frequencies of these cells in Peyer's patches was observed throughout all tested mice as the frequency of these cells is above 1% (Figure 3.2.2.3A). When observing the expression pattern of proliferation marker Ki67 in CD4⁺CD45⁺ V α 2⁺V β 6⁺ T cells, we noted that mice gavaged with ovalbumin showed a significantly higher Ki67 expression in almost all harvested organs when compared to mice gavaged with PBS or in untreated C57BL/6 mice. However, an unspecific proliferation of CD4⁺CD45⁺ V α 2⁺V β 6⁺ T cells was observed in the ileum segment of PBS-treated and untreated C57BL/6 mice, suggesting that an unspecific activation event is occurring in this particular segment of the gut. Expression of activation marker CD25 in CD4⁺CD45⁺ V α 2⁺V β 6⁺ T cells was observed to be predominantly occurring in mice that were gavaged with ovalbumin (Figure 3.2.2.3C) but when observing the expression of early activation marker CD69 we noted that mice gavaged with PBS show an increase in their frequencies throughout all harvested organs (Figure 3.2.2.3D). This latter observation indicates that the handling of the mice during the gavage procedure induces an unspecific activation of transferred CD4⁺CD45⁺ V α 2⁺V β 6⁺ T cells, as no increase in the expression of CD69 in these cells was detected in CD4⁺CD45⁺ V α 2⁺V β 6⁺ T cells recovered from organs of untreated mice.

The next step into establishing our planned in-vivo model was to test the efficiency of the retroviral transduction of NFAT-TRE-sGFP sequence into C57BL/6 splenocytes. Therefore, retroviral supernatant obtained from transfecting packaging Phoenix cells with pQC-NFAT-TRE-sGFP plasmid was prepared and pre-activated splenocytes from C57BL/6 mice were infected by spin-infection, as described on Figure 3.2.2.1. Ultimately, splenocytes were stimulated with PMA/Ionomycin for 4 hours and screened for their GFP expression via FACS (Figure 3.2.2.4).

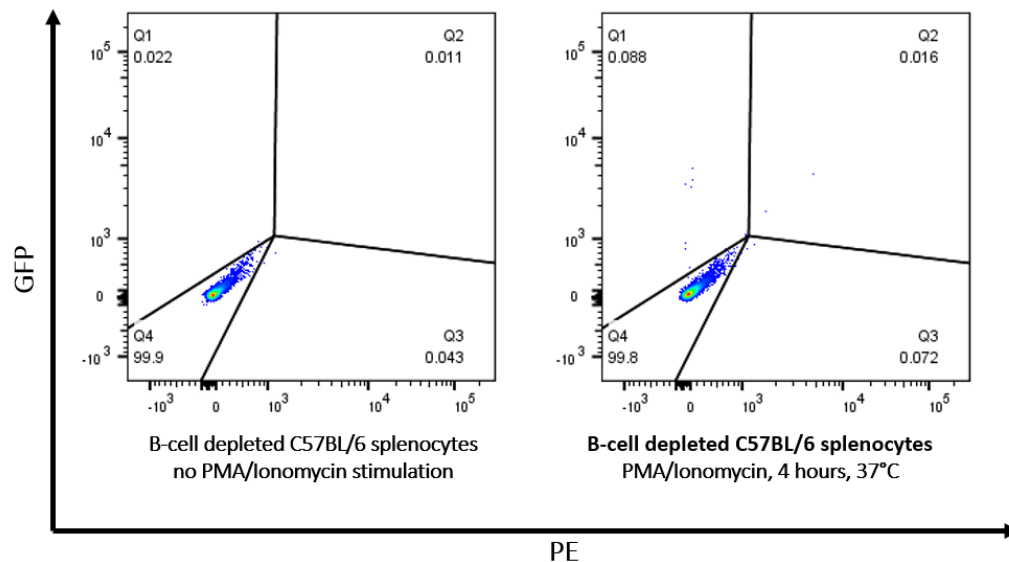


Figure 3.2.2.4. Retroviral transfection of B-cell depleted C57BL/6 splenocytes with NFAT-TRE-sGFP retroviral supernatant.

Representative FACS plots of B-cell depleted splenocytes screened by FACS after retroviral transduction with pQC-NFAT-TRE-sGFP through spin-infection at 2000 rpm for 90 minutes. Transfected cells were incubated for 48 hours at 37°C and stimulated with 50 ng/mL PMA/Ionomycin cocktail for 4 hours prior to FACS assessment. (Data is representative of 3 independent experiments).

As observed in figure 3.2.2.4, and similar to observations in figure 3.2.1.7, B-cell depleted splenocytes do not take up NFAT-TRE-sGFP as no GFP signal is detected by FACS after stimulating with PMA/Ionomycin cocktail. Taken together, it was concluded that the utilization pQC-NFAT-TRE-sGFP is not a suitable tool for assessing T cell activation events in the gut as neither hybridoma cells nor splenocytes seem to successfully integrate this sequence through retroviral transduction.

4. Discussion

4.1 Understanding the role of epithelial MyD88 signals in the pathogenesis and course of spontaneous EAE

The pathogenesis of MS is complicated and an answer to the long-standing question regarding the initial triggers of this autoimmune disease remains elusive to this day. Attempts to better understand the pathogenesis of MS by several research groups have led to the proposal of different theories that evaluate the involvement of an array of potential key players such as immune cells as the classical protagonists, or the local gut microbiota as the novel proposed candidate. Emerging evidence from studies in OSE and RR mouse models points at an important role for the resident gut microbiota in the pathogenesis of MS but it does not provide direct evidence that implicates the gut microbiota in triggering MS. For instance, a key study performed by Berer and her team was the first study of its kind to describe the triggering role of the gut microbiota in the initiation of a spontaneous demyelinating autoimmune disease, in this case EAE (Berer et al. 2011). This study is of great significance in the field of MS research as it clearly shows that the presence of an intact gut microbiota is critically required for the development of EAE. In her study, the incidence of spontaneous EAE in germ-free RR mice was severely reduced and these mice only developed full EAE disease once they were recolonized with conventional flora from SPF mice. It was discovered that the initial activation of MOG-specific T cells in these mice require the presence of the gut microbiota. Likewise, the production of anti-MOG autoantibodies is greatly reduced in germ-free RR mice, and it was promptly increased upon recolonization. Only in the presence of the gut microbiota, activated MOG-specific T cells in the GALT can aid in recruiting MOG-reactive B lymphocytes from the endogenous compartment in order to lead to full clinical EAE. Further evidence of the critical role that the gut microbiota plays in the development of EAE was also observed after a short-term antibiotic treatment of OSE mice (Gödel et al. 2015). In this study, OSE mice treated with an antibiotic cocktail for 2 weeks remained protected from developing EAE; whereas 50% of untreated mice developed spontaneous EAE. A closer look into the composition of the microbiota revealed that even a short-term antibiotic treatment is enough to modify the microbiota in a way that favors EAE development. Finally, an interesting piece of evidence comes from a study where fecal material from twin pairs discordant for MS was transplanted into germ-free RR mice (Berer et al. 2017). In this study it was reported that the transplantation of fecal material of the MS twin in germ-free RR mice results in EAE development at a higher incidence in comparison to those germ-free RR mice that

received fecal material from the healthy twin. All of these reports indisputably link the gut microbiota to the development of EAE; however, the exact mechanism behind these events is yet to be described. To this end, we decided to explore the possibility that the gut microbiota might directly influence MS development by performing a variety of experiments in tissue-specific MyD88-knock-out mice, keeping in focus those observations made in mice lacking MyD88 signaling in IECs.

The first hint that indicated that MyD88-dependent pathways in IECs modulate the severity of EAE stems from observations made during active immunization experiments performed in tissue-specific MyD88-knock-out mice using MOG₃₅₋₅₅ and CFA (Figure 3.1.1.1). Here it was observed that mice deficient of MyD88 signaling in IECs (MyD88^{ΔIEC}) developed more severe EAE when compared to littermates. Although these observations point to an important role of MyD88-dependent pathways in IECs in the development of EAE, the artificial immunological environment created through the technique in which these events occur, do not reflect the physiological conditions that otherwise take place in the actual disease pathogenesis. The reason for this is the mode of induction used by this technique that requires the inoculation of large amounts of adjuvant that may globally alter the immune reactivity in mice where EAE has been actively induced. This leads to a strong activation of cells of the innate arm of the immune system that skews for a potent pro-inflammatory response by the host.

To circumvent this, tissue-specific MyD88-knock-out mice were crossbred with OSE mice, a mouse model known to develop spontaneous EAE at a rate of 40-60% (Krishnamoorthy et al. 2006). When compared to MyD88-sufficient OSE mice (OSE x MyD88^{F/F}), OSE mice crossed with MyD88^{ΔIEC} (OSE x MyD88^{ΔIEC}) exhibit an increased EAE incidence of about 80% (Figure 3.1.1.2). These results are in agreement with observations stemmed from active EAE experiments that intrinsic MyD88 signals in IECs play a modulating role in EAE development. In order to deepen our understanding of the mechanism behind these findings, we explore several theories throughout this work and thoroughly discuss them in the following sections.

4.1.1. Influence of intrinsic MyD88 signals in IECs in the integrity of the gut epithelial cell wall and commensal gut bacterial translocation

MyD88-dependent signals in the gut, especially those that occur within IECs, are crucial for maintaining the intestinal homeostasis (Abreu 2010b). An important feature of the gut-microbe crosstalk is the physical separation of microbiota from the intestinal surface that is critical for limiting immune activation and maintaining mutualistic host-bacterial associations (Abreu 2010a; Vaishnavi et al. 2008; Vaishnavi et al. 2011). Changes in the integrity of the epithelial cell wall and the loss of the physical separation are known to lead to an overstimulation of the immune system that can contribute to the development of different autoimmune diseases such as IBD (Lee et al. 2018). When examining terminal ileum samples of MyD88^{ΔIEC} mice for histological abnormalities in their epithelial barrier, no visible differences were observed in these mice when compared to MyD88-sufficient mice (Figure 3.1.2.1). This observation goes along with reports from Frantz et al., where MyD88^{ΔIEC} mice displayed no obvious histological signs of intestinal inflammation or disruption when compared to MyD88^{F/F} control mice at 9 weeks of age or when followed up at 12 months of age (Frantz et al. 2012). An assessment of sections from colon samples by H&E staining to evaluate intestinal morphological changes in MyD88^{ΔIEC} mice is missing; however, based on the report from Frantz et al., we can speculate that examination of colon sections using the same technique would probably not find any visible histological difference between steady-state MyD88^{ΔIEC} and control mice. However, since no histological abnormalities were found in terminal ileum H&E staining of MyD88^{KO} mice, a line meant for being the positive control of this experiment, it is difficult to evaluate the results observed for MyD88^{ΔIEC} mice.

As previously mentioned, the epithelial cell barrier does not only function as a physical barrier that keeps commensal and pathogenic bacteria at bay, but the production of AMPs and the presence of a mucus layer in both small and large intestine also play an important role in limiting bacterial-epithelial cell contact as well (Frantz et al. 2012; Vaishnavi et al. 2011). Both the production of AMPs and the mucus layer by goblet cells have been reported to be MyD88-dependent. AMPs are known to be found in high concentration within the mucus layer and visualization of spatial relationships between bacteria and the intestinal surface shows that the inner mucus layer remains relatively free of bacteria, whereas the outer mucus layer retains large numbers of bacteria (Johansson et al. 2008; Vaishnavi et al. 2011). Based on this, we expected that epithelial MyD88 signal deficiency would greatly impair the production of AMPs or mucin-2 therefore facilitating the translocation of commensal bacteria beyond gut tissues. However, the involvement of any of these molecules or changes in the integrity of the epithelial cell wall

that could favor commensal bacterial translocation beyond the gut tissues appear unlikely as neither 16s rDNA in gut peripheral organs nor endotoxin A levels were detected in serum of MyD88^{ΔIEC} mice. The lack of 16s rDNA in peripheral organs and the absence of endotoxin A in serum of these mice could be explained by findings made by Diehl et al. In their report, Diehl and colleagues demonstrated that at steady-state, the local gut microbiota in an MyD88-dependent manner inhibit the transport of both commensal and pathogenic bacteria from the lumen to a key immune inductive site, the MLNs (Diehl et al. 2013). This mechanism was reported to be mediated by CD11c⁺CX₃CR1^{hi} DCs, who are responsible for trafficking of non-invasive bacteria to the MLNs was upon disturbance of the microbiota. Since no changes in the composition of the microbiota in steady-state MyD88^{ΔIEC} mice were observed, as shown Figure 3.1.4.3, it could be possible that a translocation of commensal bacteria in these mice is prevented through the mechanism proposed by Diehl and colleagues. In addition, the involvement of intrinsic MyD88 signals in B cell could also play a role in preventing bacterial translocation in MyD88^{ΔIEC} mice. Experiments done in cell-type specific MyD88-deficient mice (B cell-specific MyD88 knock-out mice) by Kirkland and colleagues showed that MyD88 signals in B cells are required for preventing the dissemination of commensal bacteria following colonic damage (Kirkland et al. 2012). This leads us to the assumption that MyD88-sufficient B cells in steady-state MyD88^{ΔIEC} mice might also aid in preventing translocation of resident gut bacteria into the gut tissues. Based on this, it is reasonable to believe that other MyD88-sufficient cells, such as B cells or DCs for example, might compensate for potential changes in the intestinal homeostasis caused by the deficiency of epithelial MyD88 signals under steady-state conditions. However, since no 16s rDNA nor endotoxin A was detected in MyD88^{KO} mice, it is difficult to interpret the results observed in MyD88^{ΔIEC} mice. Potential reasons for the lack of signs related to bacterial penetration in MyD88^{KO} mice could be related to experimental flaws. It is possible that steady-state mice do not offer the conditions necessary for assessing a possible bacterial translocation. Further evidence supporting this theory comes from studies performed by Diehl et al., and Kirkland et al., where mice were fed with non-invasive bacteria or colonic damage was induced through DSS gavage, respectively.

Although the histology performed on terminal ileum samples from steady-state MyD88^{ΔIEC} mice shown in Figure 3.1.2.1 did not reveal any major histological abnormalities, a change in the tight junction barrier function that could influence the permeability of the epithelial cell wall is still possible. Slight MyD88-dependent changes in epithelial tight junctions that could increase the permeability of the epithelial cell wall needs to be assessed through additional experiments. For that reason, a further evaluation of the epithelial cell barrier integrity included experiments that assessed the gut permeability

on MyD88^{ΔIEC} mice through gavage of FITC-conjugated dextran. These experiments demonstrated that the permeability of the gut is slightly increased in MyD88^{ΔIEC} mice; but the leakage observed in these mice was lower than the one observed in MyD88^{KO} mice. This observation suggests that epithelial MyD88 signals are partially but not fully responsible for maintaining the gut permeability in these mice. Therefore, it is plausible to conclude that although epithelial MyD88-dependent signals are known to maintain the permeability and integrity of the gut epithelial cell wall, these signals alone are not sufficient to induce dramatic changes in the permeability of the epithelial wall. Consequently, it is possible that the epithelial cell wall is not permeable enough to allow the trafficking of commensal bacteria from the intestinal lumen to systemic circulation. However, the diffusion of bacteria beyond the intestinal epithelial cell wall is not the only mechanism in which the intestinal permeability could favor EAE development in MyD88^{ΔIEC} mice.

Changes in the intestinal permeability have recently been described as an important event that triggers the onset of some autoimmune diseases. For instance, in rheumatoid arthritis (RA), reports of impaired intestinal barrier function before the clinical onset of arthritis in mice have identified the enterotoxin zonulin, a potent regulator for intestinal tight junctions secreted by intestinal epithelial cells upon stimuli from diets or microbiota, as a molecular factor that triggers the onset of arthritis by regulating intestinal barrier function (Tajik et al. 2020). A role of intestinal permeability in MS has become apparent in a study involving 22 MS patients where 73% of cases compared to the 23% in controls show abnormal intestinal permeability (Buscarinu et al. 2018). Evidence of the intestinal permeability in the development of EAE is shown by Nouri and colleagues, where an altered intestinal permeability, reduced submucosa thickness and altered tight junction expression in intestinal epithelial cells was found shortly before clinical onset (7 days post immunization with MOG₃₅₋₅₅ emulsified in CFA) and at the stage of paralysis (14 days post-immunization) (Nouri et al. 2014). In the same study, these intestinal alterations were also reported to occur in a similar manner in induced EAE by adoptive transfer in C57BL/6 mice. Additionally, a recent study showed that the degree of intestinal permeability disturbance is closely associated with EAE severity and that treatment with *Escherichia coli* strain Nissle 1917 improved intestinal barrier function thereby reducing EAE severity (Secher et al. 2017). Since the course of EAE in MyD88^{ΔIEC} mice was more severe when compared to control mice, we cannot completely discard that the slight increase of the intestinal epithelial permeability observed in MyD88^{ΔIEC} steady-state mice might be involved in EAE development.

In order to deepen our understanding of how the intestinal permeability could play a role in favoring a more severe course of EAE, additional experiments in diseased MyD88^{ΔIEC} mice would be required. To start with, performing a time-course analysis of serum zonulin levels in EAE mice could provide a hint whether the permeability and barrier function of the intestinal wall is compromised in MyD88^{ΔIEC} mice in a greater way than in control mice. Additionally, evaluating the expression of permeability tight-junction (TJ) proteins ZO-1 and occludin through histological immunofluorescence staining or through quantification of the mRNA expression level of these proteins in small intestine and colon samples could offer further insight into the effect that the intestinal permeability of MyD88^{ΔIEC} mice has in the course of EAE.

Since the targeted deletion of MyD88 in IECs is known to compromise the antibacterial immunity and because EAE requires the presence of commensal bacteria to develop, as reported by Berer et al., experiments to evaluate the expression analysis of genes that control permeability and mucus production could offer further valuable information. Experiments to determine the expression level of RegIIIγ and Muc1, Muc2 and Muc3 genes, in terminal ileum and colon of MyD88^{ΔIEC} mice in both steady-state and during EAE through qPCR could offer insights into the role these molecules play in the development and course of EAE in these mice. Furthermore, FISH staining of small intestine and colon samples fixated in Carnoy's fixative for RegIIIγ, Muc2 along with a universal 16S rRNA gene probe could provide visual clues of the bacterial location in respect to the villus tip of the epithelial cell wall. In addition, semiquantitative PCR of bacterial 16S gene using DNA isolated from the loose and firm mucus layers of small intestine and colon using guanidinium chloride (Johansson et al. 2008) could provide additional evidence on the location of the bacteria within mucus layer. We theorize that an overall defect into these components, along with the slight increase in gut permeability, could facilitate the diffusion and sampling of bacterial antigens into the lamina propria. This increase in the access of bacterial products from commensal bacteria could potentially skew MyD88^{ΔIEC} mice into developing stronger pro-inflammatory responses that could lead to a severe aEAE course.

4.1.2. Effect of intestinal epithelial MyD88 signals in cells from the innate and adaptive immune system

MyD88 –dependent signals play an important role in the prompt activation of cells from the innate immune population necessary for initial containment of an infection. Upon activation through PRR recognition, these cells (i.e., dendritic cells, macrophages, neutrophils) express an appropriate array of cytokines and co-stimulatory molecules that activate and direct the adaptive immune response required for full pathogen clearance. Based on this, we evaluated whether intrinsic MyD88 signals in IECs have an influence in Ly6C⁺Ly6G⁻ monocytes and Ly6C⁺Ly6G⁺ neutrophils of MyD88^{ΔIEC} mice. Our observations reveal that the frequencies of global Ly6C⁺Ly6G⁻ monocytes and Ly6C⁺Ly6G⁺ neutrophils remain unchanged in these mice (Figure 3.1.3.4), suggesting that epithelial MyD88 signals do not have a profound effect in these cells in steady-state mice.

A local cell within the lamina propria that could offer further insight into this proposed mechanism is the lamina propria DC. In recent years, lamina propria DCs have been extensively studied due to their involvement in initiating autoimmune reactions. Local DCs are reported to access bacterial products through different routes. First, specialized M cells within the Peyer's patches could transcytose bacterial products followed by nearby lamina propria DCs uptake. Second, bacterial products can be directly sensed by local DC through the projection of dendrites through the epithelial-cell layer. Lamina propria DCs have been reported to form tight-junction-like structures with intestinal epithelial cells that allow them to project their dendrites through the epithelial-cell layer and sample bacteria from the intestinal lumen (Rescigno et al. 2001). The projection of dendrites by lamina propria DCs across the intestinal epithelium is thought to require MyD88-dependent signaling through TLRs and the chemokine receptor CX3CR1 (Chieppa et al. 2006; Niess et al. 2005). Based on these reports, it would be of special interest to quantify the bacterial load of DCs from MyD88^{ΔIEC} mice along with both controls strains (MyD88^{KO} and MyD88^{F/F} mice) in both steady-state and diseased mice in order to evaluate whether DCs from MyD88^{ΔIEC} mice present a more pathogenic profile than control mice. In addition, it would be of great interest to include EAE experiments in MyD88^{ΔCD11c} mice to evaluate whether DC signals of MyD88 could prevent the development of EAE in these mice or whether they exhibit lower incidence in the spontaneous development of EAE when crossing these mice with OSE mice.

The involvement of intrinsic MyD88 signals of IECs in the local humoral immune response has also been acknowledged when it was discovered that polarized epithelial cells mediate the transcytosis of IgA from the lamina propria into the intestinal lumen through the upregulation of the polymeric immunoglobulin

receptor (pIgR) (Johansen and Kaetzel 2011; Kaetzel et al. 1991; Turula and Wobus 2018). In addition, epithelial TLR activation also triggers class switch recombination and IgA secretion by B cells in a T cell-independent fashion (He et al. 2007). Since the presence of IgA in the gut tissues is of great importance in locally limiting the interaction of the gut microbiota with the host, we explored whether the deletion of MyD88 in IEC have an impact in the quantities of IgA present in fecal samples and serum in steady-state MyD88^{ΔIEC} mice. We observed that the abundance of sIgA in fecal samples (Figure 3.1.3.5) as well as for the amounts of immunoglobulins IgA, IgM and IgG in serum (Figure 3.1.3.6) are not significantly affected in steady-state MyD88^{ΔIEC} mice.

Aside from the roles of epithelial MyD88 discussed in the above sections MyD88 signaling pathways are known to modulate the initiation of local adaptive immune responses in the GALT (Akira and Takeda 2004; Tezuka and Ohteki 2019; Wang et al. 2011; Uematsu et al. 2008). Adaptive immunological responses accountable for shaping the course of EAE in OSE mice are known to require the presence of the commensal gut microbiota (Berer et al. 2011). For instance, a reduction of Th17-like cells in the lamina propria and Peyer's patches of germ-free RR mice was observed. In a similar manner, the production of MOG-specific IgG2a antibodies in these mice was also reduced. Based on this, we explored the effect of MyD88-signalling in the development of EAE by profiling the local gut immune response in steady-state MyD88^{ΔIEC} mice. The local Th1 and Th17 proinflammatory responses in GALT tissues, characterized by the presence of resident CD3⁺CD4⁺ T cells that produce cytokines IFN-γ and IL-17 respectively, showed to not be influenced by the absence of epithelial MyD88-dependent signals as the frequency of these T cells do not differ between MyD88-sufficient- and MyD88^{ΔIEC} mice (Figure 3.1.3.1). The lack of changes in the frequencies of Th17-producing CD4⁺ T cells in the lamina propria of small intestine could be explained by looking at the abundance of SFB in fecal pellets of MyD88^{ΔIEC} mice depicted in Figure 3.1.4.1. SFB bacteria are known to be potent inducers of Th17-cells in the small intestine (Gaboriau-Routhiau et al. 2009; Ivanov et al. 2009; Wu et al. 2010) and in the case of MyD88^{ΔIEC} mice the abundance of these bacteria did not differ from MyD88-sufficient mice. The normal SFB abundance observed in MyD88^{ΔIEC} mice could be further explained by a report from Wang and colleagues that identified a MyD88-dependent mechanism responsible for the control of SFB within the gut microbiota (Wang et al. 2015). In this report, a mechanism involving MyD88-Stat3-dependent sensing of the microbiota by Tregs was reported to favor commensalism by promoting anti-commensal IgA responses; therefore, controlling the Th17 expansion by preventing SFB overgrowth. This study could explain the reason behind the frequencies of Th17-producing CD4⁺ T cells observed in MyD88^{ΔIEC}

mice as Tregs, although present in lower frequencies in the gut tissues, could still have functional intrinsic MyD88 signals in these mice.

When looking at the intestinal Th2 anti-inflammatory immune responses, a slight but not significant reduction in IL4 and IL-10 production by CD3⁺CD4⁺ T cells in SiLPL of MyD88^{ΔIEC} mice was observed when compared to control mice. Additionally, a significant reduction in the frequencies of regulatory T cells (Tregs) in the SiLPL of MyD88^{ΔIEC} mice was observed, further supporting the slight reduction of IL-10 in the SiLPL as FoxP3⁺ Tregs produce, although not exclusively, IL-10 in these tissues. Taken altogether, intestinal MyD88 signals alone appear to be insufficient to cause striking changes in gut adaptive immune responses of steady-state mice that would point out to an involvement of these pathways in a triggering role in the development of EAE. The alterations observed in the SiLPL are statistically not significant for Th2 cytokines but are rather subtle, and alterations caused by the lack of epithelial MyD88 signals are only significant when quantifying the frequencies of FoxP3⁺ Tregs present in this tissue. Such subtle changes could support the notion that that MyD88 signals delicately maintain the balance between pro- and anti-inflammatory responses in gut tissues (Araki et al. 2005; Gibson et al. 2008; Malvin et al. 2012; Rakoff-Nahoum et al. 2004) and point out to a modulatory role, rather than triggering one, of this pathway in the development of EAE in MyD88^{ΔIEC}. Taken together, we speculate that the exacerbated EAE observed in MyD88^{ΔIEC} mice could be the result of these mice lacking enough FoxP3⁺ Tregs in the SiLPL necessary to control the inflammatory responses that unleash the observed course of EAE.

4.1.5 Composition of the local gut microbiota in steady-state MyD88^{ΔIEC} mice

Based on reports that epithelial MyD88 signals can help shaping the microbiota composition in the gut (Wang et al. 2015; Round et al. 2011), we studied several aspects of the gut microbiota from MyD88^{ΔIEC} mice, along with control mice, in order to explore whether we could detect any changes to the microbiota that could offer hints on the mechanism behind the aEAE phenotype observed. When looking at the relative abundance of SFB across all groups, we notice that there are no significant changes resulting from the deletion of MyD88 in IECs (Figure 3.1.4.1). This, as explained in section 4.1.2, could be due to the ability of Tregs to control SFB overgrowth in a MyD88-Stat3-dependent pathway. When comparing the composition of the local gut microbiota, we also notice that there are no significant differences within the 3 groups of mice (Figure 3.1.4.3), indicating that the microbiota of steady-state MyD88^{ΔIEC} mice remains unchanged upon the absence of MyD88 in IECs. When further

analyzing the gut bacterial communities in terms of their alpha and beta diversity, epithelial MyD88 signals appear to cause no striking differences in steady-state MyD88^{ΔIEC} mice (Figure 3.1.4.2). A tendency for a slight change at the order level was observed for MyD88^{KO} mice. This tendency involves a shift towards the Clostridiales order, but this shift is not statistically significant. The microbial-host crosstalk is a bidirectional pathway in which one actively influences the other and changes in the balance from either side causes relevant changes onto the other side. Therefore, it is plausible to think that the gut microbiota in MyD88^{ΔIEC} mice could undergo major changes in their composition upon the development of EAE as no changes were observed in steady-state mice. It is possible that the bidirectional nature of the microbiota host crosstalk could favor a change in the microbiota based on the changes in the immune system that these mice could experience during EAE.

Taken altogether, we propose that the severe aEAE course observed in MyD88^{ΔIEC} mice could be due to these mice being skewed to aberrant inflammatory responses due to the effect epithelial MyD88 signals exert in the integrity of the intestinal epithelial cell wall and in the local Treg population. It is known that commensal bacteria display the same immunostimulatory molecules as pathogenic bacteria and commensal microbiota has been shown to trigger inflammation and disease if they penetrate the intestinal epithelial barrier. Therefore, we propose that the slight increased gut permeability observed in steady-state MyD88^{ΔIEC} mice could allow local DCs an easier access to bacterial antigens. These DCs could sample PAMPs from the local gut microbiota and transport these antigens to the MLNs where cells from the adaptive immune system, such as CD4⁺ T cells, can become activated. The subsequent pro-inflammatory responses caused by these events could probably not be suppressed by the local FoxP3⁺ Tregs cells due to their reduced frequencies in the small intestine. In addition, the low frequencies of IL-10 producing T cells observed in the small intestinal lamina propria could further contribute to the lower frequencies local FoxP3⁺ T regs cells, as IL-10 is thought to be required for the maintenance of this cell in the lamina propria (Denning et al. 2011). Defects in the anti-inflammatory and regulatory responses combined with a potential increase in antigen presentation by local DCs could favor uncontrolled Th1/Th17 inflammatory responses that could exacerbate the course of EAE in MyD88^{ΔIEC} mice. This, in combination with a potential reduction in AMP production and a defect in the mucus layer could cause changes in the bacterial composition of the gut microbiota that could potentially favor Th1 and Th17 inflammatory responses even further. These enhanced pro-inflammatory responses could explain the higher incidence and severity of EAE development in MyD88^{ΔIEC} mice; however, further studies are required to test this hypothesis.

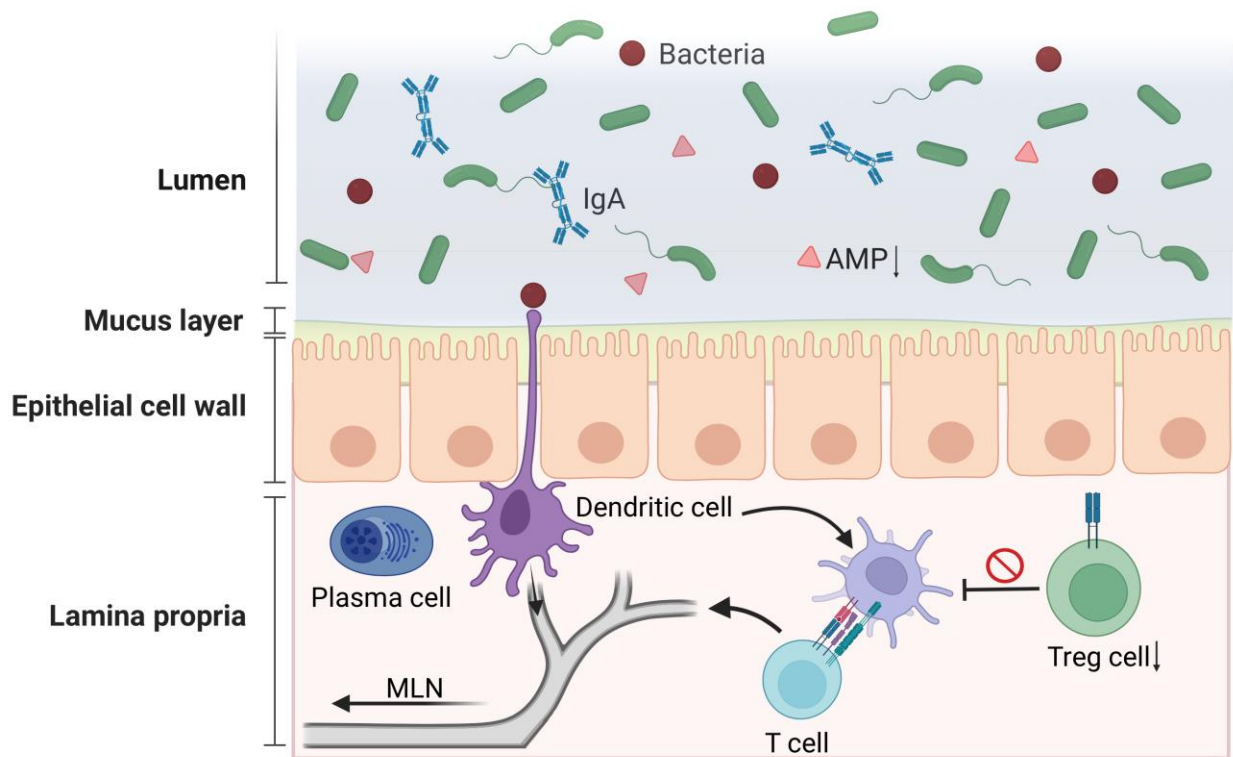


Figure 4.1. Proposed mechanism for a local gut inflammatory event that could lead to severe EAE in $MyD88^{\Delta IEC}$ mice.

Absence of MyD88 signals favors a slight increase in the permeability of the intestinal epithelial cell wall in steady-state $MyD88^{\Delta IEC}$ mice. This would allow local dendritic cells (DCs) an easier access through the epithelial cell wall to sample for commensal antigens. DCs that have taken-up commensal antigens could interact with resident T cells, activate them and initiate inflammatory responses. The inflammatory responses would not be suppressed as the frequency of local regulatory T cells (Tregs) is decreased. In addition, local dendritic cells could migrate into MLNs and activate naïve T cells and further enhance the inflammatory response. Activated T cells would ultimately migrate into the CNS and initiate EAE development (Created with Biorender.com by Veronica Solis)

4.2 The challenges of establishing in-vivo and in-vitro experiments to assess T cell activation in the gut

As of today, the etiology of MS is unknown and the triggering mechanism that develops in the early stages of the disease remains undiscovered. Several theories have been proposed to explain how MS is triggered in the periphery but so far, no consensus between these theories has been reached. A popular theory is that previous infections increase the risk of developing MS through a mechanism known as molecular mimicry. Molecular mimicry is one hypothesis suggested which could reconcile the diverse pathology and etiology of MS. Molecular mimicry occurs when peptides from pathogens share sequence or structural similarities with self-antigens, are recognized by the host and initiate autoimmune processes. In the case of MS, infection with certain virus strains and bacteria has been identified to increase the risk of developing MS (Libbey et al. 2007). Though many viruses have been shown to be associated with MS, no one virus has ever been demonstrated to be the cause of MS. However, the idea that a viral infection may play a role in MS development has a long story and this theory is supported by observations that demonstrate a link between B –cell tropic Epstein-Baar Virus (EBV) and the onset of the disease. Nearly all MS patients exhibit evidence of past EBV infection and an intermittent reactivation of the virus during the active MS course may occur along with exacerbations in relapsing remitting MS patients (Lucas et al. 2011). It has been reported that after the onset of MS, antibody responses directed against EBV antigens correlate with the activity and the progression of the disease (Christensen 2006). In addition, EBV epitopes are reported to elicit a humoral response in sera and CSF samples from MS patients, suggesting that an infection with this virus enhances inflammation in MS potentially by antibodies from the host cross-reacting to these peptides (Mameli et al. 2016; Mameli et al. 2014).

Although a potential cross-reactivity of peptides from virus is being often described in the literature for this disease, molecular mimicry in the context of MS by commensal bacterial peptides has not been proved. In order to evaluate whether bacterial antigens could trigger the early events of MS pathogenesis, we attempted to establish an in-vitro and in-vivo system. The first steps taken into establishing both in-vivo and in-vitro system were aimed to generate a retroviral plasmid that could express a protein that would allow the study of activation events on T cells. As described in section 1.4.2, the calcium-dependent translocation of NFAT upon T cell activation makes this protein a fitting candidate for this purpose. To this end, we designed a plasmid that features the insert NFAT-TRE-sGFP. This insert contains four NFAT transcriptional response elements (TRE), where NFAT molecules bind

upon following the activation of TCR-bearing cells that express the NFAT-TRE-sGFP sequence. The binding of NFAT molecules to these TRE would then drive the transcription of GFP that would ultimately allow the detection of GFP either through FACS or IHC staining. In this approach, the transduction of hybridomas (in-vitro approach) or splenocytes (in-vivo approach) with NFAT-TRE-sGFP would allow them to be studied for activation events following stimulation with either PMA/ionomycin or in the presence of APCs loaded with lysate from gut contents from mice for in-in vitro approach and endogenous stimulation for in-vivo approach . Upon activation, the detection of GFP could be performed through FACS after stimulation as GFP⁺ cells can still be detected 24 hours after stimulation based on our experiments.

4.2.1. Designing a T-cell hybridoma as in-vitro tool for antigen screening

For the in-vitro approach, the generation of a MOG-specific T cell hybridoma through PEG fusion of 2D2 splenocytes and BW5147, a T lymphoblast cell line, was performed. The goal of this approach was to establish a screening approach where MOG-specific hybridoma cells would be cultured with lysate from gut contents of mice in the presence of APCs in order to identify possible commensal bacterial antigens that could favor EAE development. When establishing the cell line, we observed that the viral infection of these hybrids with pQC-NFAT-TRE-sGFP retroviral plasmid proved unsuccessful as no GFP expression was detected after quantifying its expression by FACS. A possible explanation for the resistance of these cells to retroviral infection is the loss of the required machinery for viral particle uptake post-PEG fusion. PEG fusion is an approach that aids in the fusion of two cells; however, the procedure does not guarantee fully functional cells and it could be possible that the machinery required for taking up retroviral particles was lost or damaged during the fusion process. Furthermore, we ruled out issues with the technique itself as GFP expression was detected by FACS in 3T3, HEK293T cells lines after retroviral transduction.

Having established that the 2D2-TCH-B9 hybridomas were resistant to retroviral infection, target sequence NFAT-TRE-sGFP was cloned into a pcDNA6 plasmid to be able to generate stable hybridoma cells either by the usage of transfection reagents or through electroporation. Similar to experiments involving retroviral infection of 2D2-TCH-B9 hybridomas, these cells are unable to take up our target plasmid by any of the techniques mentioned above. A GFP expression was detected only in BW5147 control cells by FACS after PMA/Ionomycin stimulation. Interestingly, 2D2-TCH-B9 hybridoma cells were able to take up control plasmid pMAX-GFP as GFP expression was detected by in these cells by FACS.

Based on this, we assume that the size of the plasmid influences greatly the efficiency in which 2D2-TCH-B9 hybridoma cells can incorporate a given plasmid. We know that control plasmid pMAX-GFP (3486bp) is smaller than target plasmid pCDNA6-NFAT-TRE-sGFP (7405bp). This difference in size offers an explanation as to why 2D2-TCH-B9 hybridoma cells efficiently take up our control plasmid but not our target plasmid. In summary, we concluded that 2D2-TCH-B9 hybridoma cells were resistant to retroviral infection or unable to incorporate big-sized plasmids through a variety of techniques.

Having observed that BW5147 hybridoma cells easily incorporated our target sequence (Figure 3.2.1.7) through retroviral transduction, the cloning technique to achieve our stable hybridoma cell line was reversed. To this end, we first decided to introduce our target sequence into BW5147 cells to generate a stably-transduced cell line that would then be fused with 2D2 splenocytes. To this end, BW5147 were infected with NFAT-TRE-sGFP retroviral supernatant and sorted for their expression of GFP. After expanding these cells, PEG fusion with 2D2 splenocytes was performed but after culturing under selective conditions, none of the clones survived indicating that none of the clones successfully fused with 2D2 splenocytes. This was a one-time experiment that require further attempts to achieve stably-expressing NFAT-TRE-sGFP BW5147 hybridomas cells. Once achieved, experiments to test the capability of stably-expressing NFAT-TRE-sGFP BW5147 hybridomas cells to recognize MOG₃₅₋₅₅ through IL-2 ELISA or through other alternate methods such as FACS, immunohistochemistry or fluorescence microscopy and tests to determine the sensitivity of these cells would be required for establishing this method prior to screening for bacterial peptides.

4.2.2. Establishing an in-vivo approach for the study of early T cell activation events in EAE

Since our ultimate goal is to elucidate whether the commensal microbiota plays a direct role in the early activation events of autoreactive T cells in the GALT, we attempted to establish an in-vivo approach. To this end, we first performed transfer experiments in order to determine the number of cells required to transfer into recipient mice in order to have sufficient cells available in the lamina propria of the gut for analysis. The transfer of B-cell depleted splenocytes lead to the recovery of less than 1% of GFP⁺ cells from the gut tissues of recipient mice. We determined that a transfer of purified CD4⁺ T cells could improve the frequencies of recovered cells from these tissue as the cell suspension used to the transfer experiment would be devoid from other cell types that otherwise lower the amount of actual CD4⁺ T cells present in the cell suspension. A trial experiment performed (data not shown) where 18×10^6 purified, polyclonal actin-GFP CD4⁺ T cells were transferred to each mice demonstrated an increase in the percentage of GFP⁺ cells recovered from gut tissues. Of major improvement were the frequencies

observed in the ileum and colon, with frequencies of 1% and 5%, respectively. However, this experiment was performed once and variations in the frequencies of these cells are known to occur between experiments. Further replicates of this experiment are required before drawing further conclusions.

Although we knew the condition is not optimal, we performed a trial experiment in which C57BL/6 mice would receive a B-cell depleted splenocytes cell suspension from OT-II mice, a transgenic mice strain where their T cells carry a TCR recognizing OVA₃₂₃₋₃₃₉ peptide in the context of I-A^b. In this experiments, the transfer of OT-II cells to C57BL/6 mice followed by gavage with ovalbumin (OVA) showed proliferation of CD4⁺CD45⁺ Vα2⁺Vβ6⁺ T cells that was hinted by the increase of proliferation marker Ki67 in CD4⁺CD45⁺ Vα2⁺Vβ6⁺ T cells recovered from the ileum segment of PBS-treated compared to untreated C57BL/6 mice (Fig. 3.2.2.3B). This proliferation suggests that transferred CD4⁺CD45⁺ Vα2⁺Vβ6⁺ T cells that are present in the gut tissues are capable of become activating and proliferate when encountering their cognate peptide. This observation is further supported by the increase in CD25 expression by CD4⁺CD45⁺ Vα2⁺Vβ6⁺ T cells in OVA treated mice when compared control groups. However, when evaluating the expression of early activation marker CD69 in CD4⁺CD45⁺ Vα2⁺Vβ6⁺ T cells, we noted that mice gavaged with PBS or ovalbumin show an increase in their CD69 expression throughout all harvested organs. This increase in the expression of CD69 was not observed in untreated mice. These observations suggest that the handling of the mice during the gavage procedure could cause an unspecific activation of transferred CD4⁺CD45⁺ Vα2⁺Vβ6⁺ T cells. The unspecific activation of transferred cells in gut tissues observed in our experiments represents a major issue to studying early activation events in the context of EAE. Based on our experiments, we conclude that the transferred naïve CD4⁺ T cells can be activated in the gut tissues upon encountering their cognate peptide, as demonstrated by the gavage experiment. However, we observed that the handling of the mice during the gavage procedure is enough to exert unspecific activation events that could disguise real pathogen-derived activation. Furthermore, the amount of cells required for analysis still requires improvement as low numbers between 1 and 5% of total T cells for further analysis could represent a challenge when interpreting results. Recoverable cells from the gut tissues require higher numbers that could offer better opportunities for statistical analysis.

Finally, the ultimate goal to transfer NFAT-TRE-sGFP CD4⁺2D2⁺ T cells into recipient mice would seem rather unlikely as the infection of CD4⁺ T cells with this construct did not lead to GFP expression after PMA/Ionomycin stimulation. We assume that, similar to hybridoma cells, the size of pQC-NFAT-TRE-

sGFP plasmid (6803bp) might have a negative impact in the retroviral infection efficiency of T cells. In accordance to results from other colleagues, changing the vector backbone from pQC to pMSCV could improve transduction efficiency in hybridoma cells. In addition, it can be that the backbone used for delivering target sequence NFAT-TRE-SGFP is not easily taken-up by CD4⁺ T cells. An alternative approach to circumvent these issues is assessing T-cell activation events by using a GFP-labeled truncated version of NFAT-1 that is reported to translocate from the cytoplasm into the nucleus within seconds post-activation events and lasting for around one hour after stimulus is removed (Pesic et al. 2013). This approach would involve the transfer of 2D2⁺CD4⁺T cells infected with Δ NFAT-GFP into recipient mice and promptly assess for their activation status using an in-vivo setting using cutting-edge technology similar to the one described by Rakhlin and colleagues (Rakhilin et al. 2019). In their paper, Rakhilin and colleagues implanted an intravital window to image, track and study the transferred cells live in-vivo in the colonic tissue. This combined approach could offer an opportunity to visualize possible activation 2D2⁺CD4⁺T cells in relevant gut tissues. To this end, kinetic experiments would be required to identify the best possible time point for observing T cell activation events in gut tissues. Likewise, experiments to determine the ideal amount of 2D2⁺CD4⁺ T cells for adoptive transfer would be a must.

A role for the commensal bacteria in stimulating encephalitogenic T cells in the lamina propria has been demonstrated through intravital imaging in one recent study (Fang 2018). In this study, encephalitogenic, but not polyclonal, T cells display continuous calcium signaling in the lamina propria. The continuous signaling was induced by APC as encephalitogenic T cells from mice that were treated with an anti-MHC Class II blocking antibody show diminished calcium signaling. Furthermore, it was demonstrated that the commensal microbiota is relevant for this event, as encephalitogenic T cells in germ-free mice do not show any calcium signaling. This study nicely shows, once again, that the commensal microbiota is a key player in influencing the host's immune responses. However, when looking at the literature, we find that the gut microbiota influences EAE pathogenesis rather indirectly by the production of various metabolic by-products or through alternative mechanisms that skew the immune system into unleashing pro-inflammatory responses that ultimately lead to EAE. Nevertheless, such discovery would certainly revolutionize the way we see the commensal bacteria in the context of autoimmunity.

References

- Abreu, M. T. 2010a. Erratum: Toll-like receptor signalling in the intestinal epithelium: how bacterial recognition shapes intestinal function. *Nature Reviews Immunology* 10 (3):215-215.
- . 2010b. Toll-like receptor signalling in the intestinal epithelium: how bacterial recognition shapes intestinal function. *Nature Reviews Immunology* 10 (2):131-144.
- Akira, S., and K. Takeda. 2004. Toll-like receptor signalling. *Nat Rev Immunol* 4 (7):499-511.
- Araki, A., T. Kanai, T. Ishikura, S. Makita, K. Uraushihara, R. Iiyama, T. Totsuka, K. Takeda, S. Akira, and M. Watanabe. 2005. MyD88-deficient mice develop severe intestinal inflammation in dextran sodium sulfate colitis. *J Gastroenterol* 40 (1):16-23.
- Atarashi, K., J. Nishimura, T. Shima, Y. Umesaki, M. Yamamoto, M. Onoue, H. Yagita, N. Ishii, R. Evans, K. Honda, and K. Takeda. 2008. ATP drives lamina propria T(H)17 cell differentiation. *Nature* 455 (7214):808-812.
- Atarashi, K., T. Tanoue, T. Shima, A. Imaoka, T. Kuwahara, Y. Momose, G. Cheng, S. Yamasaki, T. Saito, Y. Ohba, T. Taniguchi, K. Takeda, S. Hori, Ivanov, II, Y. Umesaki, K. Itoh, and K. Honda. 2011. Induction of colonic regulatory T cells by indigenous *Clostridium* species. *Science* 331 (6015):337-341.
- Baecher-Allan, C., B. J. Kaskow, and H. L. Weiner. 2018. Multiple Sclerosis: Mechanisms and Immunotherapy. *Neuron* 97 (4):742-768.
- Berer, K., L. A. Gerdes, E. Cekanaviciute, X. Jia, L. Xiao, Z. Xia, C. Liu, L. Klotz, U. Stauffer, S. E. Baranzini, T. Kumpfel, R. Hohlfeld, G. Krishnamoorthy, and H. Wekerle. 2017. Gut microbiota from multiple sclerosis patients enables spontaneous autoimmune encephalomyelitis in mice. *Proc Natl Acad Sci U S A* 114 (40):10719-10724.
- Berer, K., and G. Krishnamoorthy. 2014. Microbial view of central nervous system autoimmunity. *FEBS Lett* 588 (22):4207-4213.
- Berer, K., M. Mues, M. Koutrolos, Z. A. Rasbi, M. Boziki, C. Johner, H. Wekerle, and G. Krishnamoorthy. 2011. Commensal microbiota and myelin autoantigen cooperate to trigger autoimmune demyelination. *Nature* 479 (7374):538-541.
- Bettelli, E., M. Pagany, H. L. Weiner, C. Lington, R. A. Sobel, and V. K. Kuchroo. 2003. Myelin oligodendrocyte glycoprotein-specific T cell receptor transgenic mice develop spontaneous autoimmune optic neuritis. *J Exp Med* 197 (9):1073-1081.
- Brownlee, W. J., T. A. Hardy, F. Fazekas, and D. H. Miller. 2017. Diagnosis of multiple sclerosis: progress and challenges. *Lancet* 389 (10076):1336-1346.
- Burgueño, J. F., and M. T. Abreu. 2020. Epithelial Toll-like receptors and their role in gut homeostasis and disease. *Nat Rev Gastroenterol Hepatol* 17 (5):263-278.
- Buscarinu, M. C., S. Romano, R. Mechelli, R. Pizzolato Umeton, M. Ferraldeschi, A. Fornasiero, R. Reniè, B. Cerasoli, E. Morena, C. Romano, N. D. Loizzo, R. Umeton, M. Salvetti, and G. Ristori. 2018. Intestinal Permeability in Relapsing-Remitting Multiple Sclerosis. *Neurotherapeutics* 15 (1):68-74.
- Cai, S. Y., D. Yu, C. J. Soroka, J. Wang, and J. L. Boyer. 2021. Hepatic NFAT signaling regulates the expression of inflammatory cytokines in cholestasis. *J Hepatol* 74 (3):550-559.
- Cario, E. 2010. Toll-like receptors in inflammatory bowel diseases: a decade later. *Inflamm Bowel Dis* 16 (9):1583-1597.
- Ciccarelli, O., F. Barkhof, B. Bodini, N. De Stefano, X. Golay, K. Nicolay, D. Pelletier, P. J. Pouwels, S. A. Smith, C. A. Wheeler-Kingshott, B. Stankoff, T. Yousry, and D. H. Miller. 2014. Pathogenesis of multiple sclerosis: insights from molecular and metabolic imaging. *Lancet Neurol* 13 (8):807-822.

- Compston, A., and A. Coles. 2002. Multiple sclerosis. *Lancet* 359 (9313):1221-1231.
- Chen, J., K. Bittinger, E. S. Charlson, C. Hoffmann, J. Lewis, G. D. Wu, R. G. Collman, F. D. Bushman, and H. Li. 2012. Associating microbiome composition with environmental covariates using generalized UniFrac distances. *Bioinformatics* 28 (16):2106-2113.
- Chieppa, M., M. Rescigno, A. Y. Huang, and R. N. Germain. 2006. Dynamic imaging of dendritic cell extension into the small bowel lumen in response to epithelial cell TLR engagement. *J Exp Med* 203 (13):2841-2852.
- Christensen, T. 2006. The role of EBV in MS pathogenesis. *Int MS J* 13 (2):52-57.
- Christo, S. N., K. R. Diener, and J. D. Hayball. 2015. The functional contribution of calcium ion flux heterogeneity in T cells. *Immunol Cell Biol* 93 (8):694-704.
- Chun, J., J. H. Lee, Y. Jung, M. Kim, S. Kim, B. K. Kim, and Y. W. Lim. 2007. EzTaxon: a web-based tool for the identification of prokaryotes based on 16S ribosomal RNA gene sequences. *Int J Syst Evol Microbiol* 57 (Pt 10):2259-2261.
- Dendrou, C. A., L. Fugger, and M. A. Friese. 2015. Immunopathology of multiple sclerosis. *Nat Rev Immunol* 15 (9):545-558.
- Denning, T. L., B. A. Norris, O. Medina-Contreras, S. Manicassamy, D. Geem, R. Madan, C. L. Karp, and B. Pulendran. 2011. Functional specializations of intestinal dendritic cell and macrophage subsets that control Th17 and regulatory T cell responses are dependent on the T cell/APC ratio, source of mouse strain, and regional localization. *J Immunol* 187 (2):733-747.
- Depaolo, R. W., F. Tang, I. Kim, M. Han, N. Levin, N. Ciletti, A. Lin, D. Anderson, O. Schneewind, and B. Jabri. 2008. Toll-like receptor 6 drives differentiation of tolerogenic dendritic cells and contributes to LcrV-mediated plague pathogenesis. *Cell Host Microbe* 4 (4):350-361.
- Derkow, K., J. M. Bauer, M. Hecker, B. K. Paap, M. Thamilasan, D. Koczan, E. Schott, K. Deuschle, J. Bellmann-Strobl, F. Paul, U. K. Zettl, K. Ruprecht, and S. Lehnardt. 2013. Multiple sclerosis: modulation of toll-like receptor (TLR) expression by interferon-beta includes upregulation of TLR7 in plasmacytoid dendritic cells. *PLoS One* 8 (8):e70626.
- DeSantis, T. Z., P. Hugenholtz, N. Larsen, M. Rojas, E. L. Brodie, K. Keller, T. Huber, D. Dalevi, P. Hu, and G. L. Andersen. 2006. Greengenes, a chimera-checked 16S rRNA gene database and workbench compatible with ARB. *Appl Environ Microbiol* 72 (7):5069-5072.
- Diehl, G. E., R. S. Longman, J.-X. Zhang, B. Breart, C. Galan, A. Cuesta, S. R. Schwab, and D. R. Littman. 2013. Microbiota restricts trafficking of bacteria to mesenteric lymph nodes by CX(3)CR1(hi) cells. *Nature* 494 (7435):116-120.
- Dyment, D. A., G. C. Ebers, and A. D. Sadovnick. 2004. Genetics of multiple sclerosis. *Lancet Neurol* 3 (2):104-110.
- Edgar, R. C. 2010. Search and clustering orders of magnitude faster than BLAST. *Bioinformatics* 26 (19):2460-2461.
- . 2013. UPPARSE: highly accurate OTU sequences from microbial amplicon reads. *Nat Methods* 10 (10):996-998.
- Edgar, R. C., B. J. Haas, J. C. Clemente, C. Quince, and R. Knight. 2011. UCHIME improves sensitivity and speed of chimera detection. *Bioinformatics* 27 (16):2194-2200.
- Endriz, J., P. P. Ho, and L. Steinman. 2017. Time correlation between mononucleosis and initial symptoms of MS. *Neurol Neuroimmunol Neuroinflamm* 4 (3):e308.
- Falk, P. G., L. V. Hooper, T. Midtvedt, and J. I. Gordon. 1998. Creating and maintaining the gastrointestinal ecosystem: what we know and need to know from gnotobiology. *Microbiol Mol Biol Rev* 62 (4):1157-1170.
- Fang, P. 2018. Visualizing the stimulation of encephalitogenic T cells in gut associated lymphoid tissue as a trigger of autoimmunity. Dissertation, LMU Munich.
- Feske, S. 2007. Calcium signalling in lymphocyte activation and disease. *Nat Rev Immunol* 7 (9):690-702.

- Frantz, A. L., E. W. Rogier, C. R. Weber, L. Shen, D. A. Cohen, L. A. Fenton, M. E. Bruno, and C. S. Kaetzel. 2012. Targeted deletion of MyD88 in intestinal epithelial cells results in compromised antibacterial immunity associated with downregulation of polymeric immunoglobulin receptor, mucin-2, and antibacterial peptides. *Mucosal Immunol* 5 (5):501-512.
- Fukata, M., K. S. Michelsen, R. Eri, L. S. Thomas, B. Hu, K. Lukasek, C. C. Nast, J. Lechago, R. Xu, Y. Naiki, A. Soliman, M. Ardit, and M. T. Abreu. 2005. Toll-like receptor-4 is required for intestinal response to epithelial injury and limiting bacterial translocation in a murine model of acute colitis. *Am J Physiol Gastrointest Liver Physiol* 288 (5):G1055-1065.
- Gaboriau-Routhiau, V., S. Rakotobe, E. Lécuyer, I. Mulder, A. Lan, C. Bridonneau, V. Rochet, A. Pisi, M. De Paepe, G. Brandi, G. Eberl, J. Snel, D. Kelly, and N. Cerf-Bensussan. 2009. The key role of segmented filamentous bacteria in the coordinated maturation of gut helper T cell responses. *Immunity* 31 (4):677-689.
- Gerth, A. J., L. Lin, M. F. Neurath, L. H. Glimcher, and S. L. Peng. 2004. An innate cell-mediated, murine ulcerative colitis-like syndrome in the absence of nuclear factor of activated T cells. *Gastroenterology* 126 (4):1115-1121.
- Gibson, D. L., C. Ma, K. S. Bergstrom, J. T. Huang, C. Man, and B. A. Vallance. 2008. MyD88 signalling plays a critical role in host defence by controlling pathogen burden and promoting epithelial cell homeostasis during *Citrobacter rodentium*-induced colitis. *Cell Microbiol* 10 (3):618-631.
- Gödel, C., B. K., G. Krishnamoorthy, and H. Wekerle. 2015. Alteration of the intestinal microbiota by short-time antibiotics protects mice from CNS-specific autoimmunity. *Journal of the Neurological Sciences* 357.
- Greer, J. M., and P. A. McCombe. 2011. Role of gender in multiple sclerosis: clinical effects and potential molecular mechanisms. *J Neuroimmunol* 234 (1-2):7-18.
- Guo, S., M. Nighot, R. Al-Sadi, T. Alhmoud, P. Nighot, and T. Y. Ma. 2015. Lipopolysaccharide Regulation of Intestinal Tight Junction Permeability Is Mediated by TLR4 Signal Transduction Pathway Activation of FAK and MyD88. *J Immunol* 195 (10):4999-5010.
- Haahr, S., A. M. Plesner, B. F. Vestergaard, and P. Hollsberg. 2004. A role of late Epstein-Barr virus infection in multiple sclerosis. *Acta Neurol Scand* 109 (4):270-275.
- Handel, A. E., G. Giovannoni, G. C. Ebers, and S. V. Ramagopalan. 2010. Environmental factors and their timing in adult-onset multiple sclerosis. *Nat Rev Neurol* 6 (3):156-166.
- Handel, A. E., M. R. Lincoln, and S. V. Ramagopalan. 2011. Of mice and men: experimental autoimmune encephalitis and multiple sclerosis. *Eur J Clin Invest* 41 (11):1254-1258.
- Harbo, H. F., R. Gold, and M. Tintore. 2013. Sex and gender issues in multiple sclerosis. *Ther Adv Neurol Disord* 6 (4):237-248.
- Harirchian, M. H., F. Fatehi, P. Sarraf, N. M. Honarvar, and S. Bitarafan. 2018. Worldwide prevalence of familial multiple sclerosis: A systematic review and meta-analysis. *Mult Scler Relat Disord* 20:43-47.
- Hauser, S. L., A. Bar-Or, G. Comi, G. Giovannoni, H. P. Hartung, B. Hemmer, F. Lublin, X. Montalban, K. W. Rammohan, K. Selmaj, A. Traboulsee, J. S. Wolinsky, D. L. Arnold, G. Klingelschmitt, D. Masterman, P. Fontoura, S. Belachew, P. Chin, N. Mairon, H. Garren, and L. Kappos. 2017. Ocrelizumab versus Interferon Beta-1a in Relapsing Multiple Sclerosis. *N Engl J Med* 376 (3):221-234.
- He, B., W. Xu, P. A. Santini, A. D. Polydorides, A. Chiu, J. Estrella, M. Shan, A. Chadburn, V. Villanacci, A. Plebani, D. M. Knowles, M. Rescigno, and A. Cerutti. 2007. Intestinal bacteria trigger T cell-independent immunoglobulin A(2) class switching by inducing epithelial-cell secretion of the cytokine APRIL. *Immunity* 26 (6):812-826.

- Hill, D. A., M. C. Siracusa, M. C. Abt, B. S. Kim, D. Kobuley, M. Kubo, T. Kambayashi, D. F. Larosa, E. D. Renner, J. S. Orange, F. D. Bushman, and D. Artis. 2012. Commensal bacteria-derived signals regulate basophil hematopoiesis and allergic inflammation. *Nat Med* 18 (4):538-546.
- Honda, K., and D. R. Littman. 2012. The microbiome in infectious disease and inflammation. *Annu Rev Immunol* 30:759-795.
- Huber, M., S. Heink, A. Pagenstecher, K. Reinhard, J. Ritter, A. Visekruna, A. Guralnik, N. Bollig, K. Jeltsch, C. Heinemann, E. Wittmann, T. Buch, O. Prazeres da Costa, A. Brustle, D. Brenner, T. W. Mak, H. W. Mittrucker, B. Tackenberg, T. Kamradt, and M. Lohoff. 2013. IL-17A secretion by CD8+ T cells supports Th17-mediated autoimmune encephalomyelitis. *J Clin Invest* 123 (1):247-260.
- Ivanov, I., K. Atarashi, N. Manel, E. L. Brodie, T. Shima, U. Karaoz, D. Wei, K. C. Goldfarb, C. A. Santee, S. V. Lynch, T. Tanoue, A. Imaoka, K. Itoh, K. Takeda, Y. Umesaki, K. Honda, and D. R. Littman. 2009. Induction of intestinal Th17 cells by segmented filamentous bacteria. *Cell* 139 (3):485-498.
- Iwahashi, M., M. Yamamura, T. Aita, A. Okamoto, A. Ueno, N. Ogawa, S. Akashi, K. Miyake, P. J. Godowski, and H. Makino. 2004. Expression of Toll-like receptor 2 on CD16+ blood monocytes and synovial tissue macrophages in rheumatoid arthritis. *Arthritis Rheum* 50 (5):1457-1467.
- Jarchum, I., M. Liu, C. Shi, M. Equinda, and E. G. Pamer. 2012. Critical role for MyD88-mediated neutrophil recruitment during *Clostridium difficile* colitis. *Infect Immun* 80 (9):2989-2996.
- Johansen, F. E., and C. S. Kaetzel. 2011. Regulation of the polymeric immunoglobulin receptor and IgA transport: new advances in environmental factors that stimulate pIgR expression and its role in mucosal immunity. *Mucosal Immunol* 4 (6):598-602.
- Johansson, M. E., M. Phillipson, J. Petersson, A. Velcich, L. Holm, and G. C. Hansson. 2008. The inner of the two Muc2 mucin-dependent mucus layers in colon is devoid of bacteria. *Proc Natl Acad Sci U S A* 105 (39):15064-15069.
- Joseph, N., B. Reicher, and M. Barda-Saad. 2014. The calcium feedback loop and T cell activation: how cytoskeleton networks control intracellular calcium flux. *Biochim Biophys Acta* 1838 (2):557-568.
- Jost, L. 2007. Partitioning diversity into independent alpha and beta components. *Ecology* 88 (10):2427-2439.
- Kaetzel, C. S., J. K. Robinson, K. R. Chintalacheruvu, J. P. Vaerman, and M. E. Lamm. 1991. The polymeric immunoglobulin receptor (secretory component) mediates transport of immune complexes across epithelial cells: a local defense function for IgA. *Proc Natl Acad Sci U S A* 88 (19):8796-8800.
- Kamada, N., S. U. Seo, G. Y. Chen, and G. Nunez. 2013. Role of the gut microbiota in immunity and inflammatory disease. *Nat Rev Immunol* 13 (5):321-335.
- Karasuyama, H., and F. Melchers. 1988. Establishment of mouse cell lines which constitutively secrete large quantities of interleukin 2, 3, 4 or 5, using modified cDNA expression vectors. *Eur J Immunol* 18 (1):97-104.
- Karmarkar, D., and K. L. Rock. 2013. Microbiota signalling through MyD88 is necessary for a systemic neutrophilic inflammatory response. *Immunology* 140 (4):483-492.
- Kebir, H., I. Ifergan, J. I. Alvarez, M. Bernard, J. Poirier, N. Arbour, P. Duquette, and A. Prat. 2009. Preferential recruitment of interferon-gamma-expressing TH17 cells in multiple sclerosis. *Ann Neurol* 66 (3):390-402.
- Kebir, H., K. Kreymborg, I. Ifergan, A. Dodelet-Devillers, R. Cayrol, M. Bernard, F. Giuliani, N. Arbour, B. Becher, and A. Prat. 2007. Human TH17 lymphocytes promote blood-brain barrier disruption and central nervous system inflammation. *Nat Med* 13 (10):1173-1175.
- Kirkland, D., A. Benson, J. Mirpuri, R. Pifer, B. Hou, A. L. DeFranco, and F. Yarovinsky. 2012. B cell-intrinsic MyD88 signaling prevents the lethal dissemination of commensal bacteria during colonic damage. *Immunity* 36 (2):228-238.

- Komatsuda, A., H. Wakui, K. Iwamoto, M. Ozawa, M. Togashi, R. Masai, N. Maki, T. Hatakeyama, and K. Sawada. 2008. Up-regulated expression of Toll-like receptors mRNAs in peripheral blood mononuclear cells from patients with systemic lupus erythematosus. *Clin Exp Immunol* 152 (3):482-487.
- Krishnamoorthy, G., H. Lassmann, H. Wekerle, and A. Holz. 2006. Spontaneous optico-spinal encephalomyelitis in a double-transgenic mouse model of autoimmune T cell/B cell cooperation. *J Clin Invest* 116 (9):2385-2392.
- Lassmann, H. 2007. Experimental models of multiple sclerosis. *Rev Neurol (Paris)* 163 (6-7):651-655.
- Lee, J. Y., V. C. Wasinger, Y. Y. Yau, E. Chuang, V. Yajnik, and R. W. Leong. 2018. Molecular Pathophysiology of Epithelial Barrier Dysfunction in Inflammatory Bowel Diseases. *Proteomes* 6 (2).
- Lee, Y. K., J. S. Menezes, Y. Umesaki, and S. K. Mazmanian. 2011. Proinflammatory T-cell responses to gut microbiota promote experimental autoimmune encephalomyelitis. *Proc Natl Acad Sci U S A* 108 Suppl 1:4615-4622.
- Liang, S. C., X. Y. Tan, D. P. Luxenberg, R. Karim, K. Dunussi-Joannopoulos, M. Collins, and L. A. Fouser. 2006. Interleukin (IL)-22 and IL-17 are coexpressed by Th17 cells and cooperatively enhance expression of antimicrobial peptides. *J Exp Med* 203 (10):2271-2279.
- Libbey, J. E., L. L. McCoy, and R. S. Fujinami. 2007. Molecular mimicry in multiple sclerosis. *Int Rev Neurobiol* 79:127-147.
- Littman, D. R., and E. G. Pamer. 2011. Role of the commensal microbiota in normal and pathogenic host immune responses. *Cell Host Microbe* 10 (4):311-323.
- Litzenburger, T., R. Fassler, J. Bauer, H. Lassmann, C. Lington, H. Wekerle, and A. Iglesias. 1998. B lymphocytes producing demyelinating autoantibodies: development and function in gene-targeted transgenic mice. *J Exp Med* 188 (1):169-180.
- Lochner, M., M. Berard, S. Sawa, S. Hauer, V. Gaboriau-Routhiau, T. D. Fernandez, J. Snel, P. Bousso, N. Cerf-Bensussan, and G. Eberl. 2011. Restricted microbiota and absence of cognate TCR antigen leads to an unbalanced generation of Th17 cells. *J Immunol* 186 (3):1531-1537.
- Lodygin, D., F. Odoardi, C. Schläger, H. Körner, A. Kitz, M. Nosov, J. van den Brandt, H. M. Reichardt, M. Haberl, and A. Flügel. 2013. A combination of fluorescent NFAT and H2B sensors uncovers dynamics of T cell activation in real time during CNS autoimmunity. *Nat Med* 19 (6):784-790.
- Lublin, F. D., and S. C. Reingold. 1996. Defining the clinical course of multiple sclerosis: results of an international survey. National Multiple Sclerosis Society (USA) Advisory Committee on Clinical Trials of New Agents in Multiple Sclerosis. *Neurology* 46 (4):907-911.
- Lublin, F. D., S. C. Reingold, J. A. Cohen, G. R. Cutter, P. S. Sørensen, A. J. Thompson, J. S. Wolinsky, L. J. Balcer, B. Banwell, F. Barkhof, B. Bebo, Jr., P. A. Calabresi, M. Clanet, G. Comi, R. J. Fox, M. S. Freedman, A. D. Goodman, M. Inglesse, L. Kappos, B. C. Kieseier, J. A. Lincoln, C. Lubetzki, A. E. Miller, X. Montalban, P. W. O'Connor, J. Petkau, C. Pozzilli, R. A. Rudick, M. P. Sormani, O. Stüve, E. Waubant, and C. H. Polman. 2014. Defining the clinical course of multiple sclerosis: the 2013 revisions. *Neurology* 83 (3):278-286.
- Lucas, R. M., A. M. Hughes, M. L. Lay, A. L. Ponsonby, D. E. Dwyer, B. V. Taylor, and M. P. Pender. 2011. Epstein-Barr virus and multiple sclerosis. *J Neurol Neurosurg Psychiatry* 82 (10):1142-1148.
- Macian, F. 2005. NFAT proteins: key regulators of T-cell development and function. *Nat Rev Immunol* 5 (6):472-484.
- Malvin, N. P., H. Seno, and T. S. Stappenbeck. 2012. Colonic epithelial response to injury requires Myd88 signaling in myeloid cells. *Mucosal Immunol* 5 (2):194-206.
- Mameli, G., E. Cocco, J. Frau, M. G. Marrosu, and L. A. Sechi. 2016. Epstein Barr Virus and Mycobacterium avium subsp. paratuberculosis peptides are recognized in sera and cerebrospinal fluid of MS patients. *Sci Rep* 6:22401.

- Mameli, G., D. Cossu, E. Cocco, S. Masala, J. Frau, M. G. Marrosu, and L. A. Sechi. 2014. Epstein-Barr virus and Mycobacterium avium subsp. paratuberculosis peptides are cross recognized by anti-myelin basic protein antibodies in multiple sclerosis patients. *J Neuroimmunol* 270 (1-2):51-55.
- Marrie, R. A. 2004. Environmental risk factors in multiple sclerosis aetiology. *Lancet Neurol* 3 (12):709-718.
- Marta, M., A. Andersson, M. Isaksson, O. Kämpe, and A. Lobell. 2008. Unexpected regulatory roles of TLR4 and TLR9 in experimental autoimmune encephalomyelitis. *Eur J Immunol* 38 (2):565-575.
- Mazmanian, S. K., J. L. Round, and D. L. Kasper. 2008. A microbial symbiosis factor prevents intestinal inflammatory disease. *Nature* 453 (7195):620-625.
- McDonald, W. I. 2000. Relapse, remission, and progression in multiple sclerosis. *N Engl J Med* 343 (20):1486-1487.
- Merad, M., P. Sathe, J. Helft, J. Miller, and A. Mortha. 2013. The dendritic cell lineage: ontogeny and function of dendritic cells and their subsets in the steady state and the inflamed setting. *Annu Rev Immunol* 31:563-604.
- Morgan, M. E., P. J. Koelink, B. Zheng, M. H. den Brok, H. J. van de Kant, H. W. Verspaget, G. Folkerts, G. J. Adema, and A. D. Kraneveld. 2014. Toll-like receptor 6 stimulation promotes T-helper 1 and 17 responses in gastrointestinal-associated lymphoid tissue and modulates murine experimental colitis. *Mucosal Immunol* 7 (5):1266-1277.
- Niess, J. H., S. Brand, X. Gu, L. Landsman, S. Jung, B. A. McCormick, J. M. Vyas, M. Boes, H. L. Ploegh, J. G. Fox, D. R. Littman, and H. C. Reinecker. 2005. CX3CR1-mediated dendritic cell access to the intestinal lumen and bacterial clearance. *Science* 307 (5707):254-258.
- Nighot, M., R. Al-Sadi, S. Guo, M. Rawat, P. Nighot, M. D. Watterson, and T. Y. Ma. 2017. Lipopolysaccharide-Induced Increase in Intestinal Epithelial Tight Permeability Is Mediated by Toll-Like Receptor 4/Myeloid Differentiation Primary Response 88 (MyD88) Activation of Myosin Light Chain Kinase Expression. *Am J Pathol* 187 (12):2698-2710.
- Nouri, M., A. Bredberg, B. Weström, and S. Lavasani. 2014. Intestinal barrier dysfunction develops at the onset of experimental autoimmune encephalomyelitis, and can be induced by adoptive transfer of auto-reactive T cells. *PLoS One* 9 (9):e106335.
- Nyirenda, M. H., E. Morandi, U. Vinkemeier, D. Constantin-Teodosiu, S. Drinkwater, M. Mee, L. King, G. Podda, G. X. Zhang, A. Ghaemmaghami, C. S. Constantinescu, A. Bar-Or, and B. Gran. 2015. TLR2 stimulation regulates the balance between regulatory T cell and Th17 function: a novel mechanism of reduced regulatory T cell function in multiple sclerosis. *J Immunol* 194 (12):5761-5774.
- Olsson, T., L. F. Barcellos, and L. Alfredsson. 2017. Interactions between genetic, lifestyle and environmental risk factors for multiple sclerosis. *Nat Rev Neurol* 13 (1):25-36.
- Pan, Z. J., S. Maier, K. Schwarz, J. Azbill, S. Akira, S. Uematsu, and A. D. Farris. 2010. Toll-like receptor 7 (TLR7) modulates anti-nucleosomal autoantibody isotype and renal complement deposition in mice exposed to syngeneic late apoptotic cells. *Ann Rheum Dis* 69 (6):1195-1199.
- Penna, A., A. Demuro, A. V. Yeromin, S. L. Zhang, O. Safrina, I. Parker, and M. D. Cahalan. 2008. The CRAC channel consists of a tetramer formed by Stim-induced dimerization of Orai dimers. *Nature* 456 (7218):116-120.
- Pesic, M., I. Bartholomäus, N. I. Kyratsous, V. Heissmeyer, H. Wekerle, and N. Kawakami. 2013. 2-photon imaging of phagocyte-mediated T cell activation in the CNS. *J Clin Invest* 123 (3):1192-1201.
- Peterson, J., S. Garges, M. Giovanni, P. McInnes, L. Wang, J. A. Schloss, V. Bonazzi, J. E. McEwen, K. A. Wetterstrand, C. Deal, C. C. Baker, V. Di Francesco, T. K. Howcroft, R. W. Karp, R. D. Lunsford, C. R. Wellington, T. Belachew, M. Wright, C. Giblin, H. David, M. Mills, R. Salomon, C. Mullins, B. Akolkar, L. Begg, C. Davis, L. Grandison, M. Humble, J. Khalsa, A. R. Little, H. Peavy, C. Pontzer,

- M. Portnoy, M. H. Sayre, P. Starke-Reed, S. Zakhari, J. Read, B. Watson, and M. Guyer. 2009. The NIH Human Microbiome Project. *Genome Res* 19 (12):2317-2323.
- Pollard, M., and N. Sharon. 1970. Responses of the Peyer's Patches in Germ-Free Mice to Antigenic Stimulation. *Infect Immun* 2 (1):96-100.
- Pollinger, B., G. Krishnamoorthy, K. Berer, H. Lassmann, M. R. Bosl, R. Dunn, H. S. Domingues, A. Holz, F. C. Kurschus, and H. Wekerle. 2009. Spontaneous relapsing-remitting EAE in the SJL/J mouse: MOG-reactive transgenic T cells recruit endogenous MOG-specific B cells. *J Exp Med* 206 (6):1303-1316.
- Prinz, M., F. Garbe, H. Schmidt, A. Mildner, I. Gutcher, K. Wolter, M. Piesche, R. Schroers, E. Weiss, C. J. Kirschning, C. D. Rochford, W. Brück, and B. Becher. 2006. Innate immunity mediated by TLR9 modulates pathogenicity in an animal model of multiple sclerosis. *J Clin Invest* 116 (2):456-464.
- Quast, C., E. Pruesse, P. Yilmaz, J. Gerken, T. Schweer, P. Yarza, J. Peplies, and F. O. Glöckner. 2013. The SILVA ribosomal RNA gene database project: improved data processing and web-based tools. *Nucleic Acids Res* 41 (Database issue):D590-596.
- Rakhilin, N., A. Garrett, C.-Y. Eom, K. R. Chavez, D. M. Small, A. R. Daniel, M. M. Kaelberer, M. A. Mejooli, Q. Huang, S. Ding, D. G. Kirsch, D. V. Bohórquez, N. Nishimura, B. B. Barth, and X. Shen. 2019. An intravital window to image the colon in real time. *Nature Communications* 10 (1):5647.
- Rakoff-Nahoum, S., J. Paglino, F. Eslami-Varzaneh, S. Edberg, and R. Medzhitov. 2004. Recognition of commensal microflora by toll-like receptors is required for intestinal homeostasis. *Cell* 118 (2):229-241.
- Ransohoff, R. M., D. A. Hafler, and C. F. Lucchinetti. 2015. Multiple sclerosis-a quiet revolution. *Nat Rev Neurol* 11 (3):134-142.
- Rescigno, M., M. Urbano, B. Valzasina, M. Francolini, G. Rotta, R. Bonasio, F. Granucci, J. P. Kraehenbuhl, and P. Ricciardi-Castagnoli. 2001. Dendritic cells express tight junction proteins and penetrate gut epithelial monolayers to sample bacteria. *Nat Immunol* 2 (4):361-367.
- Reynolds, J. M., G. J. Martinez, Y. Chung, and C. Dong. 2012. Toll-like receptor 4 signaling in T cells promotes autoimmune inflammation. *Proc Natl Acad Sci U S A* 109 (32):13064-13069.
- Reynolds, J. M., B. P. Pappu, J. Peng, G. J. Martinez, Y. Zhang, Y. Chung, L. Ma, X. O. Yang, R. I. Nurieva, Q. Tian, and C. Dong. 2010. Toll-like receptor 2 signaling in CD4(+) T lymphocytes promotes T helper 17 responses and regulates the pathogenesis of autoimmune disease. *Immunity* 32 (5):692-702.
- Rickert, R. C., J. Roes, and K. Rajewsky. 1997. B lymphocyte-specific, Cre-mediated mutagenesis in mice. *Nucleic Acids Res* 25 (6):1317-1318.
- Rodriguez, J. M., K. Murphy, C. Stanton, R. P. Ross, O. I. Kober, N. Juge, E. Avershina, K. Rudi, A. Narbad, M. C. Jenmalm, J. R. Marchesi, and M. C. Collado. 2015. The composition of the gut microbiota throughout life, with an emphasis on early life. *Microb Ecol Health Dis* 26:26050.
- Round, J. L., S. M. Lee, J. Li, G. Tran, B. Jabri, T. A. Chatila, and S. K. Mazmanian. 2011. The Toll-like receptor 2 pathway establishes colonization by a commensal of the human microbiota. *Science* 332 (6032):974-977.
- Round, J. L., R. M. O'Connell, and S. K. Mazmanian. 2010. Coordination of tolerogenic immune responses by the commensal microbiota. *J Autoimmun* 34 (3):J220-225.
- Scher, J. U., and S. B. Abramson. 2011. The microbiome and rheumatoid arthritis. *Nat Rev Rheumatol* 7 (10):569-578.
- Schrijver, I. A., M. van Meurs, M. J. Melief, C. Wim Ang, D. Buljevac, R. Ravid, M. P. Hazenberg, and J. D. Laman. 2001. Bacterial peptidoglycan and immune reactivity in the central nervous system in multiple sclerosis. *Brain* 124 (Pt 8):1544-1554.
- Secher, T., S. Kassem, M. Benamar, I. Bernard, M. Boury, F. Barreau, E. Oswald, and A. Saoudi. 2017. Oral Administration of the Probiotic Strain Escherichia coli Nissle 1917 Reduces Susceptibility to

- Neuroinflammation and Repairs Experimental Autoimmune Encephalomyelitis-Induced Intestinal Barrier Dysfunction. *Front Immunol* 8:1096.
- Serafini, B., B. Rosicarelli, D. Franciotta, R. Magliozzi, R. Reynolds, P. Cinque, L. Andreoni, P. Trivedi, M. Salvetti, A. Faggioni, and F. Aloisi. 2007. Dysregulated Epstein-Barr virus infection in the multiple sclerosis brain. *J Exp Med* 204 (12):2899-2912.
- Siewert, K., J. Malotka, N. Kawakami, H. Wekerle, R. Hohlfeld, and K. Dornmair. 2012. Unbiased identification of target antigens of CD8+ T cells with combinatorial libraries coding for short peptides. *Nat Med* 18 (5):824-828.
- Sitara, D., and A. O. Aliprantis. 2010. Transcriptional regulation of bone and joint remodeling by NFAT. *Immunol Rev* 233 (1):286-300.
- Sorensen, L. K., A. Havemose-Poulsen, S. U. Sonder, K. Bendtzen, and P. Holmstrup. 2008. Blood cell gene expression profiling in subjects with aggressive periodontitis and chronic arthritis. *J Periodontol* 79 (3):477-485.
- Stromnes, I. M., and J. M. Goverman. 2006. Active induction of experimental allergic encephalomyelitis. *Nat Protoc* 1 (4):1810-1819.
- Tajik, N., M. Frech, O. Schulz, F. Schälter, S. Lucas, V. Azizov, K. Dürholz, F. Steffen, Y. Omata, A. Rings, M. Bertog, A. Rizzo, A. Iljazovic, M. Basic, A. Kleyer, S. Culemann, G. Krönke, Y. Luo, K. Überla, U. S. Gaip, B. Frey, T. Strowig, K. Sarter, S. C. Bischoff, S. Wirtz, J. D. Cañete, F. Ciccía, G. Schett, and M. M. Zaiss. 2020. Targeting zonulin and intestinal epithelial barrier function to prevent onset of arthritis. *Nature Communications* 11 (1):1995.
- Tamura, K., G. Stecher, D. Peterson, A. Filipski, and S. Kumar. 2013. MEGA6: Molecular Evolutionary Genetics Analysis version 6.0. *Mol Biol Evol* 30 (12):2725-2729.
- Tezuka, H., and T. Ohteki. 2019. Regulation of IgA Production by Intestinal Dendritic Cells and Related Cells. *Front Immunol* 10:1891.
- Turula, H., and C. E. Wobus. 2018. The Role of the Polymeric Immunoglobulin Receptor and Secretory Immunoglobulins during Mucosal Infection and Immunity. *Viruses* 10 (5).
- Uematsu, S., K. Fujimoto, M. H. Jang, B. G. Yang, Y. J. Jung, M. Nishiyama, S. Sato, T. Tsujimura, M. Yamamoto, Y. Yokota, H. Kiyono, M. Miyasaka, K. J. Ishii, and S. Akira. 2008. Regulation of humoral and cellular gut immunity by lamina propria dendritic cells expressing Toll-like receptor 5. *Nat Immunol* 9 (7):769-776.
- Vaishnava, S., C. L. Behrendt, A. S. Ismail, L. Eckmann, and L. V. Hooper. 2008. Paneth cells directly sense gut commensals and maintain homeostasis at the intestinal host-microbial interface. *Proc Natl Acad Sci U S A* 105 (52):20858-20863.
- Vaishnava, S., M. Yamamoto, K. M. Severson, K. A. Ruhn, X. Yu, O. Koren, R. Ley, E. K. Wakeland, and L. V. Hooper. 2011. The antibacterial lectin RegIIIgamma promotes the spatial segregation of microbiota and host in the intestine. *Science* 334 (6053):255-258.
- van Langelaar, J., R. M. van der Vuurst de Vries, M. Janssen, A. F. Wierenga-Wolf, I. M. Spilt, T. A. Siepman, W. Dankers, G. Verjans, H. E. de Vries, E. Lubberts, R. Q. Hintzen, and M. M. van Luijn. 2018. T helper 17.1 cells associate with multiple sclerosis disease activity: perspectives for early intervention. *Brain* 141 (5):1334-1349.
- Vanderlugt, C. L., K. L. Neville, K. M. Nikcevic, T. N. Eagar, J. A. Bluestone, and S. D. Miller. 2000. Pathologic role and temporal appearance of newly emerging autoepitopes in relapsing experimental autoimmune encephalomyelitis. *J Immunol* 164 (2):670-678.
- Visser, L., M. J. Melief, D. van Riel, M. van Meurs, E. A. Sick, S. Inamura, J. J. Bajramovic, S. Amor, R. Q. Hintzen, L. A. Boven, B. A. t Hart, and J. D. Laman. 2006. Phagocytes containing a disease-promoting Toll-like receptor/Nod ligand are present in the brain during demyelinating disease in primates. *Am J Pathol* 169 (5):1671-1685.

- Wang, Q., G. M. Garrity, J. M. Tiedje, and J. R. Cole. 2007. Naive Bayesian classifier for rapid assignment of rRNA sequences into the new bacterial taxonomy. *Appl Environ Microbiol* 73 (16):5261-5267.
- Wang, S., L.-M. Charbonnier, M. Noval Rivas, P. Georgiev, N. Li, G. Gerber, L. Bry, and Talal A. Chatila. 2015. MyD88 Adaptor-Dependent Microbial Sensing by Regulatory T Cells Promotes Mucosal Tolerance and Enforces Commensalism. *Immunity* 43 (2):289-303.
- Wang, S., E. J. Villablanca, J. De Calisto, D. C. O. Gomes, D. D. Nguyen, E. Mizoguchi, J. C. Kagan, H.-C. Reinecker, N. Hacohen, C. Nagler, R. J. Xavier, B. Rossi-Bergmann, Y.-B. Chen, R. Blomhoff, S. B. Snapper, and J. R. Mora. 2011. MyD88-Dependent TLR1/2 Signals Educate Dendritic Cells with Gut-Specific Imprinting Properties. *The Journal of Immunology* 187 (1):141.
- Wekerle, H., K. Berer, and G. Krishnamoorthy. 2013. Remote control-triggering of brain autoimmune disease in the gut. *Curr Opin Immunol* 25 (6):683-689.
- Wen, L., R. E. Ley, P. Y. Volchkov, P. B. Stranges, L. Avanesyan, A. C. Stonebraker, C. Hu, F. S. Wong, G. L. Szot, J. A. Bluestone, J. I. Gordon, and A. V. Chervonsky. 2008. Innate immunity and intestinal microbiota in the development of Type 1 diabetes. *Nature* 455 (7216):1109-1113.
- Wu, H. J., Ivanov, II, J. Darce, K. Hattori, T. Shima, Y. Umesaki, D. R. Littman, C. Benoist, and D. Mathis. 2010. Gut-residing segmented filamentous bacteria drive autoimmune arthritis via T helper 17 cells. *Immunity* 32 (6):815-827.
- Yeshokumar, A. K., S. Narula, and B. Banwell. 2017. Pediatric multiple sclerosis. *Curr Opin Neurol* 30 (3):216-221.
- Zekki, H., D. L. Feinstein, and S. Rivest. 2002. The clinical course of experimental autoimmune encephalomyelitis is associated with a profound and sustained transcriptional activation of the genes encoding toll-like receptor 2 and CD14 in the mouse CNS. *Brain Pathol* 12 (3):308-319.

Resources & Contributions

- Experiments assessing the composition of the gut microbiota were partially performed by Dr. Monika Schaubeck.
- Phoenix cells and Δ NFAT-GFP plasmid were kindly provided by Dr. Nikolaus Kyratsous.
- Experiments of immune system profiling were performed with the support of Dr. Kerstin Berer, Birgit Kunkel, Dr. Bettina Martin.

Acknowledgements

First and foremost, I would like to dedicate these first lines to express my deepest gratitude to Prof. Hartmut Wekerle for giving me the opportunity to join his department and for allowing me to engage in the exciting field of the multiple sclerosis research. Without his constant and kind support, this PhD the completion of this PhD thesis would have not been possible.

I am as well deeply grateful to my doctor father and principal supervisor PD Dr. Naoto Kawakami for his great scientific, technical and personal support during my thesis. His unconditional support and encouragement were of utmost importance throughout my entire PhD journey. Likewise, I would like to express my appreciation to the members of my thesis advisory committee Dr. Andreas Pichlmair, PD Dr. Josef Mautner for their critical scientific input that helped steered my scientific project. Special thanks go to Dr. Gurumoorthy Krishnamoorthy for his valuable scientific advice during the realization of this project.

A heartfelt thank you I dedicate to Dr. Hans-Jörg Schäffer and Dr. Ingrid Wolf, enthusiastic members of the IMPRS-LS coordination office. Thanks to them, my experience as a member of the IMPRS-LS program made is one that is fondly carved in my memory. Their doors were always open for any concerns and were particularly supportive especially during struggling times.

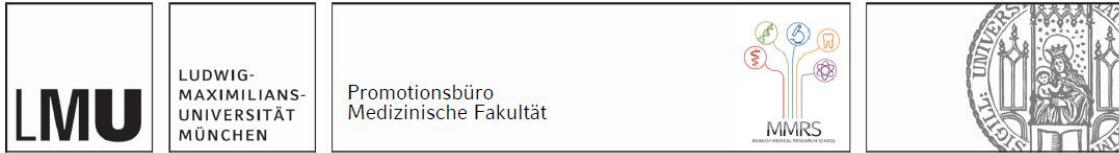
Additionally, I would like to thank members of my group Dr. Kerstin Berer, Dr. Monika Schaubek and Birgit Kunkel, for their valuable teaching, tips, tricks, and scientific input that I received during my PhD. Likewise, I thank my friends Ana, Pedro, Vidya, Amelie and Bettina for their companionship and all the good times we spent in and outside of the lab.

Furthermore, I am forever grateful to my parents in law Heike and Stefan Regula who encouraged me to finish my PhD thesis. They did not only provide me with their affectionate support but also helped me finish my PhD thesis by taking care of my beloved daughter.

My heart goes to express my endless gratitude to my husband Felix Kröner who has been my core throughout all these years. His unconditional love and support gave me the strength and courage necessary for bringing this project and thesis to an end.

Finally, yet also importantly, I heartily thank my entire family, especially my late father Roger Solís, who always believed I could reach for the stars.

Affidavit



Affidavit

Solis Gonzalez, Veronica

Surname, first name

Street

Zip code, town, country

I hereby declare, that the submitted thesis entitled:

Understanding the role of epithelial MyD88 signals in the early development of Experimental Autoimmune Encephalomyelitis (EAE)

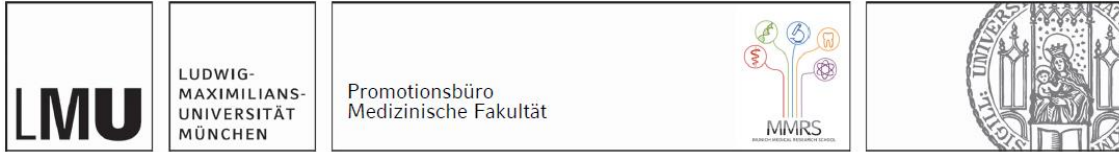
is my own work. I have only used the sources indicated and have not made unauthorized use of services of a third party. Where the work of others has been quoted or reproduced, the source is always given.

I further declare that the submitted thesis or parts thereof have not been presented as part of an examination degree to any other university.

Breunberg, 25OCT2022
place, date

Veronica E. Solis Gonzalez
Signature doctoral candidate

Confirmation of congruency



**Confirmation of congruency between printed and electronic version of
the doctoral thesis**

Solis Gonzalez, Veronica

Surname, first name

Street

Zip code, town, country

I hereby declare, that the submitted thesis entitled:

Understanding the role of epithelial MyD88 signals in the early development of Experimental Autoimmune Encephalomyelitis (EAE)

is congruent with the printed version both in content and format.

Breunberg, 25OCT2022
place, date

Veronica E. Solis Gonzalez
Signature doctoral candidate